A NEW APPROACH TO CONTROL SINGLE-LINK FLEXIBLE ARMS. PART II: Control of the Tip Position in the Presence of Joint Friction

Vicente Feliu[1], Kuldip S. Rattan[2] and H. Benjamin Brown, Jr.

CMU-RI-TR-89-14

The Robotics Institute
Carnegie Mellon University
Pittsburgh, Pennsylvania 15213

July 1989

[1]Visiting Professor, Dpto Ingeniería Eléctrica, Electrónica y Control, UNED, Ciudad Universitaria, Madrid-28040, Spain

[2]Visiting Professor, Department of Electrical Systems Engineering, Wright State University, Dayton, OH. 45435.

Unclassified
SECURITY CLASSIFICATION OF THIS PAGE

REPORT DOCUMENTATION PAGE

1a. REPORT SECURITY CLASSIFICATION Unclassified	1b. RESTRICTIVE MARKINGS
2a. SECURITY CLASSIFICATION AUTHORITY	3 DISTRIBUTION / AVAILABILITY OF REPORT Approved for public release; distribution unlimited
2b. DECLASSIFICATION / DOWNGRADING SCHEDULE	
4. PERFORMING ORGANIZATION REPORT NUMBER(S) CMU-RI-TR-89-14	5. MONITORING ORGANIZATION REPORT NUMBER(S)
6a. NAME OF PERFORMING ORGANIZATION The Robotics Institute Carnegie Mellon University 6b OFFICE SYMBOL *(If applicable)*	7a. NAME OF MONITORING ORGANIZATION
6c. ADDRESS *(City, State, and ZIP Code)* Pittsburgh, PA 15213	7b. ADDRESS *(City, State, and ZIP Code)*
8a. NAME OF FUNDING / SPONSORING ORGANIZATION 8b. OFFICE SYMBOL *(If applicable)*	9. PROCUREMENT INSTRUMENT IDENTIFICATION NUMBER
8c. ADDRESS *(City, State, and ZIP Code)*	10 SOURCE OF FUNDING NUMBERS PROGRAM ELEMENT NO. / PROJECT NO. / TASK NO. / WORK UNIT ACCESSION NO.

11. TITLE *(Include Security Classification)*
A New Approach to Control Single-Link Flexible Arms. Part II: Control of the Tip Position in the Presence of Joint Friction

12. PERSONAL AUTHOR(S)
V. Feliu, K.S. Rattan, and H.B. Brown, Jr.

13a. TYPE OF REPORT	13b. TIME COVERED	14. DATE OF REPORT *(Year, Month, Day)*	15. PAGE COUNT
Technical	FROM _____ TO _____	July 1989	69

16. SUPPLEMENTARY NOTATION

17. COSATI CODES			18. SUBJECT TERMS *(Continue on reverse if necessary and identify by block number)*
FIELD	GROUP	SUB-GROUP	

19. ABSTRACT *(Continue on reverse if necessary and identify by block number)*

This report presents a new way to control the tip position of single-link flexible arms when friction is present in the joint. In order to minimize the influence of the nonlinear components of this friction, the control scheme is composed of two nexted loops: an inner loop that controls the motor position, and an outer loop that controls the tip position.

It is demonstrated that proper design of the inner loop of this control scheme eliminates the effects of friction in controlling the tip position, and may significantly simplify the design of the tip position controller.

Three control schemes are proposed for the outer loop. All of them are based on an hybrid feedforward-feedback control scheme. The first and second schemes use only tip position feedback while the third one uses sensing of positions at several points of the beam.

Performances of the three schemes are compared under the following disturbances: a) motor position perturbations, b) unmodelled dynamics, and c) changes in the paylod.

20. DISTRIBUTION / AVAILABILITY OF ABSTRACT	21. ABSTRACT SECURITY CLASSIFICATION	
☒ UNCLASSIFIED/UNLIMITED ☐ SAME AS RPT ☐ DTIC USERS	Unclassified	
22a. NAME OF RESPONSIBLE INDIVIDUAL	22b TELEPHONE *(Include Area Code)*	22c. OFFICE SYMBOL

DD FORM 1473, 84 MAR — 83 APR edition may be used until exhausted. All other editions are obsolete.

SECURITY CLASSIFICATION OF THIS PAGE

(19 cont'd)

Experimental results are presented for the two arms described in the Part I; the three tip position control schemes are compared in both arms; and finally, conclusions are drawn.

Table of Contents

List of Figures

List of Symbols

$\mathcal{A}$: $n \times n$ constant matrix used in the dynamic model of the beam.

A : $n \times n$ constant matrix used in the state space model of a system.

$a(s)$: analog controller of the motor position control loop (feedforward term).

$a(z)$: discrete compensator for the feedforward term of the motor position control.

a_0 : independent term of $a(z)$ controller.

a_1 : term in z^{-1} of $a(z)$ controller.

$\bar{a}_i$: minimum phase zeros of the tip - motor position transfer function.

$\hat{a}_{1,1}$: element of the first row - first column of matrix $\mathcal{A}$.

$\mathcal{B}$: $n \times 1$ constant matrix used in the dynamic model of the beam.

B : $n \times 1$ constant matrix used in the state space model of a system.

$b(z)$: discrete compensator for the feedback term of the motor position control.

b_0 : independent term of $b(z)$ controller.

b_1 : term in z^{-1} of $b(z)$ controller.

$\bar{b}_i$: non-minimum phase zeros of the tip - motor position transfer function.

$\hat{b}_1$: first element of vector $\mathcal{B}$.

C : $1 \times n$ constant matrix used in the state spac model of a system.

$C(s)$: transfer function between the beam deflection from basis to tip and the coupling torque.

C_0 : constant approximation of $C(s)$.

C_i : $1 \times n$ constant matrix used to define the transfer function between mass m_i position and motor position.

CF : Coulomb friction.

C_t : motor - beam coupling torque.

$C_t^m(s)$: coupling torque estimated from the basis to tip deflection of the beam, and the transfer function $C(s)$.

D : number of sampling periods of delay of the transfer function of the inner loop.

$d(s)$: denominator of the tip - motor position transfer function.

E : elasticity coefficient of the beam.

e : error between the desired trajectory and the trajectory feasible using a bounded control signal.

e_{θ_m} : tracking error of the closed-loop system when following the desired tip trajectory.

e_δ : errors in the tip position due to perturbations.

F_n : extrnal force applied to the tip of the beam.

$F(s)$: transfer function of the feedforward term of the tip control scheme of Figure 1.

$f(z)$: discrete transfer function of the correction term used in the feedforward tip control term to compensate for inner loop dynamics.

$f_n(z)$: numerator of $f(z)$.

$f_d(z)$: denominator of $f(z)$.

$\hat{f}(s)$: transfer function of the filter used to generate the optimum feasible trajectory for the tip from the desired trajectory.

$\mathcal{G}$: matrix of transfer functions (closed-loop system) between the desired trajectories for the measured points of the beam and the actual measurements.

$G(s)$: generic continuous transfer function.

$G(z)$: equivalent discrete transfer function of $G(s)$.

$G_1(s)$: closed-loop transfer function between a motor perturbation and the tip position in the first control scheme.

$G_2(s)$: closed-loop transfer function between a motor perturbation and the tip position in the second control scheme.

$G_3(s)$: closed-loop transfer function between a motor perturbation and the tip position in the third control scheme.

$g_n(s)$: transfer function between the tip and motor positions.

$g_{nn}(s)$: numerator of the transfer function between the tip and motor positions.

$g_{nd}(s)$: denominator of the transfer function between the tip and motor positions.

$\hat{g}_n(s)$: transfer function of the optimum feedforward term.

$\hat{g}_n(z^{-1})$: transfer function of the discretized version of the optimum feedforward term.

$\hat{g}_{nn}(z^{-1})$: numerator of $\hat{g}_n(z^{-1})$.

$\hat{g}_{nd}(z^{-1})$: denominator of $\hat{g}_n(z^{-1})$.

g_n^+ : grouping of all the minimum phase factors of $g_n(s) \cdot g_n(-s)$.

g_n^- : grouping of all the non-minimum phase factors of $g_n(s) \cdot g_n(-s)$.

$\hat{g}_{ni}$: coefficient of order i of the polynomial part of $\hat{g}_n(s)$.

$\hat{g}_{np}(s)$: proper rational function part of $\hat{g}_n(s)$.

$g_{n,i}$: n row - i column element of the transfer functions matrix $\mathcal{G}$.

$g_1'(s)$: transfer function resulting from closing the positive feedback loop (second control scheme) in the single-mass beam example.

$g_n'(s)$: transfer function resulting from closing the positive feedback loop (second control scheme) in the two-mass beam case.

$g_n''(s)$: transfer function resulting from closing the positive feedback loop (second control scheme) and cancelling the minimum phase dynamics in the two-mass beam case.

$\mathcal{H}$: $1 \times n$ constant matrix used in the expression of the motor - beam coupling torque.

h_i $(1 \leq i \leq n)$: elements of matrix $\mathcal{H}$.

h_{n+1} : coefficient that expresses the influence of the motor angle on the motor - beam coupling torque.

h_{n+2} : coefficient that expresses the influence of the external torque applied to the tip of the arm on the motor - beam coupling torque.

I : cross-section inertia of the beam.

I_n : identity matrix.

$I_{UU}(s)$: transfer function obtained from the input of the beam system $u(t)$ by multiplying $u(s) \cdot u(-s)$.

$I_{UU}^+(s)$: grouping of all the minimum phase factors of $I_{UU}(s)$.

$I_{\bar{U}U}(s)$: grouping of all the non-minimum phase factors of $I_{UU}(s)$.

i^* : motor current.

i_c : feedforward current term used to compensate for Coulomb friction and motor-beam coupling.

i_l : part of the motor current that moves the linear part of the system (i less the current wasted in Coulomb friction).

$\hat{i}(s)$: current that moves the linearized and decoupled motor ($\hat{i} = i - i_c$).

$\mathcal{J}$: cost index used in optimization problems.

J : inertia of the motor.

j^* : imaginary number.

K : electromechanical constant of the D.C. motor.

$\bar{K}$: gain of the transfer function between motor and tip position.

K_c : $1 \times n$ feedback vector that represents the controller used to place the closed-loop poles of the system.

$\hat{K}_c$: part of K_c that weights the influence of states others than the tip position in the control.

k : integer used to represent sampling instants.

$\hat{k}_{c1}$: element of K_c that weights the influence the tip position in the control.

$L(s)$: generic transfer function of a closed-loop system, used in sensitivity analyses.

$\mathcal{M}$: $n \times n$ diagonal constant matrix that represents the influence of masses m_i on the dynamics of the beam.

$M(z)$: discrete transfer function of the motor control loop.

m_i $1 \leq i \leq n$: lumped mass at position i.

m_n : lumped mass at the tip of the beam.

m_n^0 : nominal lumped mass at the tip of the beam.

$m(s)$: transfer function of the motor after having removed the effects of Coulomb friction.

$\hat{m}(s)$: transfer function of the motor after decoupling and linearizing by using i_c.

$N(z)$: discrete transfer function of the feedforward term of the first control scheme.

n : number of oscillation modes.

$\bar{n}$: number of states of a system.

n_{gn} : order of the denominator of $g_n(s)$.

n_1 : number of minimum phase zeros.

n_2 : number of non-minimum phase zeros.

n_α : order of polynomial $\sum \alpha_i \cdot s^i$ in expressions (48) and (49).

$n_{\alpha'}$: number of parameters of the inner loop transfer function.

n_ϱ : number of zeros of $M(z)$ that are outside the unit circle, or are real negative.

$P(s)$: polynomial in s vector that defines the influence of the tip position measurement in the reconstruction of the state vector of the flexible arm (expression (5)).

P_p : reference trajectory, without considering non-minimum phase corrections.

p : parameter used to model the dynamics of the single-mass flexible beam (expressions (96) and (97)).

$Q(s)$: polynomial in s vector that defines the influence of the current measurement in the reconstruction of the state vector of the flexible arm (expression (5)).

$R(s)$: closed-loop controller of the tip position.

$R(z)$: discrete version of the closed-loop controller of the tip position.

$\hat{R}(s)$: closed-loop controller of the tip position using the standard pole placement design method.

R_1 : $2 \cdot n \times 2 \cdot n$ state weighting matrix in the optimization of the tip feedback controller.

R_2 : constant that weights the control signal (motor angle) in the optimization of the tip feedback controller.

$r_{1,0}$: independent coefficient of the P.D. controller used in the first control scheme for the single-mass beam.

$r_{1,1}$: first order coefficient of the P.D. controller used in the first control scheme for the single-mass beam.

$r_{2,0}$: independent coefficient of the P.D. controller used in the second control scheme.

$r_{2,1}$: first order coefficient of the P.D. controller used in the second control scheme.

$S_{L,\mu}$: sensitivity of transfer function L to changes in parameter μ.

S_{T,m_n} : sensitivity of transfer function T to changes in the tip mass.

S_{T_i,m_n} : sensitivity of the i-scheme to changes in the tip mass.

S_{T,α_i^j} : sensitivity of transfer function T to changes in the parameter i of the inner loop.

s : Laplace transform variable.

T : sampling period.

T_n : external torque applied to the tip of the arm.

$T(s)$: generic transfer functions.

$T_i(s)$: transfer function of the i-scheme.

t : time.

$U(z)$: factor of the feedforward term that is 1 if the perfect inversion of the arm dynamics is possible. If not, it is a discrete transfer function close to 1 (if the feedforward term is well designed).

$u(s)$: laplace transform of the input to the beam transfer function.

V : dynamic friction of the motor.

$W(z)$: rational function in z used to express the condition that the feedforward term must follow second order parabolas without any steady state error.

$W_n(z)$: polynomial in z^{-1}.

$X_1(z^{-1})$: z-factor of the hold in computer control systems.

$X_2(s)$: numerator of the s-terms of the hold in computer control systems.

$X_3(s)$: denominator of the s-terms of the hold in computer control systems.

x : states of the system.

x_i : i-state.

x_r : vector reference of the states.

$\hat{x}(t)$: feedforward signal.

$\mathcal{Z}$: discretization function.

z : z-transform variable.

z_p : positive zero of $g_n(s)$ transfer function.

α' : vector of dimension $n_{\alpha'}$ of parameters of the inner loop transfer function.

α'^0 : vector of parameters of the inner loop transfer function in the nominal conditions (M(s) = 1).

α_i : coefficients of the second order factor that appears in the numerator of filter (49).

α_z : absolute value of the zeros of the two-mass flexible beam.

α'_i : element i of the vector of parameters of the inner loop transfer function.

γ : control signal generated by the feedback controller of the tip position.

$\delta(z)$: discrete transfer function that represents the perturbations of the system.

$\delta_n(z)$: numerator of $\delta(z)$.

δ_1 : amplitude of the perturbation in the motor position (step).

$\delta_1(s)$: transfer function of the perturbations in the motor position (the same as ϵ).

$\delta_2(s)$: transfer function of the perturbations in the tip position.

$\epsilon(s)$: transfer function of the perturbation current applied to the motor in the robustness analysis of the nested loop scheme.

$\varepsilon(s)$: perturbation in the motor angle (the same as δ_1).

η_i^j : $i-th$ closed-loop pole od Scheme j.

Θ : vector of dimension n that represents the angular positions of the lumped masses of the beam.

$\dot{\Theta}$: vector of dimension n that represents the angular velocities of the lumped masses of the beam.

Θ_r : position reference of the lumped masses.

θ_i $1 \leq i \leq n$: angular position of mass m_i.

$\dot{\theta}_i$ $1 \leq i \leq n$: angular velocity of mass m_i.

θ_m : motor angular position.

θ_{mr} : reference of the motor angular position.

$\hat{\theta}_{mr}$: feedforward signal for the tip control.

θ_n : angular position of the tip.

θ_{nr} : reference of the angular position of the tip.

Λ : $2 \cdot n$ row vector that represents a "P.D. type" feedback controller for the tip position, in the third control scheme.

Λ_1 : n row vector that represents the "P." terms of the feedback controller for the tip position, in the third control scheme.

Λ_2 : n row vector that represents the "D." terms of the feedback controller for the tip position, in the third control scheme.

$\lambda_{i,j}$: ratio between the sensitivity to changes in the tip mass of control schemes i and j.

μ : changing parameter in the sensitivity analysis.

ν : difference between the orders of numerator and denominator of $g_n(z^{-1}) \cdot \hat{g}_n(z^{-1})$.

π : π number.

ρ : ratio between the output component due to the input command and the output component due to perturbations.

$\rho_{i,j}$: ratio between the effects of motor position perturbation in schemes i and j.

ϱ_i : zeros of the inner loop discrete transfer function that are outside the unit circle or are real negative.

$\tau_{i,j}$: ratio between the sensitivity to unmodelled motor control loop dynamics of control schemes i and j.

Υ : n column vector of transfer functions that relates the references for the position of masses m_i with the reference for the tip angle.

$\chi(s)$: transfer function that represents the coupling between the motor and the beam in the motor transfer function.

$\psi(s)$: transfer function that relates the angle of the motor with the motor-beam coupling torque.

ω_1, ω_2 : first and second vibrational modes of the two-mass flexible beam in rad/sec.

* variables are also used as integer indexes to represent elements of other vectorial variables.

Abstract

This report presents a new way to control the tip position of single-link flexible arms when friction is present in the joint. In order to minimize the influence of the nonlinear components of this friction, the control scheme is composed of two nested loops: an inner loop that controls the motor position, and an outer loop that controls the tip position.

It is demonstrated that proper design of the inner loop of this control scheme eliminates the effects of friction in controlling the tip position, and may significantly simplify the design of the tip position controller.

Three control schemes are proposed for the outer loop. All of them are based on an hybrid feedforward-feedback control scheme. The first and second schemes use only tip position feedback while the third one uses sensing of positions at several points of the beam.

Performances of the three schemes are compared under the following disturbances: a) motor position perturbations, b) unmodelled dynamics, and c) changes in the payload.

Experimental results are presented for the two arms described in the Part I; the three tip position control schemes are compared in both arms; and, finally, conclusions are drawn.

1. Introduction

Very little effort has been devoted to the control of flexible arms when static and dynamic frictions are present in the joints, in spite of this being common in practice, as was mentioned in the General Introduction (see the first report of this serie of three). The effects of friction are especially important in lightweight flexible arms, or in flexible arms moving at low speeds and accelerations.

In this second report, control of single-link flexible arms with friction in the joint is studied. A general control scheme is proposed in Section 2 to compensate for it. Existing methods to control flexible arms [1-6] are based on explicit control of the tip position. In these schemes, the controller generates a control signal, which is the current (after being properly amplified), for the DC motor that drives the arm. We propose here a new method which is based on the simultaneous control of the joint motor position and tip position, and the implementation of two nested closed loops: an inner loop that controls the motor position and another outer loop that controls the tip position. In our scheme, the tip position is controlled by using the motor position instead of the current as control signal. Friction is compensated in our scheme by using controllers of high gains in the inner loop. It is demonstrated that this can be done even in the case in which the arm is non-minimum phase.

Section 3 describes the design of the inner loop controller. Compensation of Coulomb friction and the coupling torque between the motor and the beam is carried out. It is stated that, in many cases, the dynamics of the motor position control loop is negligible compared to the dynamics of the beam (second submodel in Section 2 of Part I). This allows us to simplify the design of the outer loop. Section 4 presents the experimental results obtained when closing the inner loop in the cases of two lumped-mass flexible arms that we have built in our laboratory: a single-mass arm, and a two-mass arm (they were described in Part I). Because the first arm is minimum phase and the second non-minimum phase, all the possible cases of single-link flexible arm control are included in our experiments.

The outer control loop is described in Section 5. Three control schemes for the tip position are proposed in this report: two schemes based on classical frequency domain techniques, and a third scheme based on state-space methods. All three schemes combine a feedforward term with a feedback controller. It is shown that, with this hybrid feedforward-feedback scheme, high position accuracy may be achieved for the tip of a flexible arm. The feedforward term is designed to drive the motor in such a way that the tip of the arm approximately follows the desired trajectory. The closed-loop controller compensates for the deviations of the tip from the nominal trajectory. If the feedforward term is properly designed, these errors are small, allowing us to use simple controllers. The feedback control law is implemented in the two first schemes by sensing the tip position. The feedback law of the third scheme uses sensing of the position in several intermediate points of the arm. The second method exploits a special feature that the general control scheme proposed here exhibits: the first (lowest) natural frequency of the beam, which is the dominant one, may be easily cancelled by closing a positive feedback loop of the tip position.

Are presented in Section 6 experimental results of tip position control, that were obtained applying the three methods to our two flexible arms. Performances of the three schemes are compared in Section 7 under the following disturbances: a) motor position perturbations, b) unmodelled dynamics, and c) changes in the payload are present.

Finally, conclusions are drawn in Section 8.

2. General Control Scheme

2.1. Description

As it was mentioned in the introduction, there are many applications in which the friction must be taken into account when controlling a flexible arm. Only when friction torque is much smaller than beam torque, can it be ignored. This happens in cases such as very large flexible structures, or direct-drive arms designed for minimum friction.

Several methods have been proposed to minimize the effects of friction in the control of DC motors, that can be directly applied to the control of rigid arms. The simplest method is to use a high-gain linear feedback. This is based on the property that the robustness of a closed loop system to perturbations and changes in its parameters is improved when the open loop gain is increased (Kuo [7]). This has been used by Wu and Paul [8], for example. The main limitation of this method when applied to rigid arms is that the nonlinearities will dominate any linear compensation for small errors tending to give small permanent errors in the positioning. More significant limitation appears when this is applied to control of flexible arms, which are typically non-minimum phase systems. This means that a high-gain tip position loop leads to system instability (this is consequence of having the system zeros in the righ half-plane). Consequently, this method is unsuitable for flexible arms.

Another method for compensating friction is the use of force sensors and the mechanization of a feedback loop around the motor torque. Examples are Handlykken and Turner [9], and Cannon and Schmitz [1] (the latter is an application to flexible arms). Finally, other methods are based on the use of a calculated compensation term which is added to the current of the motor in order to compensate the friction torque. Examples are Walrath [10] that used a model of the friction in order to predict its value, and more recently Canudas et al. [11] that used a parameter identification procedure (a recursive least squares algorithm) in order to obtain this term.

In this section we propose a new simple control scheme to reduce the effects of the friction. This scheme is based on a modification of the classical high gain position closed loop procedure, in order to allow its application to flexible arms. This method does not need extra sensors (to measure the torque of the motor) and allows much simpler calculations than other compensation methods. Our control scheme also incorporates a constant feedforward term in order to remove the remaining steady state errors because of the Coulomb friction. This method practically eliminated friction nonlinearities in our flexible arms.

In order to reduce the effects of the friction, the basic control scheme of Figure 1 is proposed. This scheme has two variables: motor and tip positions: θ_m and θ_n respectively (using the nomenclature defined in Figure 1 of Part I). These two variables are controlled by two nested closed loops, and two different controllers ($R(s)$ and $a(s)$) are used, each one being designed separately according to different criteria. In Figure 1, $m(s)$ is the motor open-loop transfer function between the current and the angle of the motor. It is easy to show that $m(s)$ always has all its poles and zeros in the left half-plane. The open-loop transfer function of the flexible beam $g_n(s)$ relates the angle of the tip of the beam to the angle of the motor. $g_n(s)$ has all its poles in the left half-plane but may have (for arms with more than one vibrational mode) some zeros in the right half-plane (non-minimum phase system). $F(s)$ is an open-loop term designed in conjunction with $R(s)$.

Existing control schemes for flexible arms basically generate a current for the DC motor as function of the tip position error and/or its derivatives. If we try to compensate for friction in these schemes, by increasing the gains of the controller, the closed-loop system becomes unstable because of the right

half-plane zeros of $g_n(s)$. But in our proposed scheme, because $m(s)$ is minimum phase, the gains for the inner loop can be arbitrarily increased (using an appropiate controller $a(s)$) without making the system unstable. So, intuitively, the high gain inner loop that controls the motor position makes the system insensitive to the friction and, then, a second outer loop may be designed to control the tip position. This second loop cannot have a high gain because $g_n(s)$ is non-minimum phase, but now it does not matter because the friction effects have been nearly removed by having closed first the high gain inner loop.

2.2. Feedback compensation (sensitivity analysis)

The previous ideas justify intuitively the interest of using our control scheme. This subsection gives analytical proof of it (Rattan et al. [12]). The analysis carried out here is quite straightforward and will give a quantitative idea of how much the robustness to friction is increased by using our nested multiple loop scheme. In order to do this comparison, a typical control scheme like the one shown in Figure 2 will be used (Cannon [1], a.e.). The sensitivity characteristics of this system will be taken as representative of the existing methods because they are based on controlling the tip position using only a controller that generates a command for the current of the DC motor. So the sensitivities of all them are of the same order of magnitude. Two comparative analyses will be carried out: one checking the signal-to-noise ratio (considering that the Coulomb friction is the noise), the other checking the sensitivity to variations in the dynamic friction coefficient.

In order to do these comparative analyses, we first express the state space control scheme of Figure 2 in terms of its equivalent transfer functions.

Assume that the plant is represented by the state space equations:

$$\dot{x}(t) = A \cdot x(t) + B \cdot i_l(t), \tag{1}$$

$$\theta_n(t) = C \cdot x(t); \quad C = \begin{pmatrix} 1 & 0 & 0 & \dots & 0 \end{pmatrix}; \tag{2}$$

the system being of dimension $\bar{n}$. i_l is the part of the current given by the controller and actuator, which is applied to the linear part of the model. The remaining quantity of $i(t)$ is used to compensate for joint friction. Assume also that the controller is a row vector of dimension $\bar{n}$ of the form:

$$K_c = \begin{pmatrix} k_{c1} & \hat{K}_c \end{pmatrix}, \tag{3}$$

where $\hat{K}_c$ is a vector of dimension $\bar{n} - 1$, and k_{c1} is the coefficient corresponding to the feedback of the tip position error (error in the first state).

Differentiating the state space equations $\bar{n} - 1$ times we get:

$$\begin{pmatrix} \theta_n \\ \dot{\theta}_n \\ \ddot{\theta}_n \\ \vdots \\ \theta_n^{\angle \bar{n}-1} \end{pmatrix} = \underbrace{\begin{pmatrix} C \\ C \cdot A \\ C \cdot A^2 \\ \vdots \\ C \cdot A^{\bar{n}-1} \end{pmatrix}}_{\textit{Observability Matrix}} \cdot \begin{pmatrix} x_1 \\ x_2 \\ x_3 \\ \vdots \\ x_{\bar{n}} \end{pmatrix}$$

$$= \begin{pmatrix} 0 & 0 & 0 & \dots & 0 & 0 \\ C \cdot B & 0 & 0 & \dots & 0 & 0 \\ C \cdot A \cdot B & C \cdot B & 0 & \dots & 0 & 0 \\ \vdots & \vdots & \vdots & \vdots & \vdots & \vdots \\ C \cdot A^{\bar{n}-2} \cdot B & C \cdot A^{\bar{n}-3} \cdot B & C \cdot A^{\bar{n}-4} \cdot B & \dots & C \cdot B & 0 \end{pmatrix} \cdot \begin{pmatrix} i_l \\ \dot{i}_l \\ \ddot{i}_l \\ \vdots \\ i_l^{\angle \bar{n}-1} \end{pmatrix}; \tag{4}$$

and if the system is observable (which is true in all the models of flexible arms), then the states x of the system may be reconstructed from measurements of the input i_l and the output θ_n using a linear law of the form:

$$x(s) = P(s) \cdot \theta_n(s) + Q(s) \cdot i_l(s) \tag{5}$$

where P and Q are polynomial in s column vectors. This last equation is easily obtained from (4) by inverting the observability matrix. Substituting this in the scheme of Figure 2, substituting also the state space equation of the plant by $g_n(s) \cdot m(s)$, and operating we get the equivalent transfer function scheme shown in Figure 3. In this figure:

$$F(s) = \frac{k_{c1} \cdot m(s) \cdot g_n(s)}{K_c \cdot P(s) \cdot m(s) \cdot g_n(s) + K_c \cdot Q(s)}, \tag{6}$$

and

$$\hat{R}(s) = \frac{K_c \cdot P(s) \cdot m(s) \cdot g_n(s) + K_c \cdot Q(s)}{m(s) \cdot g_n(s)}. \tag{7}$$

Now, the comparative analysis may be done between the schemes of Figures 1 and 3.

2.2.1. Signal-to-noise ratio analysis

The signal-to-noise ratio of the output of a system is defined (Kuo [7]) as:

$$\rho = \frac{\textit{Output due to signal}}{\textit{Output due to noise}}, \tag{8}$$

and is a measure of the insensitivity of the system to perturbation signals (in this case Coulomb friction).

The comparison of the ratios of the schemes of Figures 1 and 3 is done here, for the same levels of input θ_{nr} and perturbation ϵ (which is added to the current of the motor).

Operating the nested double loop scheme we get from Figure 1 that:

$$\theta_n(s) = \frac{m(s) \cdot g_n(s)}{1 + m(s) \cdot a(s) + g_n(s) \cdot m(s) \cdot R(s) \cdot a(s)} \cdot (R(s) \cdot a(s) \cdot F(s) \cdot \theta_{nr}(s) + \epsilon(s)). \tag{9}$$

And the signal-to-noise ratio for this scheme easily follows:

$$\rho_{\theta_{nr},\epsilon} = R(s) \cdot a(s) \cdot F(s). \tag{10}$$

We get from Figure 3 that

$$\theta_n(s) = \frac{m(s) \cdot g_n(s)}{1 + g_n(s) \cdot m(s) \cdot \hat{R}(s)} \cdot (\hat{R}(s) \cdot F(s)\theta_{nr}(s) + \epsilon(s)) \tag{11}$$

$$\rho_{\theta_{nr},\epsilon} = \hat{R}(s) \cdot F(s) = k_{c1}. \tag{12}$$

Comparing both results, expression (10) may be made very large because the gains of controller $a(s)$ may be designed arbitrarily high. But k_{c1} in expression (12), and all the parameters of $R(s)$ in general, are limited by the stability margin because the system is non-minimum phase. The gains of $\hat{R}(s)$ of Figure 1 are limited for the same reason too. Therefore, expression (10) may be made larger than (12) in general, just by choosing properly the gains of the controller of the inner loop. In practice, the gains of the inner loop will be limited by the saturation of the amplifier, unmodelled high frequency dynamics, or discretization of the signals when using digital controllers. But in general case these limits are much larger than the ones imposed by the non-minimum phase characteristic.

2.2.2. Sensitivity to the dynamic friction coefficient

Dynamic friction is another component of friction. It is normally assumed to be linear, and it is included in the model of the plant. Often, however, the dynamic friction coefficient changes noticeably depending on the sense of rotation of the motor (see Figure 8 of the first report), or the position of the rotor relative to the stator (confronted poles), etc. Performing the sensitivity analysis of both systems to changes in the dynamic friction coefficient, we show here that the robustness to this parameter may be significantly improved also using our nested double loop scheme.

The sensitivity of a system, whose closed-loop transfer function is $L(s)$, to changes in a parameter μ, is defined (Kuo [7]) as

$$S_{L,\mu} = \frac{\partial L(s)}{\partial \mu} \cdot \frac{\mu}{L(s)}. \tag{13}$$

The motor submodel is described by (see Subsection 2.2 of Part I):

$$K \cdot i = J \cdot \frac{d^2\theta_m}{dt^2} + V \cdot \frac{d\theta_m}{dt} + C_t + CF \tag{14}$$

$$C_t = \mathcal{H} \cdot \Theta + h_{n+1} \cdot \theta_m + h_{n+2} \cdot T_n \tag{15}$$

In order to do this analysis, we assume that CF and T_n are 0; and, from (14),(15), we express $m(s)$ in the form:

$$m(s) = \frac{K}{J \cdot s^2 + V \cdot s + \chi(s)}, \tag{16}$$

which is the typical transfer function of a DC motor with the exception of the term $\chi(s)$, that represents the coupling between the beam and the motor. This allows us to characterize the influence of the dynamic friction coefficient V in the general transfer function.

Carrying out some calculations, we obtain that the sensitivity to V of the closed-loop system of Figure 1 is:

$$S_{L,V} = \frac{-s \cdot V}{(1 + a(s) \cdot m(s) \cdot (1 + R(s) \cdot g_n(s))) \cdot (J \cdot s^2 + V \cdot s + \chi(s))}. \tag{17}$$

The sensitivity to V of the system of Figure 3 is:

$$S_{L,V} = \frac{-s \cdot V}{(1 + \hat{R}(s) \cdot m(s) \cdot g_n(s)) \cdot (J \cdot s^2 + V \cdot s + \chi(s))}. \tag{18}$$

Comparing both sensitivities, expression (17) will normally be significantly smaller than (18) because $a(s) \cdot (1 + R(s) \cdot g_n(s)) >> \hat{R}(s) \cdot g_n(s)$. Notice again that the gains of $R(s)$ and $\hat{R}(s)$ are bounded by a stability margin, but the gain of $a(s)$ may be increased arbitrarily. Consequently, scheme of Figure 1 is more robust in general to changes in the dynamic friction than the scheme of Figure 3, by a factor of approximately $a(s)$.

2.2.3. Comparison of the characteristic equations

The previous analysis gives a quantitative justification of how the robustness of the system is increased using the two nested loops scheme. A better qualitative understanding of how the nested loops modify the stability of the system, allowing higher gains, may be obtained just by looking at the characteristic equations of the two systems.

In the standard control scheme, the robustness depends on $\hat{R}(s)$, and the characteristic equation is

$$1 + \hat{R}(s) \cdot m(s) \cdot g_n(s) = 0;$$

or, substituting $\hat{R}(s)$ by (7) in this equation:

$$1 + m(s) \cdot g_n(s) \cdot \frac{K_c \cdot P(s)}{1 + K_c \cdot Q(s)} = 0, \tag{19}$$

which expresses the characteristic equation in terms of the feedback gains. Notice that, in this last equation, the right half-plane zeros of $g_n(s)$ limit the gains K_c and, consequently, the gains of $\hat{R}(s)$.

In the proposed scheme we have, from equation (10), that the signal-to-noise robustness depends on the product $a(s) \cdot R(s)$; and, from equation (17), that the sensitivity depends on this product and also depends on an $a(s)$ term. The characteristic equation of the system is:

$$1 + a(s) \cdot m(s) \cdot (1 + g_n(s) \cdot R(s)) = 0. \tag{20}$$

and, if the factor $1 + g_n(s) \cdot R(s)$ had all its zeros in the left half-plane, then the gains of $a(s)$ could be made arbitrarily large. Because $g_n(s)$ is stable, there always exists an $R(s)$ of moderately low gains that makes the mentioned factor have all its zeros in the left half-plane (this may be justified from the root locus plot of $g_n(s) \cdot R(s)$) and, consequently, the product $a(s) \cdot R(s)$ may be arbitrarily large improving the robustness of the system.

2.3. Feedforward compensation

The scheme of Figure 1 overcomes the stability problems which are caused when implementing high gain feedback loops in non-minimum phase systems in order to increase its robustness to friction. But still small steady state errors may be present.

A feedforward term can be added to the current of the motor to remove this. This term is a constant one that changes its sign depending on the sign of the motor velocity. This term is used to compensate for an ideal Coulomb friction torque, and the value used here is the averaged one given by the identification method described in Section 5 of Part I.

3. Motor Position Control Loop

3.1. Description and Design

A main objective of the inner loop design is to remove the modelling errors and the nonlinearities introduced by the friction by means of very high gains. Another important goal is to make the response of the inner loop significantly faster than the response of the outer loop and, of course, very much faster than the motions produced by the vibrational modes of the arm. This will simplify the design of the outer loop. In fact, if the inner loop is relatively fast we can substitute for the inner loop of Figure 1 a block with unity transfer function. This allows us to study the flexible arm just as a system of $g_n(s)$ transfer function whose control signal is the angle of the motor.

In order to design the controller of the inner loop, three approaches may be used, provided that a

feedforward term is used to compensate for the Coulomb friction:

1. Design a regulator to control the linear part of the motor submodel (16). This part is minimum phase but may be quite complex, even having zeros in the imaginary axis.

2. Consider the coupling torque between the motor and the beam just as another perturbation, and design a regulator to control the reduced equation obtained from (16):

$$K \cdot i(t) = J \cdot \frac{d^2\theta_m(t)}{dt^2} + V \cdot \frac{d\theta_m(t)}{dt}. \tag{21}$$

3. Design a regulator to control the system represented by (14),(15), but using another feedforward term to compensate for the coupling between the motor and the beam. This may be estimated from measurements of a strain gauge installed in the basis of the beam, or can be calculated from the measurements of the angles of the motor and the tip, by using (15).

We use the third approach because it simplifies the design of the inner controller, and because we want explore the posibilities of estimating the coupling torque from measurements of the motor and tip position. Because the control is robust, an approximate estimation of this torque is adequate. The errors produced by this approximation will be compensated by the high gain inner loop. These points will be developed in the next subsection, and illustrated by the experiments of Section 4.

Assume in what follows that we are able to calculate by some method the coupling torque C_t between the motor and the beam. Then the system may be approximately decoupled and linearized by adding to the current the following term:

$$i_c(t) = (C_t(t) + CF(sign\ of\ motor\ velocity))/K. \tag{22}$$

Then the motor transfer function used to design the controller is reduced to the typical one for DC motors:

$$\frac{\theta_m(s)}{\hat{i}s} = \frac{K/J}{s \cdot (s + V/J)} = \hat{m}(s). \tag{23}$$

A digital controller of the form shown in Figure 4 is suggested in order to get a very fast response without overshooting. This figure represents the inner loop to control the motor position, where θ_{mr} is the commanded motor position, and $a(z)$ and $b(z)$ are phase-lead controllers. The limits in the gains of $a(z)$ (resembling $a(s)$ of Figure 1) depend upon the current limit of the amplifier of the DC motor as well as beam deflection limits. In the cases where the coupling torque is high, it is necessary to take into account in the design the current drained by the coupling compensation term. This will lower the value of the maximum current that is available for the feedback control of Figure 4. A delay term is included in this scheme in order to take into account the delay in the control signal because of the computations.

3.2. Decoupling term

Coupling torque C_t can be exactly compensated by using expression (15), if measurements of all the

angles $\theta_m, \theta_1, \ldots, \theta_n$ are available (we assume in what follows that T_n is 0). But often, we only have measurements of the motor angle θ_m and the tip angle θ_n. Under these circumstances, the coupling torque has to be approximated from an expression

$$C_t^*(s) = C(s) \cdot (\theta_m(s) - \theta_n(s)), \tag{24}$$

where $C(s)$ is a transfer function to be designed.

If we denote

$$C_t(s) = \Psi(s) \cdot \theta_m(s); \tag{25}$$

then the $C(s)$ that exactly compensates the coupling torque can be calculated from the expression

$$C(s) = \frac{\Psi(s)}{1 - g_n(s)}. \tag{26}$$

But $C(s)$ usually has its poles in the imaginary axis. This kind of transfer function is difficult to implement, especially in a computer, because discretizations easily produce unstable compensators.

The simplest approach is to assume that $C(s)$ is a constant. Selecting the adequate value for this constant, compensator (24) cancels exactly the low frequency behavior of C_t (up to the first natural frequency of the beam). Notice that, in this case, $C_t(s)$ and $C_t^*(s)$ have the same poles (resonant frequencies), they only differ in their zeros.

If we want to improve the compensation at middle and high frequencies, more complex transfer functions $C(s)$ can be tested. Coefficients of $C(s)$ may be obtained from optimization techniques (Feliu [13]) that minimize the error between the spectrum of the coupling torque ant its estimation (in this case, the error between $\Psi(s)$ and $C(s) \cdot (1 - g_n(s))$.

4. Motor Control Experimental Results

The validity of the control scheme proposed in Sections 2 and 3 is tested here. We show that the inner loop removes nearly completely the nonlinear effects of Coulomb friction and time-changing dynamic friction. We show too that the assumption of the dynamics of the motor control loop being faster than the dynamics of the beam is normally achieved. The two lumped-mass arms described and modelled in Section 6 of Part I are used here: a single-mass flexible arm, and a two-mass flexible arm.

4.1. Single-mass flexible arm

The inner loop incorporates compensation terms for the Coulomb friction and the coupling between the motor and the beam. In the case of the single-mass flexible arm, this coupling may be expressed in terms of the difference between the angle of the motor and the angle of the tip of the beam. Motor

control is built according to the scheme of Figure 4, where the parameters estimated in Section 6 of Part I are used for the compensations. The sampling period of this loop is 3 *msec*.

An optimization program was developed to get the best controllers using the model obtained for the motor. The settling time (considering an error less than 1%) of the response of the motor to step commands in the motor angle reference input was minimized. Step inputs were assumed as references for the inner loop because, in order to get a good control action, the command angle for the motor should experience very sharp changes. In fact in our experiments the motor angle varied much faster than the angle of the tip. The following constraints were used in the design:

1. $b_0 - b_1 = 1$: in order to guarantee the zero steady state error of the motor position response.
2. $a_0 - a_1 = 15$: in order to limit the peak of the current of the motor. It was dimensioned taking into account that a step of amplitude 400 *mrad.* should produce a peak of 6 *amps*.
3. The response cannot exhibit any overshooting.

The optimum controllers were:

$$a(z) = 17.442 - 2.442 \cdot z^{-1} \tag{27}$$

$$b(z) = 6.667 - 5.667 \cdot z^{-1}. \tag{28}$$

The coupling torque compensation term is given by (equation (34) of Part I):

$$C_t = 0.674 \ \ lb.in./rad. \cdot (\theta_m - \theta_1). \tag{29}$$

Figures 5 to 12 show the position responses, to step commands, of the motor loop closed with these controllers, for different values of the Coulomb friction feedforward compensation term (motor-beam decoupling term is being used). These responses were obtained keeping the tip of the arm fixed in the zero angle position. This means that, in the steady state of this experiment, there is always a coupling torque C_t caused by the bending of 50 *mrad.* existing between the angle of the motor and the angle of the tip. Analyzing permanent errors in these figures, we conclude that the best compensation term is obtained assuming an equivalent Coulomb friction of a value between 0.1318 *amps.* and 0.1367 *amps*. The value estimated from the frequency method of Section 5 of Part I was 0.132 *amp.*, which sustantially agrees with the values obtained from this closed-loop motor experiment. The estimates of Coulomb friction obtained from standard temporal methods were 0.161 *amps.* for positive velocities, and 0.152 *amps.* for negative velocities (see Figure 8 of Part I). Figures 11 and 12 show that bad compensation is achieved using these values, and that, therefore, the estimate of Coulomb friction given by our method is more accurate. When the Coulomb friction compensator has a value higher than the real value of the Coulomb friction (Figures 10-12), a permanent ripple appears as a result of using excessive compensation.

Notice that a transient ripple appears in Figures 5-12. This is because of the method of estimating the actual velocity of the motor, used to calculate the sign of the compensation term. This estimation is done by substracting the motor position value of the previous sample from the value of the actual sample. It produces a delay in the estimate of the sign of the velocity, causing this transient effect. This effect

may be easily avoided defining a limit value. If the difference between the actual motor position and the previous one is larger (in absolute value) than this limit, then the general compensation algorithm is applied. If it is smaller, then the algorithm looks at the error between the desired and actual motor positions, and the sign of the Coulomb friction compensation is the sign of this error, in order have it corrected. The value for this limit was obtained experimentally. Good results were achieved using a limit of 2 *mrad.*

Figure 13 shows the comparison between the simulated response, using the obtained optimum controller with all the compensation terms, and the experimental one. The above limit value of 2 *mrad.* was used. Both responses are very close and demonstrate the validity of the parameters estimated in Part I, and of the compensation terms obtained from them. These responses were obtained keeping again the tip of the arm fixed in the zero angle position. The coupling torque C_t, caused by the bending of 200 *mrad.* existing between the angle of the motor and the angle of the tip, is very noticeable. The zero steady state error shown for the experimental data demonstrates the effectiveness of compensation achieved for the Coulomb friction and for the coupling of the motor with the beam. The settling time achieved for the motor is 33 *msec.* which is significantly faster than the dynamics of the beam. This allows us to assume that the equivalent transfer function of all the inner loop is 1, which simplifies the design of the outer loop in the next sections.

Figure 14 shows the response, when the compensation friction term is removed, of the same experiment of Figure 13; and Figure 15 when the decoupling term is removed. These results show that these compensation terms do not improve significantly the dynamic response of this system, but they practically eliminate the steady state errors.

4.2. Two-mass flexible arm

We use the same motor here as in the previous case. Then the dynamics of the motor submodel are the same as in the single-mass arm, with exception of the coupling torque. This torque is represented now by equation (40) of Part I:

$$C_t = -6.159 \cdot \theta_1 + 2.053 \cdot \theta_2 + 4.106 \cdot \theta_m. \tag{30}$$

Consequence of all this is that the same controllers $a(z)$ and $b(z)$ of the previous arm may be used here, as well as the same Coulomb friction compensation term. Only the decoupling term has to be redesigned. We will consider here two cases: a) we only have measurements of the tip and motor positions θ_1 and θ_m; b) we have measurements of all the positions θ_1, θ_2 and θ_m.

4.2.1. Decoupling from tip position measurements

From expression (30), and taking into account the dynamic model of the beam (equation (39) of Part I), we get that the coupling torque may be expressed as a function of the measured variables:

$$C_t(s) = 2.05274 \cdot \frac{1591.625 + 2 \cdot s^2}{1682.575 + s^2} \cdot (\theta_m(s) - \theta_2(s)). \tag{31}$$

We implemented a decoupling term using this expression, and we were unable to compensate for the second natural frequency of the beam. Moreover, depending on the discretization method used for

this decoupling compensator, sometimes the system became unstable. This supports the statement of Subsection 3.2. about the difficulty of implementing such decoupling terms when the transfer function $C(s)$ has imaginary poles.

We try now to decoupling the motor from the beam by using the simplest compensator: $C(s) = C_0$. We use the characteristic $C_t(s)/\theta_m(s)$ instead of C_t in the following analysis. This can be obtained from (31) substituting $\theta_2(s)$ by $g_2(s) \cdot \theta_m(s)$. If we use the term $C_0 \cdot (\theta_m(s) - \theta_2(s))/\theta_m(s)$ as an approximation to the above characteristic, where C_0 is chosen in such a way that steady state differences are removed, then this term has the same poles as $C_t(s)/\theta_m(s)$, and they just differ in the zeros. These differences only affect to the behavior at frequencies higher than the first natural frequency. For our arm, this decoupling term is:

$$C_t(t) = 1.941 \cdot (\theta_m(t) - \theta_n(t)). \tag{32}$$

The plot of the magnitude characteristics of the frequency responses of both transfer functions is shown in Figure 16, and illustrates these statements.

The same closed-loop control experiment was done here as in the first example: the motor was moved with step motor position reference commands while the tip of the arm was kept fixed in the zero angle position (the middle mass was left free). The experimental response of the inner loop, with all its compensating terms, is shown in Figure 17. We observe that this response is still significantly faster than the dynamics of the beam (the settling time for the 5 % position error is about 60 *msec.*), in spite of having now considerably more inertia to move (higher coupling torque). We can notice also that the steady state error is small again, and that a small ripple is present because of the uncompensated high frequency coupling dynamics. The frequency of this ripple is about 5.8 *Hz*. This corresponds to the range of the mismatching frequencies of Figure 16 in the neighbourhood of the second resonant frequency (6.3 *Hz.*). Figure 18 shows the response without the decoupling compensator. We notice again that the use of this term does not affect the temporal response of the motor (probably because of the high gains used in the controller $a(z)$), but its use improves noticeably the steady state, removing the permanent error that otherwise appears in Figure 18.

4.2.2. Decoupling from intermediate measurements

If we use the Selspot camera, we are able to simultaneously track several LED's. Placing two LED's, one on each lumped mass, we can use expression (30) in order to exactly decouple the motor from the beam. The response of the motor position control loop, using this decoupling term, is shown in Figure 19. This result is sustantially better than the one obtained from only measuring tip and motor positions.

5. Tip Position Control Loop

5.1. General Scheme

5.1.1. Basic Concepts

This section studies the control of the tip position. Sections 2 to 4 showed that the use of adequate compensators and high gain controllers in the inner loop allows us to remove the effects of the friction. Once this has been achieved, the inner loop may be represented, for tip position control purposes, as a linear system of constant coefficients whose input is the desired angle of the motor θ_{mr}, and the output is the actual angle of the motor θ_m.

Another important result attained by closing the inner loop is that, because high gains are used in the motor position controller, the response of this inner loop may be quite fast compared with the dynamics of the mechanical beam. This means that we can assume in many cases that this inner loop may be represented by a unity transfer function. This is especially true in lightweight flexible arms. When the reaction torque of the flexible arm is important compared with the motor input torque then this assumption no longer remains true. But it still may be used as an approximation in the design of the tip position control loop, and correction terms may be added later in order to compensate for the delays that appear in the response of the servocontrolled motor.

Assuming the previous statement, the only dynamics to take into account are those of the beam submodel, which are given by the transfer function $g_n(s)$ of Figure 1. This transfer function relates the angle of the motor (input) with the tip position (output). This assumption allows us greatly simplify the design of the tip controller and to relate in an easy way the commanded trajectories with the mechanical limitations of the beam, as the maximum stress in the structure for example. These two facts suggest that the two nested closed loops scheme here proposed is of general interest, and may be useful even in the case where the friction in the joints is not important.

Several approaches may be used to control the tip position, either from state space or frequency domain techniques, or either using feedback or feedforward controllers.

Feedforward terms have been often used in the control of rigid arms : Craig [14], Khosla and Kanade [15] a.e. The feedforward term generates, in these schemes, a torque (current) to drive the arm that is function of the desired trajectory. The feedback control loop compensates for the tracking errors produced by perturbations. Feedforward functions may be generated off-line previous to the motion, but it is desirable to be able to generate them in real time in order to face unexpected changes in the trajectory as for example happens in robots with sensors. Feedforward functions have been used to drive flexible structures without exciting the resonant modes (Meckl and Seering [16] a.e.), but they are complex and difficult to use for real time control, especially when several resonant modes have to be considered.

The other approach is the design of feedback controllers to actively damp the vibrations produced when moving these flexible structures. Several methods have been proposed and experimental results are available. Examples are Cannon et al. [1], Matsuno et al. [2] and, recently Kotnick et al. [17] . Most of these methods are based on state space techniques. They use optimal control and normally need to reconstruct from tip and motor measurements some states of the system by using observers or filters.

A simple general scheme is proposed here that combines a feedforward term with a feedback controller. Three different feedback schemes are described here. It is shown that, with our simple scheme, high

positioning performances may be achieved for the tip of a flexible arm. In this scheme, the feedforward term is mainly responsible for driving the motor in such a way that the tip of the arm follows the desired trajectory. The closed-loop controller compensates for the deviations of the tip from the nominal trajectory. If the feedforward term is properly designed, these errors will be small allowig us to use very simple controllers to compensate for them.

The feedforward term is studied in Subsection 5.2 neglecting dynamics of the inner loop. A correction term is also proposed in this subsection to take into account the dynamics of this loop. Feedback controllers are described in Subsection 5.3.

5.1.2. Error Analysis

The scheme proposed here combines a feedforward term very simple to generate, with a simple feedback controller. We show that we can get controls that provide high dynamic performance by using some simple rules from the classical frequency domain control methods. Combined feedforward/feedback control schemes have been used before for flexible structures, as for example Dougherty et al. [18], that used acceleration feedforward in the pointing control of the Space Telescope, or recently Gebler [19], that used an approximate feedforward term to control a two degree of freedom flexible arm. Our feedforward term differs in that it uses motor angle rather than torque as the generated signal. Thus the feedforward term may be defined as the inverse of the dynamics of the beam (in the minimum phase case). This term is simpler than the terms generated in the above mentioned methods, and can be easily computed in real time.

Figure 20 represents this scheme. We have included in the arm model two kinds of perturbations, one in the angle of the motor and other in the angle of the tip. The first one ($\delta_1(s)$) models residual errors in the positioning of the motor because of the Coulomb friction, residual errors in modelling the dynamics of the motor (because of changes in the dynamic friction for example), errors because of the assumption that the transfer function of the inner loop is equal to one, and even errors because of unexpected permanent bending in the beam. The worst errors are those due to the Coulomb friction and the permanent bending of the beam because they cause steady state errors. This is modelled by a step input: $\delta_1(s) = \delta_1/s$. The second perturbation ($\delta_2(s)$) models deviations of the tip from the desired trajectory because of external disturbances. Perturbation $\delta_2(s)$ is modelled in this case by a polynomial in s because it is a transient error. Finally, notice that in Figure 20, $g_n(s) = g_{nn}(s)/g_{nd}(s)$.

5.1.2.1. Discretization.

The system of Figure 20 is a hybrid system in the sense that it has analog and discrete components. In order to simplify the design, a discretization of the analog blocks is done, and a digital controller in the $z - plane$ is designed. The discretization is done using the residues formula for continuous-discrete equivalent sampled systems with generalized holds (Feliu [20], e.g.):

$$G(z) = X_1(z^{-1}) \cdot \mathcal{Z}[G(s) \cdot X_2(s)/X_3(s)], \tag{33}$$

where $G(s)$ is the transfer function of the continuous plant, and X_1, X_2 and X_3 are polynomials that characterize the hold and its interpolation properties.

This way of discretization is preferred to others (Tustin transform for example) because it gives an exact matching between the discrete and analogical signals at sampling instants (VanLandingham [21],

e.g.).

The following assumption is made: if we sample the angle of the motor θ_m with period T, then this signal may be approximately reconstructed from its samples by interpolating between the samples by straight lines. It can be shown that it is equivalent to reconstruct the signal from its samples using a first order non-causal hold. In this case:

$$X_1(z^{-1}) = z \cdot (1 - z^{-1})^2, \quad X_2(s) = 1/T, \quad X_3(s) = s^2, \tag{34}$$

and $g_n(z)$ is obtained from (33) using this hold and making $G(s) = g_n(s)$. Transfer function $\hat{m}(z)$ is the sampled-data equivalent transfer function of the motor $\hat{m}(s)$ after having removed the Coulomb friction and the beam-motor coupling by using compensating terms. A zero order hold is used to obtain this discrete transfer function from expression (33). Now $G(s) = \hat{m}(s)$, and:

$$X_1(z^{-1}) = 1 - z^{-1}, \quad X_2(s) = 1, \quad X_3(s) = s. \tag{35}$$

The partial scheme of Figure 21, that does not include the perturbations, illustrates this discretization process. The scheme of Figure 22 is obtained where:

$$M(z) = \frac{a(z) \cdot \hat{m}(z)}{1 + a(z) \cdot b(z) \cdot \hat{m}(z)}. \tag{36}$$

It can be easily shown that the two mentioned perturbations may be grouped for control purposes in a unique perturbation $\delta(z)$ (Fig. 22). It is now of the form:

$$\delta(z) = \frac{\delta_n(z^{-1})}{g_{nd}(z^{-1}) \cdot (1 - z^{-1})}, \tag{37}$$

δ_n being a polynomial in z^{-1}, and $g_{nd}(z^{-1})$ the denominator of $g_n(z)$. The factor $1 - z^{-1}$ of the denominator is produced by the pole in the origin of perturbation δ_1, and numerator δ_n is a combination of both perturbations δ_1 and δ_2.

The only approximation made for deriving Figure 22 is the mentioned interpolation. Transfer functions $\hat{m}(z)$ and $M(z)$ are exact in the sense that they model exactly the behavior of the motor and inner loop at sampling instants because the input to the motor comes from a D/A converter and it is adequately modelled by a zero order hold.

5.1.2.2. Analysis.

From the block diagram of Figure 22 we get:

$$\frac{\theta_n(z)}{\theta_{nr}(z)} = \frac{M(z) \cdot g_n(z) \cdot (R(z) + N(z))}{1 + M(z) \cdot g_n(z) \cdot R(z)} \tag{38}$$

$$\frac{\theta_n(z)}{\delta(z)} = \frac{1}{1 + M(z) \cdot g_n(z) \cdot R(z)}. \tag{39}$$

If the feedforward term is of the form:

$$N(z) = g_n^{-1}(z) \cdot M^{-1}(z) \cdot U(z), \tag{40}$$

then the error in θ_n due to the reference trajectory (assuming no perturbations) is:

$$e_{\theta_{nr}}(z) = \frac{1 - U(z)}{1 + M(z) \cdot g_n(z) \cdot R(z)} \cdot \theta_{nr}(z). \tag{41}$$

The error due to the perturbations is, combining (37) and (39):

$$e_\delta(z) = \frac{\delta_n(z)/(g_{nd}(z^{-1}) \cdot (1 - z^{-1}))}{1 + M(z) \cdot g_n(z) \cdot R(z)}. \tag{42}$$

The steady state error analysis indicates that it is necessary to use a controller with integral feedback to eliminate steady state errors. So, it suggests that $R(z)$ should be a *P.I.D.* controller.

5.2. Open-Loop Control

Expression (41) gives a very straightforward criterion for choosing the feedforward term: the closer $U(z)$ is to 1, the less $e_{\theta_{nr}}(z)$ is. Ideally, we just need to make $U(z)$ equal to 1 to get a zero tracking error. $U(z) = 1$ means that the feedforward term does the perfect inversion of the dynamics of the arm which is expressed as a relation between the commanded angle for the motor and the angle of the tip. But, unfortunately, it is not possible to do this in many cases when trying to control flexible arms. There are three causes that preclude the use of the perfect inversion of the system as a feedforward:

1. Transfer function $g_n(s)$ (or $g_n(z)$) is normally non-minimum phase. It means that this transfer function has zeros in the right half-plane. When inverting it, the feedforward term becomes unstable producing unbounded control signals.
2. Transfer function $M(z)$ is non-minimum phase or has zeros such that their real component is negative. The same as above applies here when $M(z)$ is non-minimum phase. In the other case, the inverted term remains stable but the feedforward control signal generated is extremely oscillatory.
3. Delays in $M(z)$. When inverting it, the feedforward term becomes noncausal. If the feedforward control signal is precomputed, it is not a problem. But it impedes the real time generation of this signal. It is important to mention that $g_n(z)$ does not present this problem because it was calculated using a non causal hold.

Notice that the first problem is related to the inversion of the dynamics of $g_n(s)$, and the other two to the inversion of the dynamics of the inner loop. So, if the inner loop is much faster than the dynamics of the beam, we can assume that $M(z) = 1$ and we just have to face the first problem. Subsubsection 5.2.1. is devoted to the study of this simplified case. The profile of the tip trajectory is deduced in Subsubsection 5.2.2., assuming this simplified case. The general case, where the dynamics of the inner loop are included in the feedforward term, is studied in Subsubsection 5.2.3.

5.2.1. Feedforward term

An original method is proposed here that allows us to generalize the use of the inverse dynamics feedforward term to non-minimum phase systems. It will be seen that in this case an approximate inverse dynamics term is generated that minimizes the differences between the desired and actual behavior of the tip of the arm.

Let us assume a stable system whose transfer function is $g_n(s)$. Assume that we want its output to follow a nominal trajectory, represented by its Laplace transform $u(s)$, as close as possible minimizing the *ISE* error (integral squared error):

$$ISE = \int_0^{\infty} e^2(t) \cdot dt = \frac{1}{2 \cdot \pi \cdot j} \cdot \int_{-j \cdot \infty}^{j \cdot \infty} e(s) \cdot e(-s) \cdot ds. \tag{43}$$

Then the feedforward term (see Figure 23) that optimizes this with the constraint of being stable is given by the expression:

$$\hat{g}_n(s) = \frac{\left[\frac{g_n(-s) \cdot I_{UU}(s)}{g_n^-(s) \cdot I_{UU}^-(s)}\right]_+}{g_n^+(s) \cdot I_{UU}^+(s)}, \tag{44}$$

where:

$$g_n(s) \cdot g_n(-s) = g_n^+(s) \cdot g_n^-(s),$$

$g_n^+(s)$ groups all the poles and zeros of $g_n(s) \cdot g_n(-s)$ that are in the left half-plane, and $g_n^-(s)$ all which are in the right half-plane;

$$I_{UU}(s) = u(s) \cdot u(-s) = I_{UU}^+(s) \cdot I_{UU}^-(s),$$

where again $I_{UU}^+(s)$ groups all the poles and zeros of $I_{UU}(s)$ in the left half-plane and $I_{UU}^-(s)$ all which are in the right half-plane; and

$$\frac{g_n(-s) \cdot I_{UU}(s)}{g_n^-(s) \cdot I_{UU}^-(s)} = \left[\frac{g_n(-s) \cdot I_{UU}(s)}{g_n^-(s) \cdot I_{UU}^-(s)}\right]_+ + \left[\frac{g_n(-s) \cdot I_{UU}(s)}{g_n^-(s) \cdot I_{UU}^-(s)}\right]_-,$$

where, assuming that the partial fraction expansion of the left hand member of the above equation has been done, the + term represents the grouping of the fractions corresponding to the roots placed in the left half-plane and the - term represents the grouping of the ones corresponding to the roots in the right half-plane.

This method is just a slight modification for open-loop control of the technique to obtain optimal controllers described and demonstrated in Gupta and Hasdorff [22]. Notice that we are minimizing a cost of the form

$$\mathcal{J} = \int_{-j\cdot\infty}^{j\cdot\infty} [u(s)\cdot(1-\hat{g}_n(s)\cdot g_n(s))]\cdot[u(-s)\cdot(1-\hat{g}_n(-s)\cdot g_n(-s))]\cdot ds,$$

therefore if $g_n(s)$ is minimum phase, then $\hat{g}_n(s) = g_n^{-1}(s)$ and, as consequence of all this, the continuous feedforward term in this simplified case will be of the form

$$N(s) = \hat{g}_n(s).$$

This method allows us to design an analog feedforward term that nearly cancels (if non-minimum phase system) or completely cancels (if minimum phase) the dynamics of $g_n(s)$. If we denote the desired trajectory for the tip position as P_p, the tip will not follow exactly this reference in the non-minimum case. Instead, it will follow a new reference profile θ_{nr} obtained from passing P_p through a filter whose transfer function can be easily seen that is $g_n(s)\cdot\hat{g}_n(s)$. Then:

$$\theta_{nr}(s) = g_n(s)\cdot\hat{g}_n(s)\cdot P_p(s). \tag{45}$$

In the minimum phase case, this filter will be 1. The property of this filter, according to (43), is that the new reference trajectory $\theta_{nr}(t)$ is as close as possible to the desired reference $P_p(t)$, but taking into account the constraint of a bounded θ_{mr}.

Finally, we have to mention that, in the scheme of Figure 22, the feedforward term is discrete. This term is implemented by generating the signal $\hat{x}(t)$ of Figure 23 and sampling it with period T to produce the sequence $\hat{x}(k)$ used in the control as it is shown in Figure 24. A discrete version of formula (44) also exists that directly gives a discrete feedforward term $\hat{g}_n(z)$. We preferred to use the continuous version and then sample the output because it is easier to compute and because the use of the discrete version can easily produce feedforward terms with the problem stated above of having stable poles with negative real component, generating a high frequency oscillatory control signal.

It will be stated in the next subsubsection that the nominal trajectories used in this work for the tip position are second order parabolas. It can be easily shown that, for this class of trajectories, $\hat{x}(k)$ may be generated from the samples of the nominal trajectory $\theta_{nr}(k)$ passing this sequence through a block $N(z)$ (see Fig. 22) whose transfer function is:

$$\hat{g}_n(z^{-1}) = \frac{2\cdot(1-z^{-1})^3}{T^2\cdot z^{-1}\cdot(1+z^{-1})}\cdot\mathcal{Z}\left[\frac{\hat{g}_n(s)}{s^3}\right] = N(z) \tag{46}$$

5.2.2. Trajectories

Most of the work done on closed-loop control of flexible arms is based on the use of step functions as command signals because they are easy to generate, and the responses of the arm to such inputs may be easily analyzed. But the command signals typically utilized in existing industrial and research robots are parabolic trajectories of order at least two. This is because the desired trajectories for a robot need to have bounded derivatives until at least the second order, in order to take into account the mechanical limitations of the arm. In fact, the second derivative of the trajectory is its acceleration, whose value

is bounded by the maximum torque permissible in the mechanical structure and, in some cases, by the maximum current allowed in the motor.

These considerations are also important in flexible arms. If the purpose of a flexible arm is to carry a load at a high speed using a lightweight arm, the acceleration must be limited to prevent excesive bending in the structure that could damage it.

Further, it is apparent that relaxing the sharpness of the trajectory allows the arm to follow the trajectory better, avoiding in some cases undesired movements (overshooting) that may be produced using step inputs, and avoiding excessive control signals that can saturate the amplifiers. For example, Cannon et al. [1] reported this beneficial effect in the control of flexible arms when rounding the corners of the steps.

In the opposite sense, sophisticated trajectories have been used to open-loop drive flexible structures. Different optimization criteria have been used that take into account the limitations of the mechanical structure: Farrenkopf [23], Turner and Junkins [24] or Meckl and Seering [16], a.e. The generation of trajectories using these techniques is computationally laborious making them not suitable for on-line control of flexible arms with several vibrating modes, when computer capacity is limited.

In this subsection we propose a family of trajectories that compromise the above considerations. They must be simple enough to be generated in real time (and to allow a real time generation of the feedforward control signal), but they must take into account the physical limitations of the mechanical structure. The simplest trajectories that fulfill this are the parabolic trajectories. For this reason they are usually utilized in rigid arms. We are going to show here that they can also be utilized for minimum phase flexible arms, but not for non-minimum phase flexible arms because the feedforward signal cannot be generated in this case. We propose here a family of trajectories for this last case. We call them quasi-parabolic trajectories.

These trajectories are represented in Figure 25. They are characterized by the fact of being very similar to the parabolic trajectories, but having bounded derivatives up to forth order. The acceleration profile of the quasi-parabolic trajectory is the same as the parabolic trajectory with a slight rounding in the corners. So, the quasi-parabolic trajectory behaves most of the time as a parabolic trajectory. Only in very small intervals of time, that correspond to the changes in the acceleration, both trajectories behave differently.

5.2.2.1. Choosing the trajectory

Here we give a criterion for choosing between the two trajectories described in Figure 25. We will also justify the necessity of the quasi-parabolic trajectories.

In order to calculate the feedforward term, we assume in expression (44) that the nominal trajectory is a parabola whose Laplace transform is $u(s) = 2/s^3$. Taking this into account and operating (44) we get the general expression used in this paper to calculate the feedforward term:

$$\hat{g}_n(s) = \frac{s^3}{g_n^+(s)} \cdot \left[\frac{g_n(-s)}{g_n^-(s) \cdot s^3} \right]_+ , \tag{47}$$

and assuming that $g_n(s)$ is of the form:

$$g_n(s) = \bar{K} \cdot \frac{\prod_{i=1}^{n_1}(s - \bar{a}_i) \cdot \prod_{j=1}^{n_2}(s - \bar{b}_j)}{d(s)}$$

where $\bar{a}_i < 0, 1 \leq i \leq n_1; \bar{b}_j > 0, 1 \leq j \leq n_2$, and all the roots of $d(s)$ are in the left half-plane, operating we obtain that:

$$\hat{g}_n(s) = \frac{d(s) \cdot (\alpha_2 \cdot s^2 + \alpha_1 \cdot s + \alpha_0)}{\bar{K} \cdot \prod_{i=1}^{n_1}(s - \bar{a}_i) \cdot \prod_{j=1}^{n_2}(s + \bar{b}_j)} \tag{48}$$

where the α coefficients are obtained from the partial fraction expansion of $\frac{\prod_{j=1}^{n_2}(s + \bar{b}_j)}{s^3 \cdot \prod_{j=1}^{n_2}(s - \bar{b}_j)}$, $\alpha_0, \alpha_1, \alpha_2$ being the coefficients corresponding to the terms whose denominators are s, s^2, s^3 respectively The filter of expression (45) is then

$$g_n(s) \cdot \hat{g}_n(s) = (\alpha_2 \quad s^2 + \alpha_1 \cdot s + \alpha_0) \cdot \frac{\prod_{j=1}^{n_2}(s - b_j)}{\prod_{j=1}^{n_2}(s + b_j)}, \tag{49}$$

and the following lemma is deduced, that justifies the necessity of the quasi-parabolic trajectories.

Lemma 1:

Assume we want to control a flexible arm using parabolic or nearly parabolic commands, and we want to use a feedforward term to drive the arm. Then, with the exception of rare degenerate cases, the order of the numerator of the feedforward term $\hat{g}_n(s)$, calculated from (47), may exceed the order of the denominator by a value of 2 if $g_n(s)$ is minimum phase, or by a maximum value of 4 if $g_n(s)$ is non-minimum phase.

This lemma is easily proven using equation (48). If the system is minimum phase, then $\alpha_2 = \alpha_1 = 0$. If it is non-minimum phase, in general these coefficients will be nonzero. We denote the order of this polynomial as n_α. Moreover, the difference between the order of the denominator of $g_n(s)$ and the order of its numerator is 2 because of the form of the dynamic model of the beam (see equation (13) of Part I Report), with the exception of the rare cases in which the n element of vector $\mathcal{B}$ is 0. Then we find that the difference between the order of the numerator and denominator of $\hat{g}_n(s)$ is $n_\alpha + 2$ which is always less than or equal to 4.

If the system is minimum phase then this number is 2. If it is non-minimum phase, may be up to 4, and the lemma is proven.

Notice that the feedforward term may then be expressed as

$$\hat{g}_n(s) = \hat{g}_{n4} \cdot s^4 + \hat{g}_{n3} \cdot s^3 + \hat{g}_{n2} \cdot s^2 + \hat{g}_{n1} \cdot s + \hat{g}_{n0} + \hat{g}_{np}(s), \tag{50}$$

where $\hat{g}_{n0}, \ldots, \hat{g}_{n4}$ are constants that may take the 0 value, and $\hat{g}_{np}(s)$ is a proper rational function in s. Notice also that, as result of this, the difference between the orders of the numerator and denominator of $\hat{g}_n(s)$ gives the order of the maximum derivative of the nominal trajectory needed to generate the feedforward signal, and that consequently has to be bounded. From this and the previous lemma it follows that parabolas (bounded up to the second derivative) can be used for minimum phase systems, but normally cannot be used for non-minimum phase systems. Quasi-parabolic trajectories with derivatives bounded up to the fourth order may be used in these cases.

Finally, when we use quasi-parabolic trajectories, the feedforward term of expression (47) is just an approximation (it was obtained for a parabolic reference). But because of the closeness between these two kinds of trajectories, this approximation is normally sufficient.

5.2.2.2. Designing the parameters of the trajectory

The parameters of the trajectory: maximum acceleration and second derivative of the acceleration, may be designed approximately from expression (50), taking into account the physical limitations of the mechanical structure. In general, these limitations may be expressed in terms of the coupling torque between the beam and the motor, which may be expressed as a function of the beam deflection:

$$C_t(s) = C(s) \cdot deflection(s), \tag{51}$$

where $C(s)$ is scalar for massless beam case.

This deflection may then be expressed as

$$deflection(s) = [\hat{g}_{n4} \cdot s^4 + \hat{g}_{n3} \cdot s^3 + \hat{g}_{n2} \cdot s^2 + \hat{g}_{n1} \cdot s + (\hat{g}_{n0} - 1) + \hat{g}_{np}(s)] \cdot \theta_{nr}(s) \tag{52}$$

and, in many cases, the deflection may be kept between the safe boundaries just by choosing an appropiate value for the maximum derivative of θ_{nr}, needed to compute the above expression. This will be illustrated with examples.

For massless beam, stresses at all points will be proportional to deflection. So torque limit is proportional to deflection.

Another physical limitation is the maximum current allowable in the motor. Conditions for the derivatives of the trajectory may be obtained from (50) in conjunction with the model of the motor. But they are normally quite more complex than the conditions derived from (52) for the deflection. Moreover, in our two flexible arms, the above developed mechanical condition is more restrictive than the one obtained from the motor current limit, making unnecessary the consideration of this last constraint.

5.2.3. Considering inner loop dynamics

We mentioned before that, if the inner loop is fast enough compared with the outer loop, then $M(z) = 1$. In this case, problems 2) and 3) described in the beginning of Subsection 5.2. do not exist, the procedure

described in Subsubsection 5.2.1. applies, and the feedforward term is significantly simplified. It will be seen in the experiments of the next section that this assumption is very often true when controlling lightweight arms, although there are cases in which the dynamics of the inner loop must be taken into account. In these cases, the problems caused by the non-minimum phase zeros of $M(z)$ may be overcome by using the discrete version of the method described in the previous section. But the oscillations caused by the inversion of the zeros that have a negative real component cannot be removed. In order to avoid both kinds of problems as well as the above stated noncausality problem, an optimization method with constraints is proposed.

Assume the system has n_ϱ zeros in the situations described in the case 2). Let us call them ϱ_i. Assume also there are D delays in $M(z)$ (D poles in the origin). Then a feedforward term of the following form may be used:

$$N(z) = \hat{g}_n(z^{-1}) \cdot M^{-1}(z) \cdot \left[\prod_{i=1}^{n_\varrho} \frac{1 - \varrho_i \cdot z^{-1}}{1 - \varrho_i} \right] \cdot z^{-D} \cdot f(z) = g_n^{-1}(z^{-1}) \cdot M^{-1}(z) \cdot U(z), \tag{53}$$

where $\hat{g}_n(z^{-1}) = \hat{g}_{nn}(z^{-1})/\hat{g}_{nd}(z^{-1})$ is the term calculated in Subsubsection 5.2.1. from $g_n(s)$, $g_n(z^{-1}) = g_{nn}(z^{-1})/g_{nd}(z^{-1})$, and $f(z) = f_n(z)/f_d(z)$ is a correction term whose calculation is the objective of this subsubsection.

It has been mentioned that trajectories based on second order parabolas are used here. It seems desiderable to make the arm follow these parabolas without steady state error. In order to guarantee this, it can be easily seen from equation (41) that the following condition must be fulfilled:

$$1 - U(z) = (1 - z^{-1})^2 \cdot W(z), \tag{54}$$

W being a rational function in z. Combining this with equation (53) we get:

$$\prod_{i=1}^{n_\varrho}(1-\varrho_i)\cdot \hat{g}_{nd}(z^{-1})\cdot g_{nd}(z^{-1})\cdot f_d(z) - \prod_{i=1}^{n_\varrho}(1-\varrho_i\cdot z^{-1})\cdot z^{-D}\cdot \hat{g}_{nn}(z^{-1})\cdot g_{nn}(z^{-1})\cdot f_n(z) = (1-z^{-1})\cdot W_n(z), \tag{55}$$

where $W_n(z)$ is a polynomial. Transfer function $f(z)$ may be calculated in such a way that the tracking error is minimized. Again we propose to minimize the integral squared error of (41):

$$Cost = \sum_{k=0}^{\infty} e^2(k).$$

But now, apart from the stability condition as given in Subsubsection 5.2.1., the following constraints should be also fulfilled by the feedforward term:

- Zero steady state tracking error of a parabola (equation (55)).
- No stable poles in the left half plane.
- It must be a causal term (no zeros in the origin). This condition is optional, depending on if a real time feedforward term is wanted or not.

A numerical method is proposed to calculate the optimum $f(z)$ that accomplishes all these conditions. Previous to its calculation, the form of $f(z)$ should be defined (orders of numerator and denominator). This is given by the following lemma.

Lemma 2:

Assume that the difference between the orders of the numerator and denominator of $\hat{g}_n(z^{-1}) \cdot g_n(z^{-1})$ is ν, n_ϱ is the number of zeros causing problem 2), and D is the number of delays of $M(z)$. Then the minimum order of the denominator of $f(z)$ that accomplishes the above optimization constraints is given (exceptuating degeneracies) by:

$$order\ f_d(z) = n_\varrho + D + \nu + 1 \tag{56}$$

and the order of the numerator is

$$order\ f_n(z) = 1. \tag{57}$$

This lemma may be easily proved taking into account that the accomplishment of the constraints implies that a number of order $f_d(z)$ parameters must be tuned to make $f(z)$ stable, plus two parameters more in order to make $1 - U(z)$ have two zeros at 1 (null tracking error condition).

Knowing the order of the $f(z)$ transfer function, its coefficients can be chosen in such a way to optimize the above defined cost. Some of the existing numerical search methods may be used to get the optimum parameters of $f(z)$.

5.3. Closed-loop control

5.3.1. Classical control using tip position feedback

The use of a controller with an integral term is proposed, in order to remove permanent errors (Fig. 26). We mentioned before that the use of a feedforward term allows us to simplify this controller. Often, simple PID controllers may be used to get good positioning performances. Moreover, the examples will show that if a perfect compensation of Coulomb friction is provided, the feedback controller may even be simpler because the integral action is not needed. All this allows us to use high sampling rates improving the general behavior of the digital control system.

These controllers may be easily designed using, for example, classical frequency domain techniques. The function of this controller is to compensate for the deviation of the tip position from the desired trajectory. To move the arm to the desired angle, most of the control action required is provided by the feedforward term. When the arm is not moving and a deviation from the reference position is produced by an external disturbance, the control action to recover the desired position is provided by the controller $R(z)$. The fact that this controller compensates for only small deviations allows us to use high gains (when the system is minimum phase) without saturating the amplifier of the motor. This produces a significant improvement in the dynamic performances of the controlled system.

5.3.2. Control that cancels the first natural frequency by using tip position feedback

This scheme is composed of two loops: a loop that cancels the first natural frequency, and a classical P.D. controller with a feedforward term as shown in Figure 27. The control components are designed in three steps:

1. A positive unity feedback loop is closed to remove the first vibrational mode. This loop *always* removes the first vibrational mode because $g_n(0) = 1$ in all flexible arms.
2. A compensator is designed that cancels the poles of the remaining system, and its minimum phase zeros.
3. A P.D. controller is designed (in the case of a single non-minimum phase zero) with a feedforward term. In the case of more than one non-minimum phase zeros, a controller designed using the standard pole assignment technique may be used, instead of the P.D. controller.

The feedforward term is designed here using the procedure described in Subsection 5.2., but taking into account that now the $g_n(s)$ transfer function that has to be used is the resulting from steps 1 and 2 of the above described method.

5.3.3. Control using feedback of position at several points of the beam

The general scheme of this controller is also composed of two terms: the feedforward term discussed in Subsection 5.2., and a feedback controller that uses the measurements of positions at intermediate points of the beam.

Feedback controllers may be designed using any of the standard control design methods. Good results are achieved using optimization techniques ([25], e.g.) to design a controller: $\gamma(s) = -A \cdot x(t)$ that drives x from an initial state to the zero state minimizing a cost function of the form:

$$\mathcal{J} = \int_{t=0}^{\infty} (x^T(t) \cdot R_1 \cdot x(t) + R_2 \cdot \theta_{mr}^2(t)) \cdot dt \tag{58}$$

where $R_1 \in \Re^{2 \cdot n \times 2 \cdot n}, R_2 \in \Re$ are weighting matrices, and $x \in \Re^{2 \cdot n}$ is the state vector of the system. From equation (13) of Part I, and making $T_n = F_n = 0$, we get the state equation of the system:

$$\dot{x}(t) = \underbrace{\begin{pmatrix} 0 & I_n \\ E \cdot I \cdot \mathcal{M}^{-1} \cdot A & 0 \end{pmatrix}}_{A} \cdot x(t) + \underbrace{\begin{pmatrix} 0 \\ E \cdot I \cdot \mathcal{M}^{-1} \cdot B \end{pmatrix}}_{B} \cdot \theta_m(t) \tag{59}$$

where $x^T(t) = \begin{pmatrix} \Theta^T & \dot{\Theta}^T \end{pmatrix}$, and $I_n \in \Re^{n \times n}$ is the identity matrix. This model is simpler than models used in other approaches (that relate $\theta_n(t)$ and $\theta_m(t)$ with $i(t)$), producing simpler controllers.

If there were dynamic friction in the tip, then F_n would be proportional to the speed of the tip mass and a coefficient would appear in the position $(2 \cdot n, 2 \cdot n)$ of matrix A of the before equation.

This feedback scheme uses the errors between the desired and the actual states to generate the control signal. Defining $\Lambda = \begin{pmatrix} \Lambda_1 & \Lambda_2 \end{pmatrix}$; $\Lambda_1, \Lambda_2 \in \Re^{1\times n}$ we can express the control signal (γ) as a function of the measured variables: $\gamma(s) = (\Lambda_1 + \Lambda_2 \cdot s) \cdot (\Theta_r(s) - \Theta(s))$.

The reference vector for the measured variables (Θ_r) may be obtained from the reference θ_{nr} by using the following expression:

$$\Theta_r(s) = \Upsilon(s) \cdot \theta_{nr}, \tag{60}$$

$$\Upsilon(s) = \begin{pmatrix} C_1 \cdot Adj(\mathcal{M} \cdot s^2 - E \cdot I \cdot \mathcal{A}) \cdot E \cdot I \cdot \mathcal{B} \\ C_2.Adj(\mathcal{M} \cdot s^2 - E \cdot I \cdot \mathcal{A}) \cdot E \cdot I \cdot \mathcal{B} \\ \vdots \\ C_n.Adj(\mathcal{M} \cdot s^2 - E \cdot I \cdot \mathcal{A}) \cdot E \cdot I \cdot \mathcal{B} \end{pmatrix} \cdot \frac{1}{C_n.Adj(\mathcal{M} \cdot s^2 - E \cdot I \cdot \mathcal{A}) \cdot E \cdot I \cdot \mathcal{B}} \tag{61}$$

where $C_i = \begin{pmatrix} 0 & \dots & 0 & 1 & 0 & \dots & 0 \end{pmatrix}$ the 1 being in the $i-th$ column. These last equations are obtained from equation (16) of Part I. Logically $\Upsilon_n = 1$ results.

In the case of a non-minimum phase system, the denominator of Υ has some positive real component roots. But they are cancelled with the zeros of filter (49), leaving $\Theta_r(t)$ bounded. Cancellation may be exactly done because all these terms are computed.

This feedback control scheme presents important advantages over other existing schemes when implementing it with a digital computer. Other control methods need to reconstruct the whole state x from measurements of the motor and tip of the arm by means of filters or observers. They involve a large amount of computation. In many cases, these reconstructions are distorted by the noise of the measured signals making the control difficult. But in our case, because a) we have simplified the arm dynamics by closing the motor position loop, and b) we are using more sensing in the beam, all the states may be easily obtained: positions are measured and velocities may be approximated by the simple difference equation $\dot{\Theta}(k \cdot T) = (\Theta(k \cdot T) - \Theta((k-1) \cdot T))/T$ where T is the sampling period and k is an integer. Because only the first derivative of measured signals is needed, this approximation of the velocities of the mass points is reasonable in many cases, even having relatively high levels of measurement noise.

Figure 28 shows the details of this control scheme. Notice that first derivatives of the position error signals are used instead of first derivatives of the position states.

5.3.3.1. Influence of the payload

We study in this subsection how changes in the payload affect the dynamics of the controlled system.

Inner loop

The motor position control loop is not directly affected by changes in the payload. Payload influences the dynamics of this loop only through the coupling torque between the motor and the beam. This coupling is being compensated by using expression (15) to estimate the coupling torque from position measurements. Coefficients h_i are independent of the payload and consequently no term of the inner loop needs to be tuned as a function of the payload.

Payload affects this loop indirectly if we consider the saturation limits of the motor current. If the payload is too high, the current saturates and control performance deteriorates. But for the normal range of payloads, performance of this inner loop may be considered invariant.

Feedforward term

Because of the *Zero Invariancy Property* described in Part I, the filter expressed in (49) is independent on the load, and variations in the feedforward term (48) are due only to the factor $d(s)/\bar{K}$. So $\hat{g}_n(s)$ can be easily tuned to payload changes by changing only one parameter in its numerator as it will be illustrated in the example.

Feedback term

The gain factor and poles of the closed-loop transfer functions matrix $\mathcal{G}$ $(\Theta(s) = \mathcal{G}(s) \cdot \Theta_r(s))$ change with the payload. But zeros of the transfer functions $g_{n,i}$; $1 \leq i \leq n$ of the last row of this matrix remain constant. Notice that these transfer functions characterize the closed-loop dynamic behavior of the tip of the arm.

Proof of zeros invariancy: the closed-loop state equation (without the feedforward term) is:

$$\dot{x}(t) = \begin{pmatrix} 0 & I_n \\ E.I.\mathcal{M}^{-1}.(\mathcal{A} - \mathcal{B}.\Lambda_1) & -E.I.\mathcal{M}^{-1}.\mathcal{B}.\Lambda_2 \end{pmatrix} \cdot x(t) + \begin{pmatrix} 0 & 0 \\ E.I.\mathcal{M}^{-1}.\mathcal{B}.\Lambda_1 & E.I.\mathcal{M}^{-1}.\mathcal{B}.\Lambda_2 \end{pmatrix} \cdot x_r(t)$$

$$\Theta(t) = \begin{pmatrix} I_n & 0 \end{pmatrix} \cdot x(t),$$

where x_r is the state reference; and operating:

$$\Theta(s) = (s^2 \cdot \mathcal{M} + s \cdot E \cdot I \cdot \mathcal{B} \cdot \Lambda_2 + E \cdot I \cdot (-\mathcal{A} + \mathcal{B} \cdot \Lambda_1))^{-1} \cdot E \cdot I \cdot \mathcal{B} \cdot (\Lambda_1 + s \cdot \Lambda_2) \cdot \Theta_r(s).$$

In this expression, $\mathcal{G}(s)$ shows the same dependence of $\mathcal{M}$ as expression (16) of Part I. Then, the same reasoning that supports the *Zeros Invariancy Property* is applied here to demonstrate this.

Finally, only numerators of Υ are affected by changes in the payload. Their dependence on m_n is similar to the dependence of $\hat{g}_n(s)$.

6. Tip Control Experimental Results

Control methods described in this report are applied here to our two flexible arms, whose dynamics were modelled in Part I. Experimental results are shown.

6.1. Single-mass flexible arm

6.1.1. Discretization

This system has only one vibrational mode and it is minimum phase. The transfer function of the beam was found to be (see Part I):

$$g_1(s) = \frac{43.75}{s^2 + 0.06 \cdot s + 43.75}. \tag{62}$$

Applying the discretization method suggested in Subsubsection 5.1.2.1. we get:

$$g_1(z) = 0.6583 \cdot 10^{-4} \cdot \frac{1 + 3.984848485 \cdot z^{-1} + z^{-2}}{1 - 1.999423 \cdot z^{-1} + 0.999817 \cdot z^{-2}}. \tag{63}$$

And the sampled data equivalent transfer function of the inner loop is

$$M(z) = \frac{0.0309247 \cdot z^{-2} \cdot (1 + 0.857737056 \cdot z^{-1} - 0.139691015 \cdot z^{-2})}{1 - 1.993393 \cdot z^{-1} + 1.199567748 \cdot z^{-2} + 0.00159364 \cdot z^{-3} - 0.179119249 \cdot z^{-4} + 0.0244809 \cdot z^{-5}}. \tag{64}$$

We can notice that $M(z)$ has a delay $D = 2$, and a zero in -0.99774394.

6.1.2. Open-loop control

6.1.2.1. Simplified feedforward term

The settling time to a step input of the inner loop was found to be 30 *msec*. So it is much faster than the dynamics of the beam and it may be assumed that $M(z) = 1$.

Because $g_1(s)$ is minimum phase, we get from (48) that $\hat{g}_1(s) = g_1^{-1}(s)$. And because of the assumption $M(z) = 1$, we have that the feedforward signal $\hat{x}(k)$ is given directly by sampling the output of $\hat{g}_1(s)$.

Because the system is minimum phase we use the parabolic trajectory to command the arm. The only parameter to calculate there is the maximum acceleration and this can be easily obtained from equation (50), taking into account that in this case $C(s)$ of expression (51) is a constant. It means that the torque is directly proportional to the deflection. The maximum allowed deflection for this beam is 400 *mrad.* (23 *degrees*). Using equation (50) we get the simple expression:

$$deflection = acceleration/43.75, \tag{65}$$

and, therefore, the maximum acceleration is 8750 $mrad/sec^2$. We have assumed a deflection of 200 *mrad.*

(50 % of the maximum deflection) to calculate this acceleration, in order to allow some extra deflection for the action of the controller $R(z)$. Figure 29 shows the resulting feedforward signal.

6.1.2.2. Complete feedforward term

Because there is a zero of $M(z)$ in the left half-plane ($n_q = 1$), and a delay of two sampling periods ($D = 2$), the inverse of $M(z)$ cannot be directly used for a real time feedforward compensation of its dynamics. In the experiments carried out here, the feedforward term is precomputed so, the delays are not a problem. In order to cancel the effects of the left half-plane zero in -0.997744 then, according to Subsubsection 5.2.3., $M^{-1}(z)$ is multiplied by the factor $(1 + 0.997744 \cdot z^{-1})/1.997744$. And a corrective $f(z)$ term is calculated taking into account the conditions stated in those subsubsection:

$$f(z) = \frac{1.20912 - 0.870105 \cdot z^{-1}}{1 - 0.661 \cdot z^{-1}}.$$

Notice that, according to Lemma 2, the order of the denominator should have been 2. This is a degenerate case where the coefficient corresponding to z^{-2} is 0. Figure 30 shows the implementation scheme of this feedforward term, and Figure 31 shows the feedforward signal generated.

From comparing Figures 29 and 31 we see that both feedforward signals are quite similar. The only significant difference is given by some impulses produced at the instants when the value of the acceleration changes. These impulses tend to speed up the motor in these changes, in order to compensate the dynamics of $M(z)$. Experiments showed that including the dynamics of $M(z)$ in the feedforward term did not produce any significant improvement in the control of this arm. So in what follows, we will use the simplified feedforward signal shown in Figure 29.

6.1.3. Closed-loop control using the first scheme

The first scheme coincides with the third one in the case of a single-mass flexible arm.

$R(z)$ was chosen to be a simple digital P.I.D. controller and was obtained by minimizing the time needed by the arm to recover its desired position when changes in the position were produced because of external perturbations. The perturbation model represented by equation (37) was used. We assumed that we had a combination of two perturbations : a permanent error position perturbation in the angle of the motor, and a perturbation on the tip because of erroneous initial conditions. The resulting optimum controller was

$$R(z) = \frac{100 \cdot (1 - 0.98 \cdot z^{-1}) \cdot (1 - 0.99 \cdot z^{-1})}{(1 - z^{-1}) \cdot (1 - 0.61 \cdot z^{-1})}.$$

Figure 32 shows the tip response of the parabolic profile. It shows that the arm slightly leads the reference because of the feedforward term. The settling time is of 0.22 *sec*. A comparison between the angle of the tip and the angle of the motor is given in Figure 33, showing that the dynamics of the inner loop is very much faster than the outer loop, and the movements required are larger.

6.1.4. Closed-loop control using the second scheme

For the case of a flexible beam with only one vibrational mode, a very simple decoupling loop can be implemented that reduces the dynamics of the system to a double integrator. This is done by simply closing a positive unity gain feedback loop around the tip position, and premultiplying by $1/\omega_n^2$ (1/43.75), as shown in Figure 34.

The transfer function of the beam is given by expression (62). It is transformed into

$$g_1'(s) = \frac{1}{s^2 + 0.06 \cdot s},$$

which is approximately a double integrator (the first order term of the denominator can be neglected).

A simple analog P.D. controller was designed and was then discretized using the Tustin transform [21]. The discrete transfer function of the digital controller is given by

$$R(z) = 3281.25 \cdot \frac{1 - 0.987 \cdot z^{-1}}{1 - 0.74 \cdot z^{-1}}.$$

The feedforward term is, in this case, a pure second order derivative term s^2, that generates a signal which is the acceleration of the parabolic profile (a piecewise constant signal).

Figure 35 shows the tip position response to the second order parabolic trajectory. A comparison between the angle of the tip and the angle of the motor is given in Figure 36. Figure 37 shows the motor position and its reference input.

6.2. Two-mass flexible arm

6.2.1. Open-loop control

6.2.1.1. Trajectory design

The beam is non-minimum phase. Then, according with Subsubsection 5.2.2., we choose a quasi-parabolic profile. Acceleration and second derivative of the acceleration are chosen taking into account mechanical constraints (maximum allowable deflection of the beam). They are: acceleration = 7875 $mrad./sec^2$., 2nd derivative of acceleration = 8648646 $mrad./sec^4$..

Filter (49) is in this case:

$$g_n(s) \cdot \hat{g}_n(s) = (1 + 0.05605 \cdot s + 0.00157075 \cdot s^2) \cdot \frac{35.683 - s}{35.683 + s} \qquad (66)$$

Figure 38 shows the ideal quasi-parabolic trajectory $P_p(s)$ that drives the tip from -100 *mrad.* to 100 *mrad.*, and the optimized reference trajectory $\theta_{nr}(s)$ resulting from passing P_p through this filter.

6.2.1.2. Feedforward term

It is given by expression (48) (expressed in function of the payload m_2):

$$\hat{g}_n(s) = (0.12136 \cdot m_2 \cdot s^4 + (176.6032 \cdot m_2 + 2.6791) \cdot s^2 + 852.81575) \cdot \frac{1 + 0.05605 \cdot s + 0.00157075 \cdot s^2}{0.6697676 \cdot (s + 35.68333)^2} \quad (67)$$

m_2 appears only in the first factor. Then this feedforward term may be easily tuned as function of the payload using the scheme shown in Figure 39. Particularizing to our example ($m_2 = 0.12136$ *lb.*):

$$\hat{g}_n(s) = (s^4 + 1637.1 \cdot s^2 + 57903.3175) \cdot \frac{1 + 0.05605 \cdot s + 0.00157075 \cdot s^2}{45.475 \cdot (s + 35.68333)^2} \quad (68)$$

6.2.2. Closed-loop control using the first scheme

In the inner loop, the motor was decoupled approximately from the beam by using expression (32).

The feedforward term expressed in (68) was implemented, and a digital P.D. controller was used whose parameters were experimentally tuned. It was of the form

$$R(z) = 4.891 \cdot \frac{1 - 0.98511 \cdot z^{-1}}{1 - 0.94174 \cdot z^{-1}}$$

Figure 40 shows the tip response to the quasi-parabolic profile. Notice that the first vibrational mode is completely cancelled, and the second one is reduced to a small damped ripple (the amplitude of the largest ripple is less than 3% of the step amplitude). The settling time is 0.3 *sec.* Figure 41 shows the comparison between the angle of the motor and the angle of the tip, and Figure 42 shows the tip position control action provided by the feedforward term compared with the one provided by the controller $R(z)$. Notice that the use of a P.I.D. controller has not been necessary because the effective compensation of the Coulomb friction and static coupling torque carried out in the inner loop removed the permanent errors.

A more complex controller could have been designed here in order to remove the remaining ripple, and include some integral action, as was suggested in Subsubsection 5.3.1. However, this has not been done because the purpose of this example was to show that it is possible to control flexible arms of relatively complex dynamics with a simple feedback controller (in this case with a P.D. controller) if a proper feedforward term is used. This feedforward term was shown to be easy to generate. Therefore, flexible arms of complex dynamics may be controlled using control units of modest computing capabilities.

6.2.3. Closed-loop control using the second scheme

We use here the same method as in 6.2.2. to decouple the motor from the beam.

The transfer function of the two-mass flexible beam is :

$$g_n(s) = \frac{-\bar{K} \cdot (s^2 - \alpha_z^2)}{(s^2 + \omega_1^2) \cdot (s^2 + \omega_2^2)},$$

where ω_1 and ω_2 are the natural frequencies of the two vibration modes; and $\bar{K} = \omega_1^2 \cdot \omega_2^2 / \alpha_z^2$.

The method to design the tip position controller is :

1. Cancellation of the first (lowest frequency) vibration mode by closing the positive feedback:

$$g_n'(s) = \frac{-\bar{K} \cdot (s^2 - \alpha_z^2)}{s^2 \cdot (s^2 + \omega_1^2 + \omega_2^2 + \bar{K})}.$$

2. Cancellation of the remaining minimum phase dynamics. We use a compensator of the form :

$$\frac{s^2 + \omega_1^2 + \omega_2^2 + \bar{K}}{\bar{K} \cdot (s + \alpha_z)},$$

to reduce the dynamics of the beam to

$$g_n''(s) = \frac{\alpha_z - s}{s^2}. \tag{69}$$

3. Feedforward term. We apply expressions (48)-(49), but using $g_n''(s)$ instead of $g_n(s)$. We get that the feedforward term of scheme of Figure 34 is of the form:

$$\frac{s^2}{s + \alpha_z} \cdot (1 + \frac{2}{\alpha_z} \cdot s + \frac{2}{\alpha_z^2} \cdot s^2)$$

It is easy to prove that the filter of expression (49) is the same in all three methods.

4. Feedback controller: a P.D. controller is used to place the poles of system (69) in the desired locations. Again, the controller is designed in the s-plane and then discretized. The discrete transfer function of this system is shown in Figure 43.

Figure 44 shows the reference and the experimental tip position and Figure 45 shows a comparison between the tip response and the response of the middle mass (θ_1). A comparison between the tip position response and the angle of the motor is given in Figure 46 whereas Figure 47 gives a comparison between the commanded and the actual motor position. Figure 48 shows the output of the feedforward term.

6.2.4. Closed-loop control using the third scheme

We first need to calculate $\Upsilon(s)$, that gives the references for the measured variables. Using (61) we get:

$$\Upsilon(s) = \begin{pmatrix} 545.7 \cdot (s^2 + 106.10833) \\ -45.465 \cdot (s^2 - 1273.3) \end{pmatrix} \cdot \frac{1}{-45.465 \cdot (s^2 - 1273.3)}. \tag{70}$$

The numerator of the first element of vector Υ may be tuned, as a function of the payload, in the same way as the feedforward term.

Figure 49 shows the plots of the references $\theta_{1r}(t), \theta_{2r}(t)$ and $\theta_{mr}(t)$ (feedforward term).

In order to get the feedback controller, we chose a cost function (58) of the form: $R_1 = diag(1,2,0,0)$, $R_2 = 1$, where we weighted the tip position twice the middle mass and motor positions. The optimum controller that minimizes this cost is:

$$\Lambda = \begin{pmatrix} 0.4428 & 0.5572 & 0.0534 & 0.1828 \end{pmatrix}. \tag{71}$$

This places the closed-loop poles at $-3.79 \pm j \cdot 7.375, -6.61 \pm j \cdot 40.506$.

Because of the limited speed of our computer, the feedback loop had to be implemented with a sampling period of 6 *msec.* (twice that of the motor control loop).

Figure 50 shows the tip response, Figure 51 the response of the middle mass, and Figure 52 the motor response compared with the middle mass and tip responses.

The 4-th parabola reaches the target position in 0.36 *sec.* Figure 50 shows that the tip reaches this position with an error less than 2% in 0.4 *sec.* Then fast and accurate motions are achieved for this arm. Tracking errors in Figure 50 are significantly smaller when the trajectory is slower. Notice the high level of noise of the camera measurements θ_1 and θ_2.

7. Comparative Study of the Three Tip Position Control Methods

7.1. Introduction

We showed in this report that tip position control of flexible arms with friction in the joint may be achieved by using a robust scheme composed of two nested loops. We showed too that the design of the inner loop is quite straightforward consisting of a simple *P.D.* controller, but the design of the outer loop may be approached in several ways. Three methods have been proposed here: a feedforward based control scheme, a method that removes the first natural frequency of the beam, and a method that uses position measurements at intermediate points of the beam. All three methods have been experimentally tested exhibiting similar behavior when tracking a specified trajectory. In order to decide which one is the best, we study theoretically in this section the sensitivity of them to several disturbances that are likely to happen.

In the ideal case, when there are no perturbations, these three control schemes produce the same dynamic behavior in the arm. This section compares their performances when perturbations and unmodelled dynamics are present. In particular, three cases are considered: external disturbances at the motor, unmodelled dynamics in the inner loop, and changes in the carried load.

Because we compare here *control schemes* instead of *controllers*, such analysis is quite complicated. A standarization criterion had to be defined among control schemes, in order to compare controllers of the different schemes wih equivalent characteristics. The criterion chosen was to compare controllers that placed the closed-loop dominant poles in the same positions, and secondary poles as close as possible.

The three schemes are normalized in Subsection 7.2. An analytical study of the behavior of these methods in the presence of the three mentioned disturbances is carried out in Subsection 7.3. And the results of this study are applied to our two arms in Subsection 7.4.

7.2. Normalization of the three schemes

The three schemes are represented in Figures 53-55. The first scheme is the feedforward based control scheme, the second is the method that removes the first natural frequency of the beam, and the third one is the method that uses sensing at intermediate points of the beam.

We denote as "beam" in Figure 55 the model of equation (13) of Part I (assuming no forces or torques applied at the tip):

$$\mathcal{M} \cdot \frac{d^2\Theta}{dt^2} = E \cdot I \cdot [\mathcal{A} \cdot \Theta + \mathcal{B} \cdot \theta_m], \tag{72}$$

where $\mathcal{M} = diag(m_1, m_2, \ldots, m_n), \Theta^T = (\theta_1, \theta_2, \ldots, \theta_n), \mathcal{A}$ is an $n \times n$ constant matrix, and $\mathcal{B}$ is a constant $n \times 1$ column vectors. $\mathcal{A}$ and $\mathcal{B}$ depend only on the geometry of the beam. The values of the lumped masses only influence the matrix $\mathcal{M}$.

This model is exact in the case of lumped-mass flexible arms, m_i being the lumped masses; and is a reasonable approximation in the case of flexible arms distributed-mass, represented by m_i, $(i < n)$ coefficients, which are related in some way with the distribution of masses along the beam, and m_n being the tip payload. We easily obtain from equation (72) that

$$\Theta(s) = (\mathcal{M} \cdot s^2 - \mathcal{A})^{-1} \cdot \mathcal{B} \cdot \theta_m(s). \tag{73}$$

These three methods are based on the assumption that the response of the motor θ_m (after having closed the motor position inner loop), to changes in its reference θ_{mr}, is faster than beam dynamics, and, therefore, that the dynamics of the inner loop are represented by the unity transfer function ($M(s) = 1$).

The three methods differ in the importance given to the "a priori" knowledge of the plant (represented by the model) relative to the importance given to the on-line measured signals. The use of the flexible arm model in the control reduces the number of variables to be measured. A way of using this model is by implementing a controller with a feedforward component. This term can be computed off-line, and allows us to simplify the feedback component of the controller, that uses on-line measurements. Some advantages from the stability point of view have been reported [26] for these schemes when applied to rigid arms, that seem to be extendable to flexible arms. But these schemes are more sensitive to changes in the parameters of the plant than other schemes, this being especially critical in flexible arms because of their undamped nature.

The three schemes have a feedforward component, but the first scheme is the one that relies most on

the model of the arm. All the driving action is carried on by the feedforward term in this scheme, being generated from the desired tip position trajectory and the model of the arm. The measurements of the tip position are used only to correct small perturbations when following the desired trajectory.

The second scheme uses measurements of the tip position to compensate for tracking errors (as in the first method), but these measurements are also used to cancel the first natural frequency of the beam, which is the dominant frequency in most of flexible beams. The positive unity gain feedback loop shown in Figure 54 always removes the first vibrating mode, independently of the transfer function of the beam. Higher modes are canceled by implementing the inverse of the minimum phase factors of the transfer function resulting after having closed the above positive feedback loop. The feedforward term used here is much simpler than the one used in the first scheme. Now, part of the driving action is generated from on-line measurements of the tip position, through the positive unity feedback.

The third scheme uses sensing at several points of the structure allowing us to simplify the feedback controller. It includes the feedforward term of the first scheme. But now the feedback loop does not depend so strongly on the model because it uses multiple sensing.

We denote the filter $g_n(s) \cdot \hat{g}_n(s)$ as $\hat{f}(s)$.

In the ideal case, when there are no perturbations, the three schemes give the same response $\theta_n(s) = \hat{f}(s) \cdot P_p(s)$. Consequently, we will denote this signal as θ_{nr} and we will use it as reference for the feedback controller.

Differences among the three control schemes appear when there are perturbations that have to be compensated by a feedback controller $R(s)$. This is developed in the next subsection.

7.3. Comparative study

Three types of disturbances are considered here. Our three control systems are compared studying their responses to them.

The first disturbance represents errors in the position when following a trajectory. This is the disturbance used in most of the perturbation analyses. In our flexible arms, they may be produced by external disturbances, or by any remaining effect of the Coulomb friction, e.g..

The second disturbance is specific to the control method proposed here: it is produced by the unmodelled dynamics of the inner loop. As it was mentioned, a unity transfer function was assumed for the inner loop. This is only approximate. In general, it is given by a transfer function $M(s, \alpha')$, where $\alpha' \in \Re^{n_{\alpha'}}$ represents a vector of parameters $\alpha'_i, 1 \leq i \leq n_{\alpha'}$. We denote as α'^0 the set of parameters α'_i that make $M(s, \alpha') = 1$. The sensitivity of the system to small variations of α' around α'^0 will be studied as an index of which control scheme best supports the assumption $M(s) = 1$.

The third disturbance considered here is produced by changes in the tip payload.

As commented in Subsection 7.1., we have chosen the normalizing criterion that equivalent control schemes are the ones that have their closed-loop poles in the same locations (if possible). Then, in what follows, we assume that the controllers $R(s)$ of each scheme have been designed in such a way that all three schemes have the same dominant closed-loop poles, and the secondary poles are placed as close as possible to each other.

For the sake of simplicity, we assume here that the number of right half-plane zeros is 0 or 1. This assumption covers many practical cases. Expressions similar to the ones shown here may be obtained for higher numbers of positive zeros. In what follows, z_p is the positive zero. If there is not a positive zero, we use the convention of making $z_p = \infty$.

7.3.1. Perturbation in the motor position

We denote this perturbation as $\varepsilon(s)$ and it is added to the reference motor position signal:

$$\theta_m(s) = \theta_{mr}(s) + \varepsilon(s). \tag{74}$$

Figure 56 represents this for the first control scheme.

From schemes of Figures 53-55 we get:

first scheme:

$$\frac{\theta_n(s)}{\varepsilon(s)} = G_1(s) = \frac{g_n(s)}{1 + R_1(s) \cdot g_n(s)}, \tag{75}$$

second scheme:

$$\frac{\theta_n(s)}{\varepsilon(s)} = G_2(s) = \frac{g_n(s)}{(1 - g_n(s)) \cdot (1 + \frac{\hat{I}(s) \cdot R_2(s)}{s^2})}, \tag{76}$$

third scheme:

$$\frac{\theta_n(s)}{\varepsilon(s)} = G_3(s) = \frac{g_n(s)}{1 + g_n(s) \cdot (\Lambda_1 + \Lambda_2 \cdot s) \cdot \Upsilon(s)}. \tag{77}$$

We denote from now on G_1, G_2, G_3 as the transfer functions corresponding to schemes 1, 2 and 3 respectively; and $R_1, R_2, \Lambda_1 + \Lambda_2 \cdot s$ as the feedback controllers in these schemes.

Assuming that the order of the denominator of $g_n(s)$ is n_{gn}, expression (76) shows that $n_{gn} - 2$ poles of the closed-loop system are fixed in Scheme 2, and are given by the zeros of $(1 - g_n(s))/s^2$. This fixed poles are normally far away from the origin, being of secondary importance compared with the dominant poles that can be assigned. If we have 0 or 1 positive zeros, two dominant poles may be arbitrarily placed by a *P.D.* controller: $R_2(s) = r_{2,0} + r_{2,1} \cdot s$.

We define the index $\rho_{i,j}(s) = \frac{G_i(s)}{G_j(s)}; i, j \leq 3$ to compare these schemes. Assuming that the controllers do not increase the order of the system we have:

$$\rho_{2,1}(s) = \frac{1 + R_1(s) \cdot g_n(s)}{s^2 + f(s) \cdot R_2(s)} \cdot \frac{s^2}{1 - g_n(s)} = \frac{\prod_{i=1}^{n_{gn}} (s - \eta_i^1)}{(1 - r_{2,1} \cdot z_p) \cdot \prod_{i=1}^{n_{gn}} (s - \eta_i^2)} \tag{78}$$

$$\rho_{3,1}(s) = \frac{G_3(s)}{G_1(s)} = \frac{1 + R_1(s) \cdot g_n(s)}{1 + g_n(s) \cdot (\Lambda_1 + \Lambda_2 \cdot s) \cdot \Upsilon(s)} = \frac{\prod_{i=1}^{n_{gn}} (s - \eta_i^1)}{\prod_{i=1}^{n_{gn}} (s - \eta_i^3)} \tag{79}$$

where η_i^j is the $i - th$ closed-loop pole of Scheme j.

And $\rho_{3,2}$ may be obtained from

$$\rho_{3,2}(s) = \rho_{3,1}(s) / \rho_{2,1}(s). \tag{80}$$

Expression (78) is used to compare the frequency characteristics of schemes 1 and 2. If $| \rho_{2,1}(j \cdot \omega) | < 1$, then Scheme 2 attenuates more than 1 the component of frequency ω of the spectrum of the perturbation ε. If $| \rho_{2,1}(j \cdot \omega) | > 1$, then Scheme 1 attenuates more this frequency. Expressions (79) and (80) are used in the same sense.

7.3.2. Unmodelled dynamics

We consider the dynamics of the inner loop $M(s)$ in this subsection. In order to compare the effects of $M(s)$ in the overall performance of the three schemes, we assume that small variations in the parameters $\alpha_i', i \leq n_{\alpha'}$ may happen around the parameter values vector α'^0 that gives the ideal $M(s) = 1$. Then we use the sensitivity function [7]:

$$S_{T,\alpha_i'} = | \frac{\partial T(s)}{\partial \alpha_i'} \cdot \frac{\alpha_i'}{T(s)} |_{\alpha' = \alpha'^0}, \tag{81}$$

where $T(s)$ is the transfer function that relates the output $\theta_n(s)$ with the input $P_p(s)$, and α_i' is the parameter of $M(s)$ that varies. The scheme most appropiate for a design assuming $M(s) = 1$ will be the one that exhibits the smallest sensitivity to changes in the parameters α'.

First we analyze the effects of $M(s)$ in open loop control (just using the feedforward terms of schemes 1-3). Then we study the case of the complete schemes, including their feedforward and feedback terms.

7.3.2.1. Open-loop control

Schemes 1 and 3 use the same feedforward term, intermediate sensing is only used in Scheme 3 for the feedback control. Then, we only have to compare here schemes 1 and 2.

We get from Figures 53, 54 that

first scheme:

$$\frac{\theta_n(s)}{P_p(s)} = T_1(s) = \hat{f}(s) \cdot M(s), \tag{82}$$

second scheme:

$$\frac{\theta_n(s)}{P_p(s)} = T_2(s) = \hat{f}(s) \cdot \frac{M(s) \cdot (1 - g_n(s))}{1 - M(s) \cdot g_n(s)}. \tag{83}$$

And the sensitivity functions with respect to a parameter α_i' of $M(s)$ are:

$$S_{T_1,\alpha_i'} = \frac{\partial M(s)}{\partial \alpha_i'} \cdot \alpha_i'^0 \tag{84}$$

$$S_{T_2,\alpha_i'} = \frac{1}{1 - g_n(s)} \cdot \frac{\partial M(s)}{\partial \alpha_i'} \cdot \alpha_i'^0 \tag{85}$$

for the first and second scheme respectively.

The beam does not exhibit any deflection when the arm is stopped. Then, applying the *Final Value Theorem* [7], we have that $g_n(0) = 1$ and $lim_{\omega \to 0} \mid g_n(s)/(1-g_n(s)) \mid = \infty$ in (85). Consequently, comparing expressions (84) and (85), we get that Scheme 1 is much better than Scheme 2 at low frequencies (up to the first natural frequency), while at high frequencies both schemes are similar ($lim_{\omega \to \infty} g_n(s) = 0 \Rightarrow lim_{\omega \to \infty} \frac{1}{1-g_n(s)} = 1$). At medium frequencies, both sensitivity functions are of the same order.

Low frequencies dominate in the spectrum of reference signal P_p. Therefore open loop control of Scheme 1 is more insensitive to the dynamics of the inner loop $M(s)$ than Scheme 2.

7.3.2.2. Closed-loop control

We get from Figures 53-55, using expression (81) and particularizing $\alpha' = \alpha'^0$ (or $M(s) = 1$), that:

Scheme 1:

$$\frac{\theta_n(s)}{P_p(s)} = T_1(s) = \hat{f}(s) \cdot M(s) \cdot \frac{1 + g_n(s) \cdot R_1(s)}{1 + g_n(s) \cdot M(s) \cdot R_1(s)} \Rightarrow$$

$$\Rightarrow S_{T_1,\alpha_i'} = \frac{1}{1 + g_n(s) \cdot R_1(s)} \cdot \frac{\partial M(s)}{\partial \alpha_i'} \cdot \alpha_i'^0. \tag{86}$$

Scheme 2:

$$\frac{\theta_n(s)}{P_p(s)} = T_2(s) = \hat{f}(s) \cdot (1 - g_n(s)) \cdot (1 + \frac{R_2(s) \cdot \hat{f}(s)}{s^2}) \cdot \frac{M(s)}{1 + M(s) \cdot (\hat{f}(s) \cdot R_2(s) \cdot \frac{1-g_n(s)}{s^2} - g_n(s))} \Rightarrow$$

$$\Rightarrow S_{T_2,\alpha_i'} = \frac{1}{(1-g_n(s))\cdot(1+\frac{\hat{f}(s)\cdot R_2(s)}{s^2})}\cdot\frac{\partial M(s)}{\partial \alpha_i'}\cdot\alpha_i'^0. \tag{87}$$

Scheme 3:

$$\frac{\theta_n(s)}{P_p(s)} = T_3(s) = \hat{f}(s)\cdot\frac{M(s)\cdot(1+g_n(s)\cdot(\Lambda_1+\Lambda_2\cdot s)\cdot\Upsilon(s))}{1+g_n(s)\cdot(\Lambda_1+\Lambda_2\cdot s)\cdot\Upsilon(s)} \Rightarrow$$

$$\Rightarrow S_{T_3,\alpha_i'} = \frac{1}{1+g_n(s)\cdot(\Lambda_1+\Lambda_2\cdot s)\cdot\Upsilon(s)}\cdot\frac{\partial M(s)}{\partial \alpha_i'}\cdot\alpha_i'^0. \tag{88}$$

We define indexes $\tau_{i,j}(s) = S_{T_i,\alpha_k'}(s)/S_{T_j,\alpha_k'}(s)$; $i,j \leq 3$. Like in Subsubsection 7.3.1., if $\mid \tau_{i,j}(j\cdot\omega) \mid < 1$, then Scheme i is better (less sensitive) than Scheme j; and Scheme j is better than i if $\mid \tau_{i,j}(j\cdot\omega) \mid > 1$. Operating with expressions (86)-(88) we get that

$$\tau_{i,j}(s) = \rho_{i,j}(s); \qquad \forall i,j. \tag{89}$$

7.3.3. Changes in the payload

We use in this subsubsection the sensitivity function:

$$S_{T,m_n} = \mid \frac{\partial T(s)}{\partial m_n}\cdot\frac{m_n}{T(s)} \mid_{m_n=m_n^0}, \tag{90}$$

where m_n is the tip payload, and m_n^0 is the nominal tip payload for which the controllers have been designed. Model (72)-(73) expresses the dependence on the payload, so we use this to study the sensitivity in the three schemes.

Scheme 1:

$$S_{T_1,m_n} = -s^2\cdot C_n\cdot(\mathcal{M}\cdot s^2 - \mathcal{A} + R_1(s)\cdot\mathcal{B}\cdot C_n)^{-1}\cdot C_n^T\cdot m_n^0 = \frac{1}{g_n(s)\cdot(1+R_1(s)\cdot g_n(s))}\cdot\frac{\partial g_n(s)}{\partial m_n}\cdot m_n^0 \tag{91}$$

Scheme 2:

$$S_{T_2,m_n} = -s^2\cdot C_n\cdot(\mathcal{M}\cdot s^2 - \mathcal{A} - \mathcal{B}\cdot C_n + R_2(s)\cdot\frac{\hat{f}(s)\cdot(1-g_n(s))}{g_n(s)\cdot s^2}\cdot B\cdot C_n)^{-1}\cdot C_n^T\cdot m_n^0 =$$

$$= \frac{1}{g_n(s)\cdot(1-g_n(s))\cdot(1+\frac{\hat{f}(s)\cdot R_2(s)}{s^2})}\cdot\frac{\partial g_n(s)}{\partial m_n}\cdot m_n^0 \tag{92}$$

Scheme 3:

$$S_{T_3,m_n} = -s^2 \cdot C_n \cdot (\mathcal{M} \cdot s^2 - \mathcal{A} + \mathcal{B} \cdot (\Lambda_1 + \Lambda_2 \cdot s))^{-1} \cdot C_n^T \cdot m_n^0 =$$

$$= \frac{1 - g_n^2(s) \cdot (\Lambda_1 + \Lambda_2 \cdot s) \cdot \frac{\partial \Upsilon(s)}{\partial m_n} / \frac{\partial g_n(s)}{\partial m_n}}{g_n(s) \cdot (1 + g_n(s) \cdot (\Lambda_1 + \Lambda_2 \cdot s) \cdot \Upsilon(s))} \cdot \frac{\partial g_n(s)}{\partial m_n} \cdot m_n^0. \tag{93}$$

We define indexes $\lambda_{i,j}(s) = S_{T_i,m_n}(s)/S_{T_j,m_n}(s); i,j \leq 3$ with the same meaning as in Subsubsections 7.3.1-2. We have now:

$$\lambda_{2,1}(s) = \rho_{2,1}(s) \tag{94}$$

$$\lambda_{3,1}(s) = \rho_{3,1}(s) \cdot (1 - g_n^2(s) \cdot (\Lambda_1 + \Lambda_2 \cdot s) \cdot \frac{\frac{\partial \Upsilon(s)}{\partial m_n}}{\frac{\partial g_n(s)}{\partial m_n}}) \tag{95}$$

7.4. Application to our flexible arms

The above considerations are applied here to the cases of flexible arms with one and two vibrational modes. We use as examples the two flexible arms that we have built in our laboratory.

Expressions obtained in Subsection 7.3. are exact for flexible arms that can be modelled as lumped masses. In the case of flexible arms with distributed masses, the analyses of subsubsections 7.3.1. and 7.3.2. are exact if we assume that the infinite dimension dynamic models of these arms have been properly truncated. The expressions of Subsubsection 7.3.3. are just approximate because they use the assumption that matrices $\mathcal{A}, \mathcal{B}$ do not depend on the mass of the tip. This is a good approximation in many cases.

7.4.1. One vibrational mode case

In general, the model of a single vibrational mode flexible beam is given by

$$m_1 \cdot s^2 \cdot \theta_1(s) = -p \cdot \theta_1(s) + p \cdot \theta_m(s), \tag{96}$$

or by

$$g_1(s) = \frac{p/m_1}{s^2 + p/m_1}. \tag{97}$$

the resonant frequency being $\omega_1 = \sqrt{p/m_1}$.

In this case, schemes 1 and 3 coincide. Then we only compare here schemes 1 and 2.

The system described by (97) is minimum phase $\Rightarrow \hat{f}(s) = 1$, and has only two poles $\Rightarrow$ *P.D.* controllers may place the poles of this system wherever we want. Denoting $R_1(s) = r_{1,0} + r_{1,1} \cdot s, R_2(s) = r_{2,0} + r_{2,1} \cdot s$, and taking into account that closed-loop poles of schemes 1 and 2 are placed in the same location we get that $\rho_{2,1} = 1$. This means that both closed-loop schemes exhibit the same behavior in presence of disturbances 1 and 2. We get from (94) that $\lambda_{2,1} = \rho_{2,1}$. Then both schemes exhibit the same sensitivity to changes in the payload.

In the case of having $M(s)$ unmodelled dynamics in the open loop control, we get from (84)-(85) that $\tau_{2,1}(\omega) = 1 - \frac{\omega_1^2}{\omega^2}$ which agrees with subsubsection 7.3.2.1. (see Fig. 57).

The parameters of our single-mass flexible arm are: $m_1 = 0.12136\ lb., p = 5.3095 \Rightarrow \omega_1 = 6.614\ rad./sec.$ We place the closed-loop poles at -5.03 and -32.58. Then the controllers designed to achieve this are: $R_1(s) = 0.86 \cdot s + 2.748, R_2(s) = 37.61 \cdot s + 163.98$.

7.4.2. Two vibrational modes case

The identified parameters of our two-mass flexible beam are (Part I):

$$\mathcal{A} = \begin{pmatrix} 0.12136 & 0 \\ 0 & 0.12136 \end{pmatrix}, \quad \mathcal{A} = \begin{pmatrix} -176.6032 & 110.377 \\ 27.59425 & -22.0754 \end{pmatrix}, \quad \mathcal{B} = \begin{pmatrix} 66.2262 \\ -5.51885 \end{pmatrix}. \tag{98}$$

We get from this:

$$g_n(s) = \frac{\omega_1^2 \cdot \omega_2^2}{\alpha_z^2} \cdot \frac{\alpha_z^2 - s^2}{(s^2 + \omega_1^2) \cdot (s^2 + \omega_2^2)} \tag{99}$$

where $\omega_1 = 6.014\ rad./sec., \omega_2 = 40.0116\ rad./sec., \alpha_z = 35.683$.

Dominant poles of the closed-loop system are placed at $-3.79 \pm j \cdot 7.375$. This is a good compromise between the error in the response and the amplitude of the control signal. The plant has four poles, and the controllers are designed in such a way that they do not increase the complexity of the system, the number of closed-loop poles remaining four.

We use here the following controllers:

- $\Lambda = \begin{pmatrix} 0.4428 + 0.0534 \cdot s & 0.5572 + 0.1828 \cdot s \end{pmatrix}$, that places the closed-loop poles at: $-3.79 \pm j \cdot 7.375$, $-6.61 \pm j \cdot 40.506$.
- We chose a controller R_1 that placed the dominant poles in the same positions as the dominant poles of Scheme 3, and the secondary poles in positions close to the secondary poles of Scheme 3. In fact, we imposed as proximity criterion between secondary poles to have the same real component. The controller designed was $R_1(s) = -0.457438 \cdot (s^2 - 6.58135 \cdot s + 23.45615)/(s + 35.683)$, that placed the closed-loop poles at: $-3.79 \pm j \cdot 7.375$, $-6.61 \pm j \cdot 23.35$. The pole of R_1 was $-\alpha_z$, that cancelled the negative zero of the plant.

- $R_2(s) = 7.5226 \cdot (s + 7.21292)$, that places the closed-loop poles at: $-3.79 \pm j \cdot 7.375$, $\pm j \cdot 41.02$. The secondary poles of this scheme are fixed.

These controllers are compared in the next paragraphs.

7.4.2.1. Position disturbances

We first compare Schemes 1 and 2.

If we denote as η_3^1 and η_4^1 the pair of secondary conjugate poles that appear in the closed-loop transfer function of Scheme 1, we get from (78):

$$\rho_{2,1}(s) = \frac{1}{1 - r_{2,1}/\alpha_z} \cdot \frac{(s - \eta_3^1) \cdot (s - \eta_4^1)}{s^2 + \omega_1^2 + \omega_2^2 + \omega_1^2 \cdot \omega_2^2/\alpha_z^2}. \tag{100}$$

We compare the frequency characteristics of the two schemes making $s = j \cdot \omega$ in the above expression. At high frequencies $\rho = 1/(1 - r_{2,1}/\alpha_z)$. The Routh-Hurwitz stability criterion states that $0 < r_{2,1} < \alpha_z$ is condition for the stability of Scheme 2. Then $\rho_{2,1} > 1$ at high frequencies.

At low frequencies we have that:

$$\rho_{2,1} = \frac{\eta_3^1 \cdot \eta_4^1}{(1 - \frac{r_{2,1}}{\alpha_z}) \cdot (\omega_1^2 + \omega_2^2 + \frac{\omega_1^2 \cdot \omega_2^2}{\alpha_z^2})} \tag{101}$$

The function $\rho_{2,1}(\omega)$ is plotted in Figure 58. It shows that Scheme 2 removes better than 1 low and medium frequency components of the perturbation, and removes worst high frequencies. If high frequency components of normal position disturbances are small, then we conclude that Scheme 2 removes better than 1 position perturbations. While secondary poles of Scheme 2 are fixed, secondary poles of Scheme 1 may be placed with certain limitations. It can be shown that Scheme 2 behaves better than 1 independently of the placement of these poles.

A similar analysis is done to compare Schemes 3 and 1. Figure 58 plots $\rho_{3,1}(\omega)$ too. It shows that Scheme 3 behaves better than 1 at low frequencies, independently of the secondary poles of Scheme 1, and that both schemes behave approximately the same at high frequencies. So we conclude that Scheme 3 is better than 1.

Substracting $\rho_{3,1}$ and $\rho_{2,1}$ in Figure 58, we get $\rho_{3,2}$. Scheme 3 behaves better than 2 at all frequencies. The secondary poles of Scheme 3 can be arbitrarily assigned while the secondary poles of 2 are fixed. It means that, with a proper design, we can make Scheme 3 remove considerably better than Scheme 2 position perturbations.

7.4.2.2. Unmodelled dynamics

Expression (89) means that the results of the previous analysis are valid also for unmodelled dynamics in the motor position control loop.

7.4.2.3. Payload changes

Comparison between schemes 1 and 2 made in 7.4.2.1. remains valid in this case, because of expression (94).

Operating (95) we have that

$$\lambda_{3,1}(s) = \rho_{3,1}(s) \cdot (1 + \hat{b}_1 \cdot \frac{(\Lambda_1 + \Lambda_2 \cdot s) \cdot \begin{pmatrix} 1 \\ 0 \end{pmatrix}}{m_1 \cdot s^2 - \hat{a}_{1,1}}). \tag{102}$$

$\lambda_{3,1}(j \cdot \omega)$ is plotted in Figure 59, and shows that Scheme 3 is better than 1 at low frequencies, which are the most significant.

From (94) we have that $\lambda_{3,2}(s) = \lambda_{3,1}(s)/\rho_{2,1}(s)$. And comparing Figure 58 with Figure 59 we get that Scheme 3 is slightly better than Scheme 2 both at low and high frequencies. Again, a proper choice of the secondary poles in Scheme 3 would make it significantly better than Scheme 2 and, hence, than Scheme 1.

8. Conclusions

This report studied the control of the tip position of flexible arms with friction in the joints. A new general method for their control has been proposed. This is a robust control scheme, proposed in order to reduce the effects of friction and the effects of the inaccuracies in its modelling. The method consists of designing two loops: an inner loop that considers basically the dynamics of the motor (a compensator is designed that decouples the motor from the beam) and a second loop that considers the dynamics of the flexible beam. The first control loop can be designed using any standard method. It must have high gains in order to remove the effects of the friction in the control of the motor position. The second loop requires the use of sophisticated techniques in order to drive the beam without producing oscillations.

In order to design the outer loop, some new ideas have been explored. The use of a simple feedforward term has been proposed in conjunction with the use of feedback controllers. The design method for the feedforward term was generalized in order to include non-minimum phase systems. Also, a method to include the dynamics of the inner loop in the feedforward term (when it is necessary) was proposed. The use of parabolic or quasi-parabolic command profiles is also proposed. These trajectories are adequate enough to be generated in real-time, as well as the corresponding feedforward terms, but are complex to take into account the physical limitations of the beam (the maximum allowable torque). Some criteria to choose these trajectories and their parameters have been proposed. It was found that only two kind of trajectories are needed: parabolas for minimum phase systems and quasi-parabolas of up to fourth finite derivatives for non-minimum phase systems. This result does not depend on the number of zeros that the system has in the right-half plane. The use of these trajectories allows us to also improve the dynamic response of the system because they facilitate the control action, when compared with step references.

Three feedback schemes have been proposed to control the tip position. The first one uses a simple controller to place the poles of the beam where desired, using only tip measurements. The second one uses a positive feedback loop to remove the first vibrational mode, and then cancels all the minimum phase dynamics of the beam. The third one uses position measurements of intermediate points of the beam in addition to the tip position measurement. The feedforward signal is basically the same in all

three schemes, but the feedforward controller is modified in the second scheme, to take into account the positive feedback loop.

All three schemes give the same response in ideal conditions, but they differ in their behavior when disturbances are present. Three types of disturbances were used to compare them: perturbations in the tip position, unmodelled dynamics in the inner loop, and changes in the payload. The second type of perturbation happens because of our particular control structure, which assumes that the response of the motor position loop is instantaneous compared to the response of the outer loop, while in reality there is always a delay (time constant of inner loop dynamics).

An analytical comparative study of the three methods was carried out in Section 7. Expressions obtained there demonstrated that Scheme 3 is the scheme less sensitive to all the disturbances. Then follows Scheme 2, and Scheme 1 is the most sensitive. The results of this section can be summarized as:

- When the system only has one vibrational mode, all three schemes are equivalent.
- Having fixed the closed-loop dominant poles, the sensitivity characteristic of Scheme 3 may be considerably improved by placing the secondary closed-loop poles as far away as possible from the origin.
- Secondary poles of Scheme 2 are fixed, a disadvantage compared with Scheme 3.
- Scheme 2 exhibits the worst characteristic of the three schemes at high frequencies.
- Secondary poles may be moved in Scheme 1, but not arbitrarily placed (as in Scheme 3). Independently of where they are placed, Scheme 1 presents worse performance at low frequencies than Scheme 2.

All these methods have been applied to a class of very slender flexible arms. These arms could be moved very fast, but the effects of friction are important and should be considered. Since, the coupling torque is relatively small, the design of the inner loop is simple (when designing the controllers, the current needed to decouple the motor from the beam was not taken into account in the saturation condition for the current of the motor). This allowed us to obtain a very fast response of the inner loop. These techniques were applied to two of these arms, one that had only one vibrational mode and was minimum phase, and other that had two vibrational modes and was non-minimum phase, with satisfactory results. The designed controllers were simple and provided fast and precise motion of the tip.

Finally, these control schemes are general, and can be applied to heavier flexible arms. However, in this case (depending on the dimension of the motor), the compensation in the inner loop for the coupling between the motor and the beam will be large. This will make the design of controllers for this loop more complex and the assumption of $M(s) = 1$ will not hold, making necessary corrections in the feedforward (Subsubsection 5.2.3.) and feedback terms.

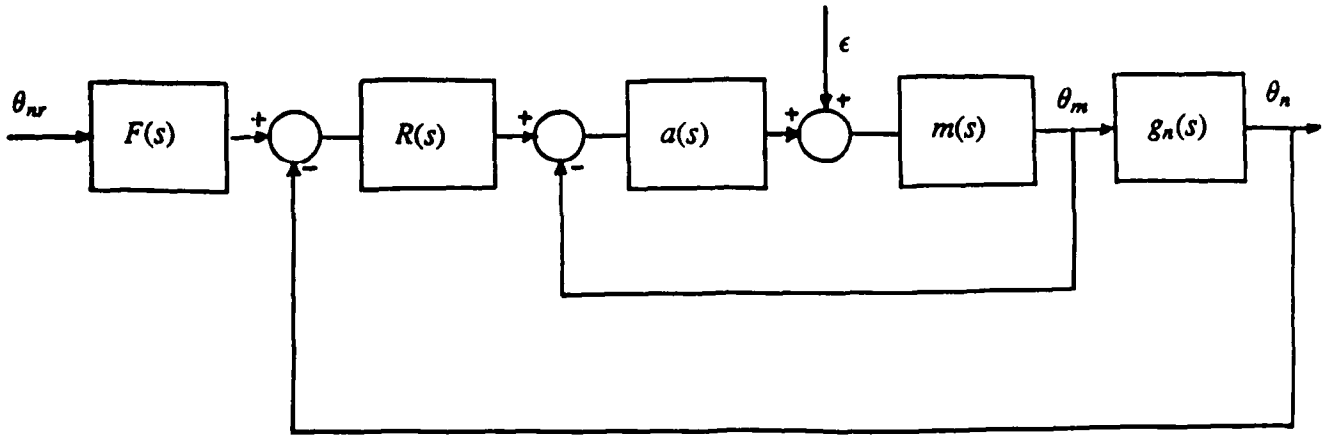

Figure 1: Proposed general control scheme

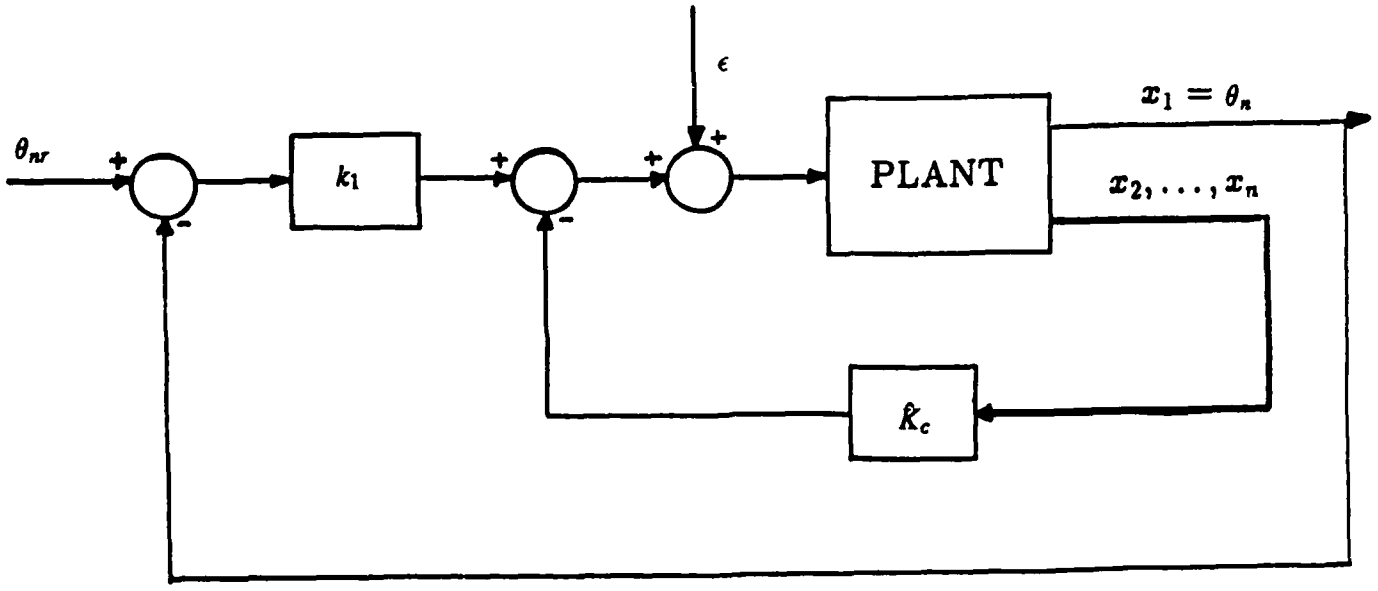

Figure 2: Standard controller for flexible arms (optimum controller)

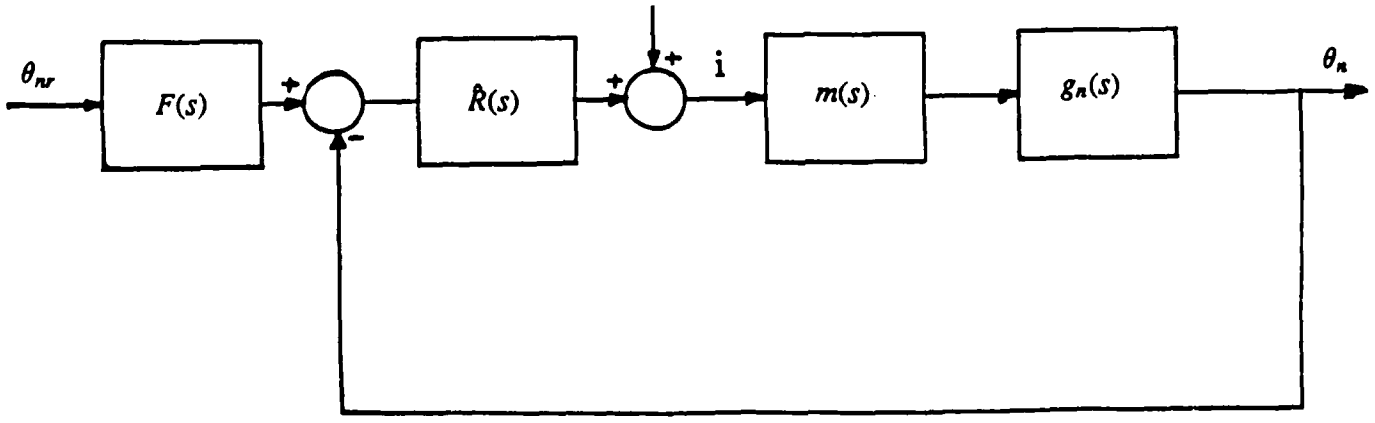

Figure 3: Scheme of Figure 2 expressed in terms of transfer functions

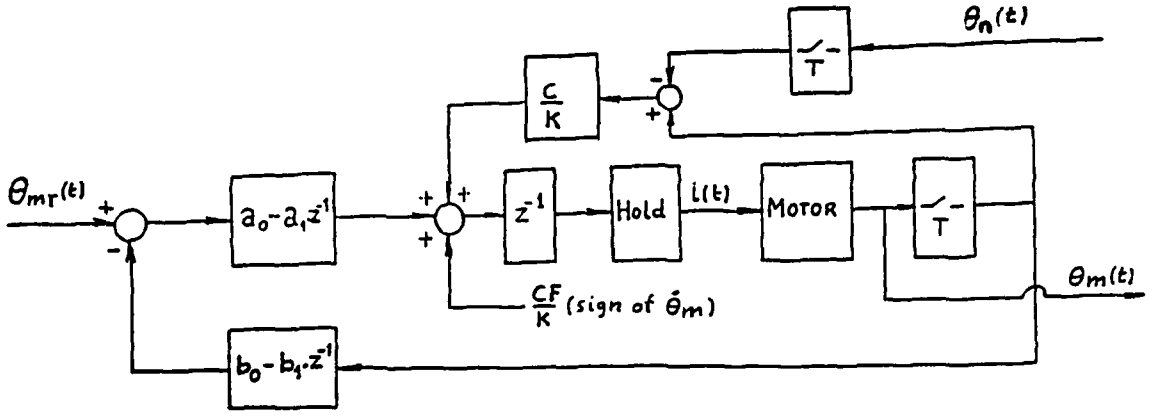

Figure 4: Computer control of the motor position

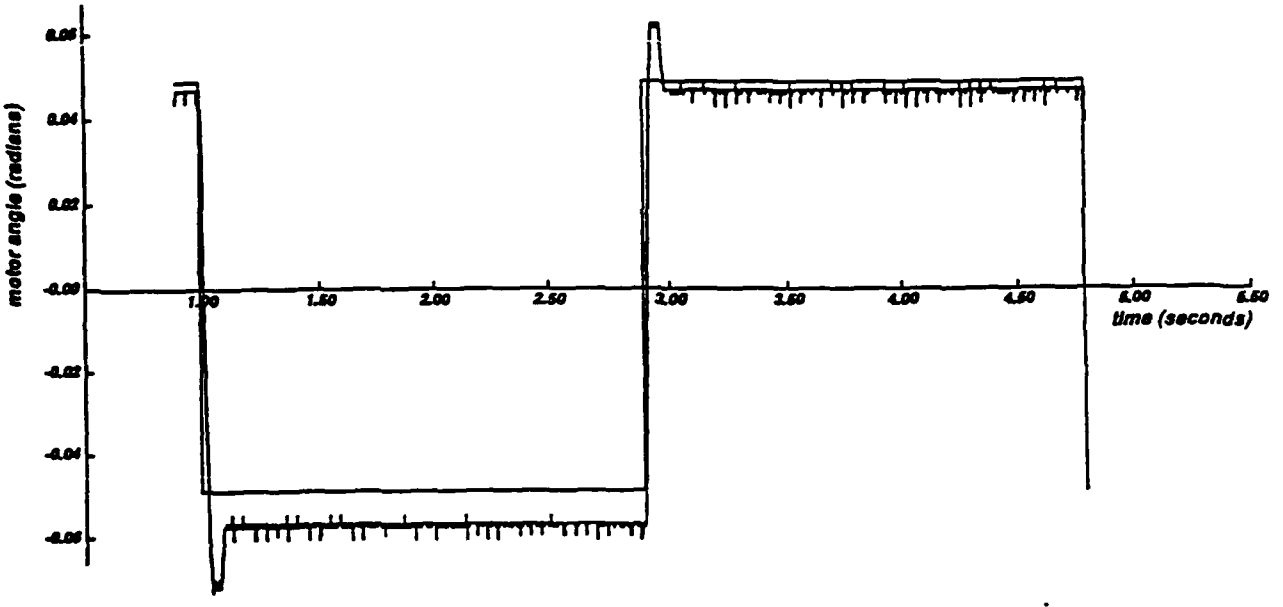

Figure 5: Closed-loop motor position response using coupling torque compensation, and a Coulomb friction compensation of ± 0 *amps*. (single-mass beam)

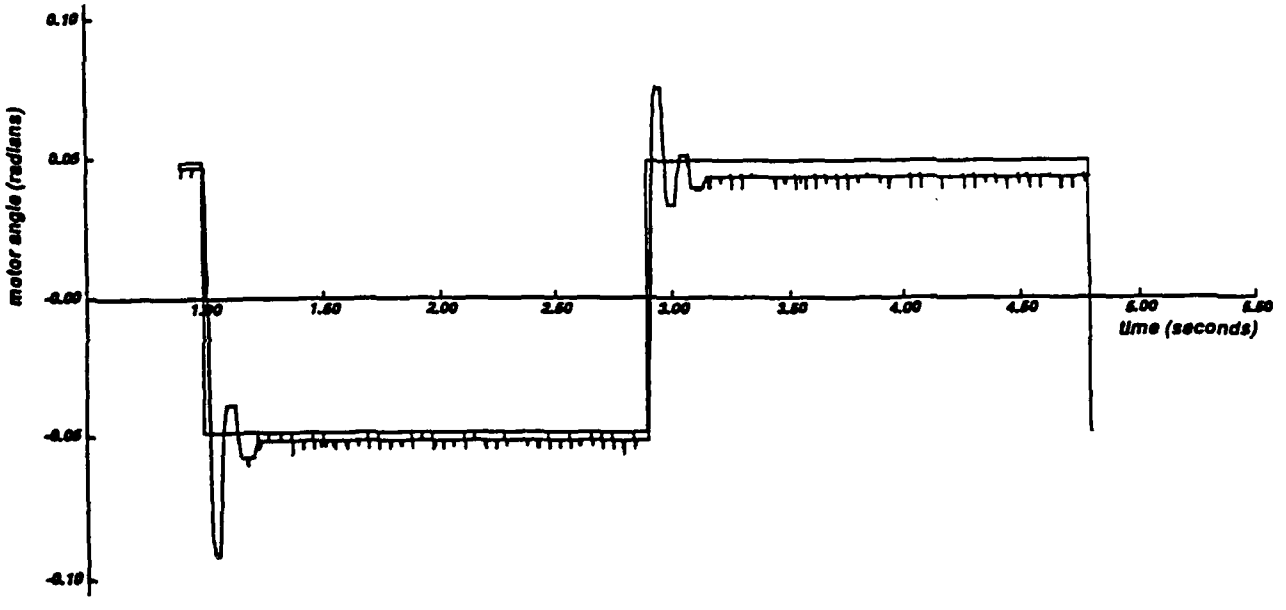

Figure 6: Closed-loop motor position response using coupling torque compensation, and a Coulomb friction compensation of ± 0.09766 *amps*. (single-mass beam)

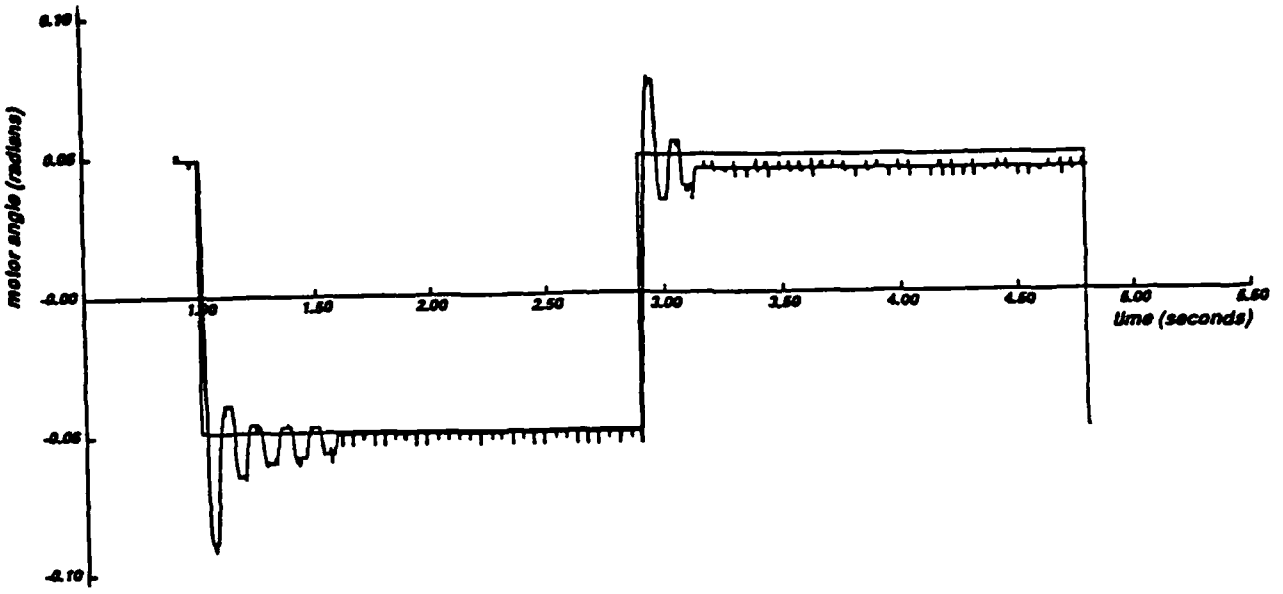

Figure 7: Closed-loop motor position response using coupling torque compensation, and a Coulomb friction compensation of ± 0.1172 *amps*. (single-mass beam)

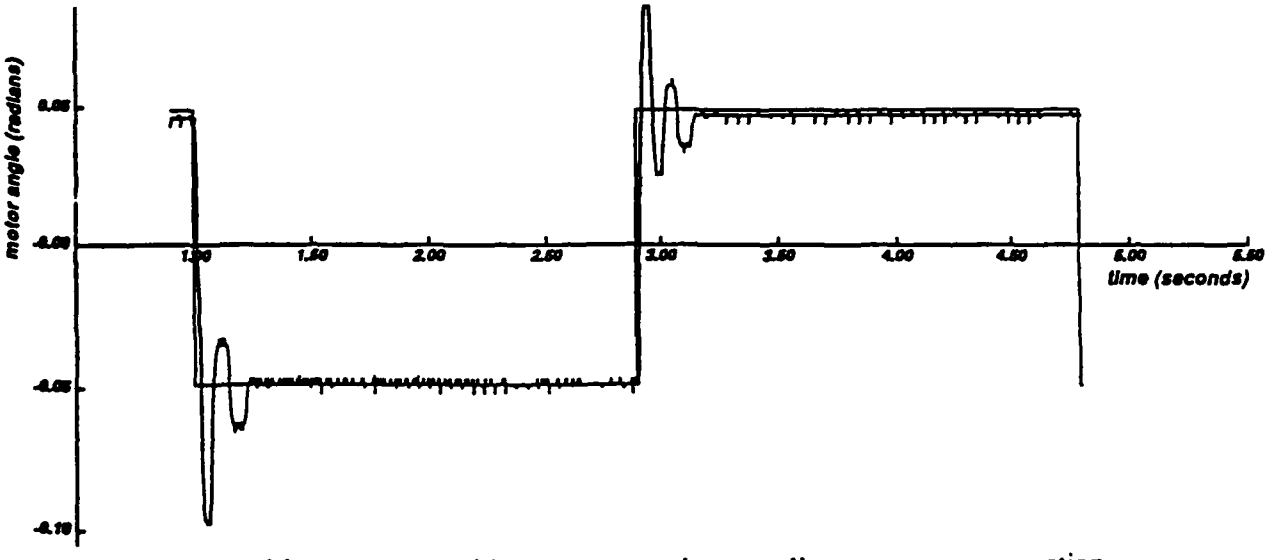

Figure 8: Closed-loop motor position response using coupling torque compensation, and a Coulomb friction compensation of ± 0.127 *amps*. (single-mass beam)

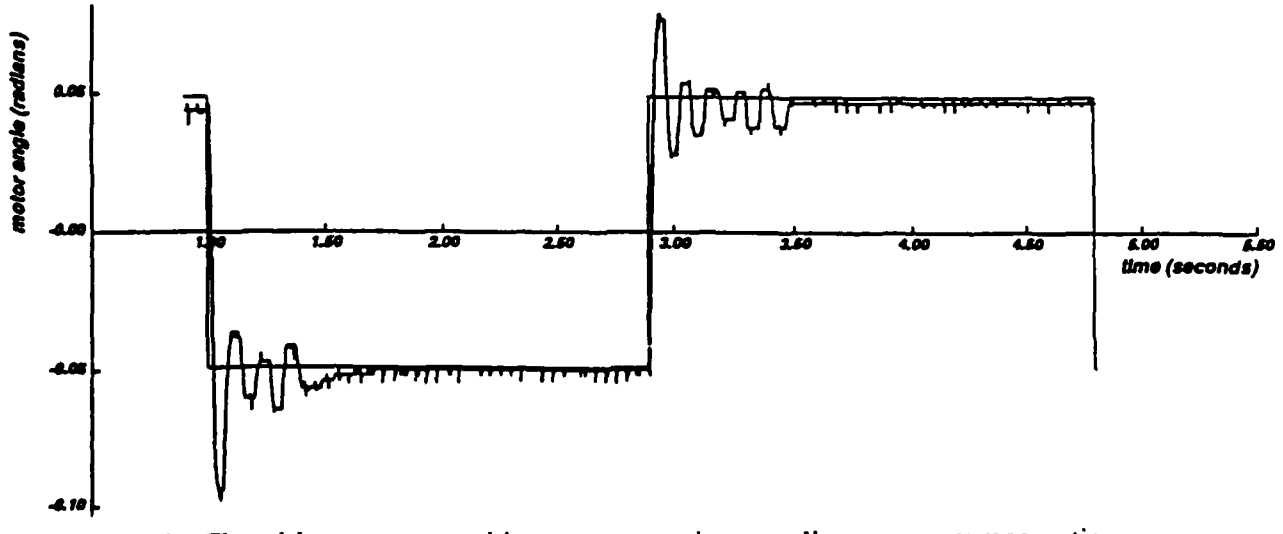

Figure 9: Closed-loop motor position response using coupling torque compensation, and a Coulomb friction compensation of ± 0.1318 *amps*. (single-mass beam)

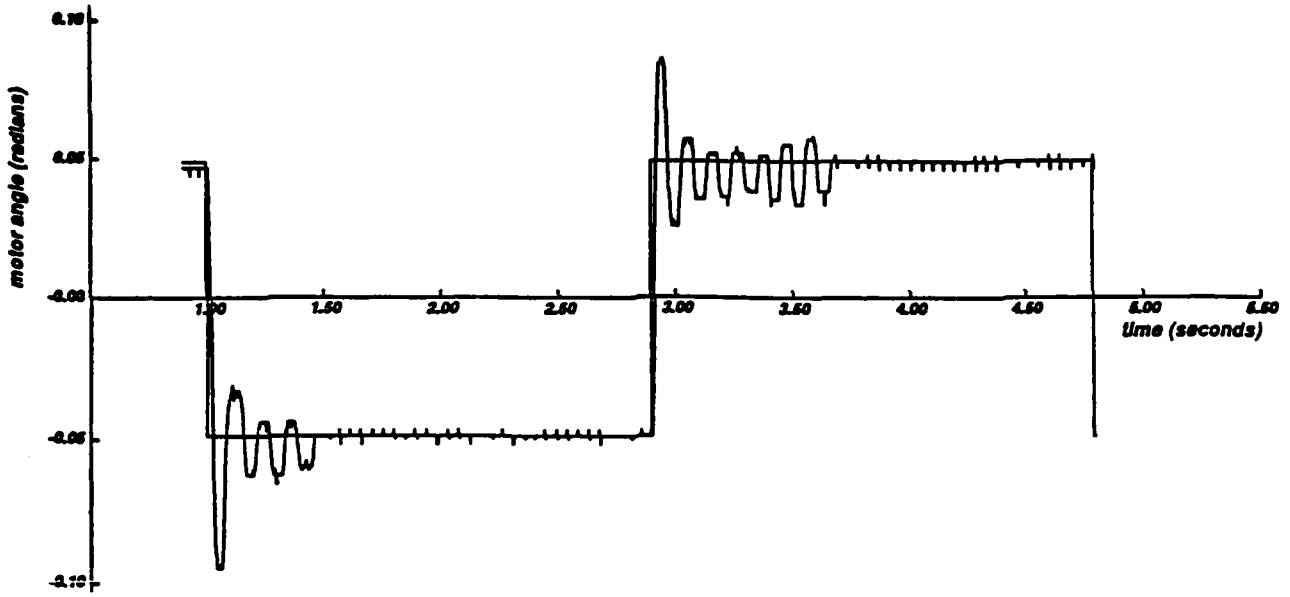

Figure 10: Closed-loop motor position response using coupling torque compensation, and a Coulomb friction compensation of ± 0.1367 *amps*. (single-mass beam)

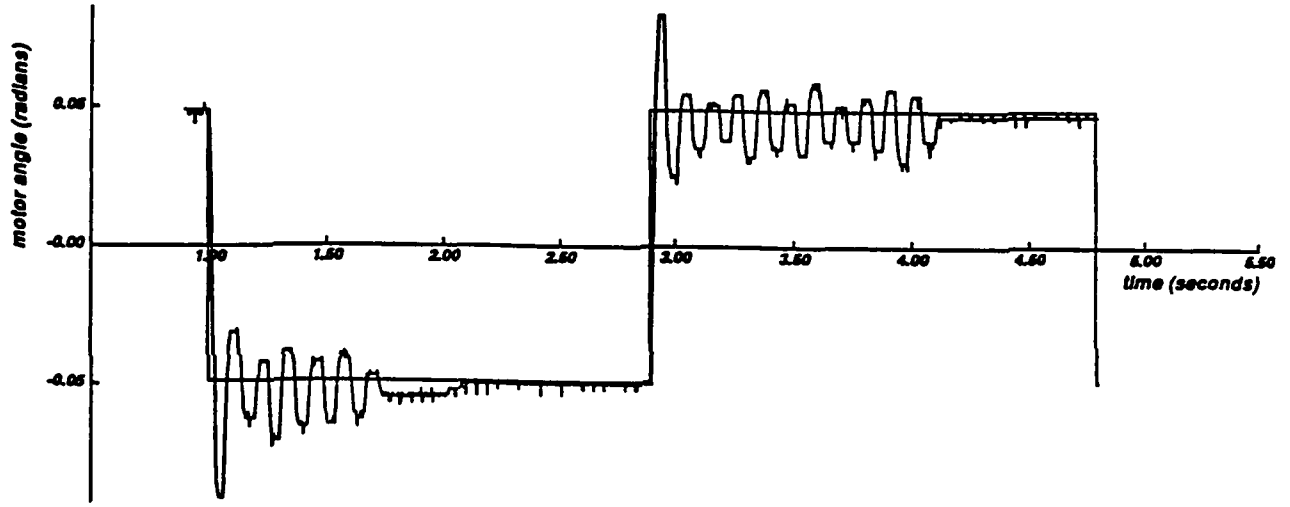

Figure 11: Closed-loop motor position response using coupling torque compensation, and a Coulomb friction compensation of ± 0.1465 *amps*. (single-mass beam)

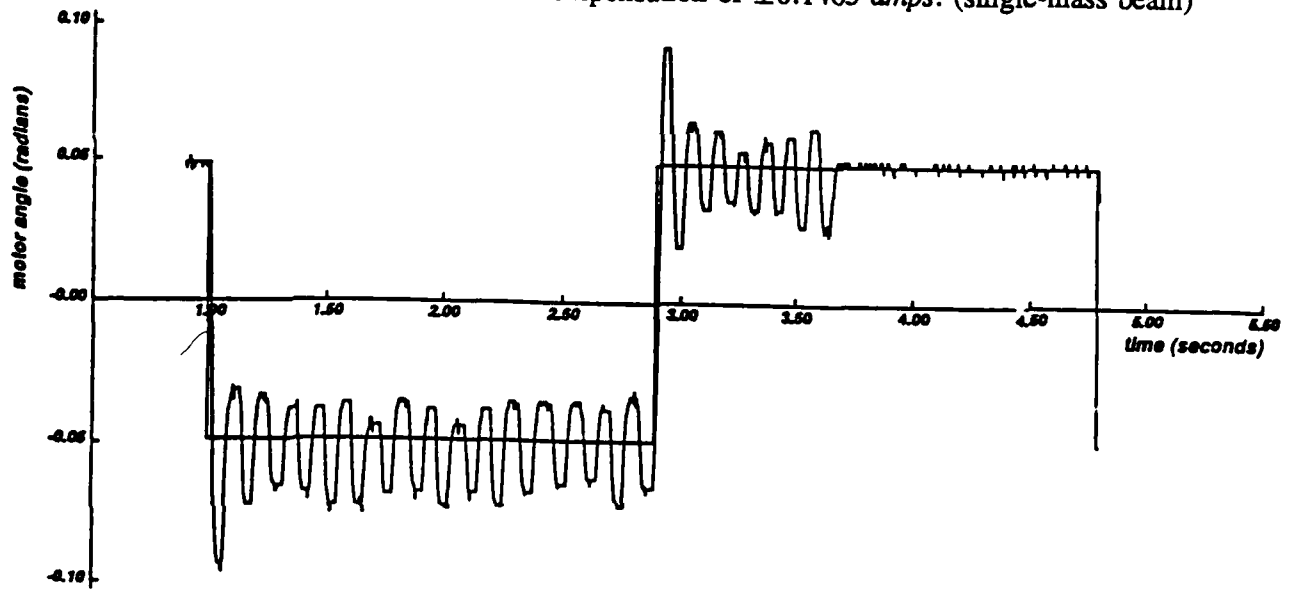

Figure 12: Closed-loop motor position response using coupling torque compensation. and a Coulomb friction compensation of ± 0.15625 *amps*. (single-mass beam)

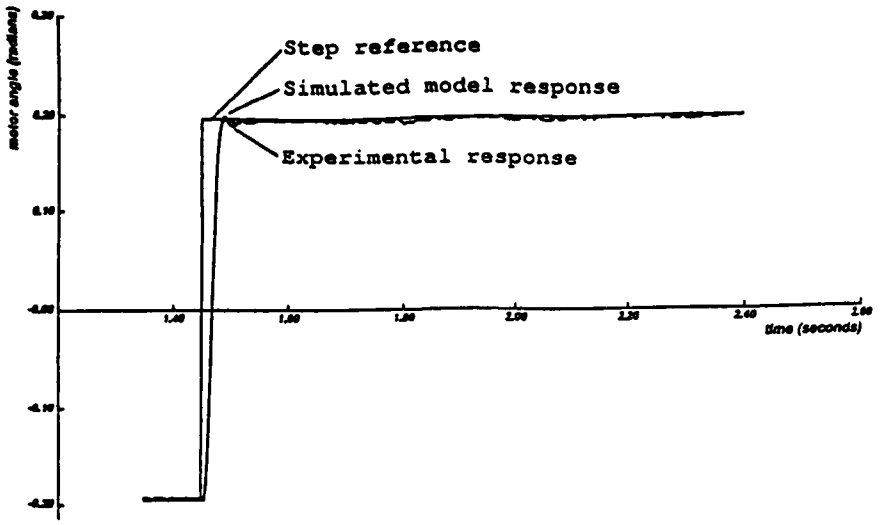

Figure 13: Closed-loop motor position response using coupling torque compensation, a Coulomb friction compensation of ± 0.132 *amps*., and a limit of 2 *mrad*. (single-mass beam)

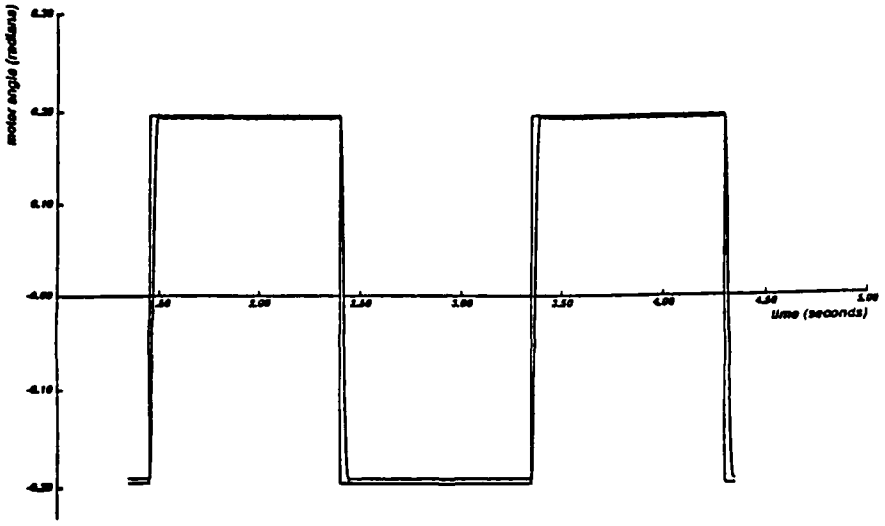

Figure 14: Closed-loop motor position response using coupling torque compensation, but not Coulomb friction compensation (single-mass beam)

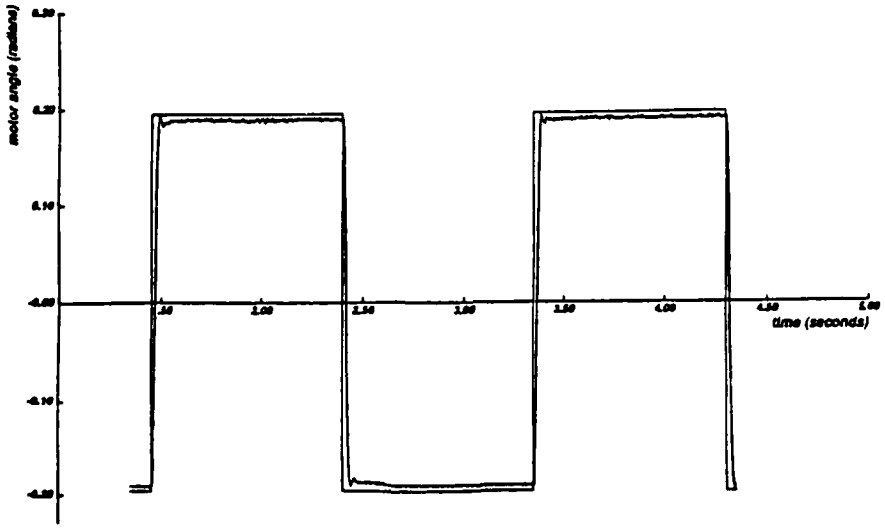

Figure 15: Closed-loop motor position response using a Coulomb friction compensation of ± 0.132 *amps*. with a limit of 2 *mrad*., but not coupling torque compensation (single-mass beam)

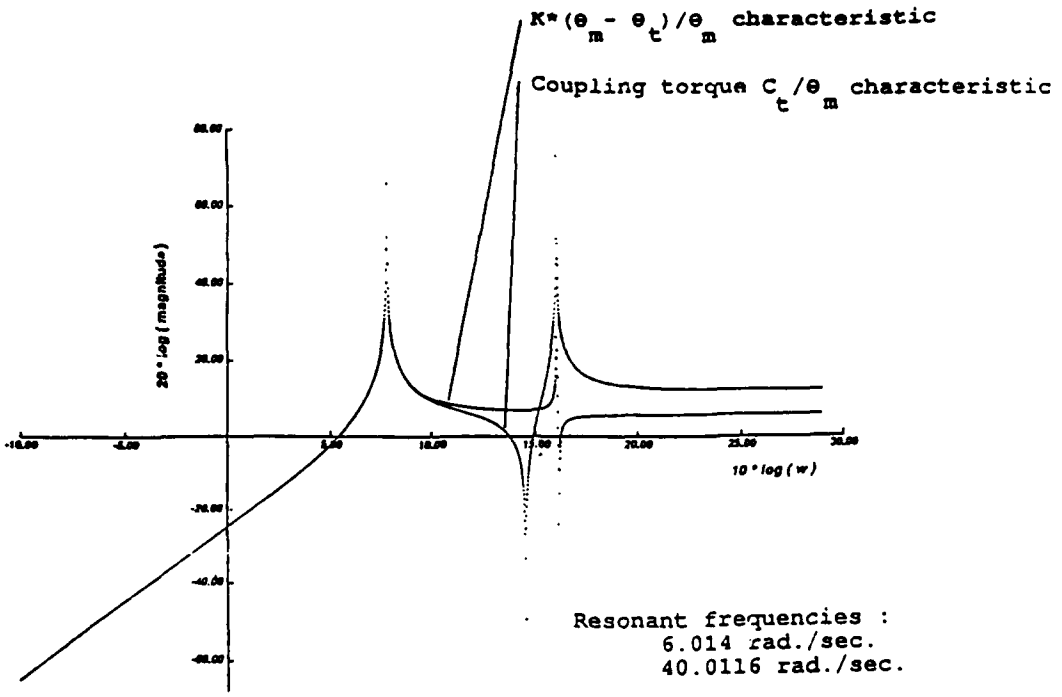

Figure 16: Magnitude of the frequency responses of the exact and approximate decoupling (expression (32)) in the two-mass beam

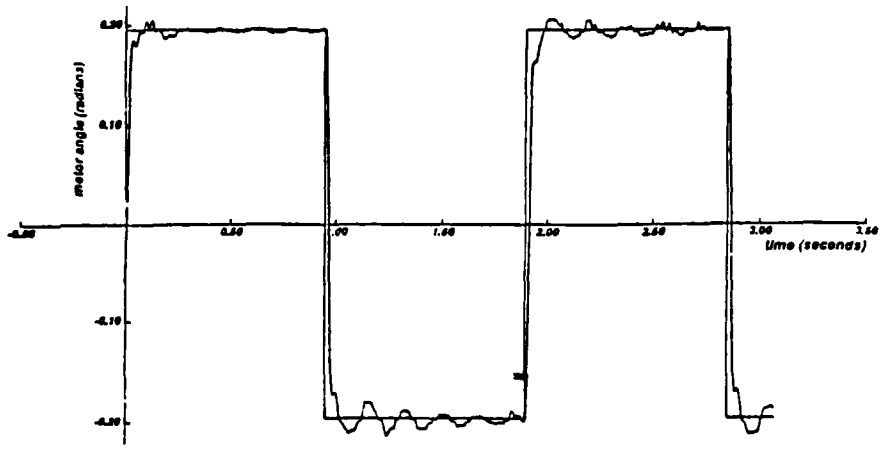

Figure 17: Closed-loop motor position response using Coulomb friction compensation of ± 0.132 *amps.* with a limit of 2 *mrad.*, and motor-beam decoupling (expression (32)) (two-mass beam)

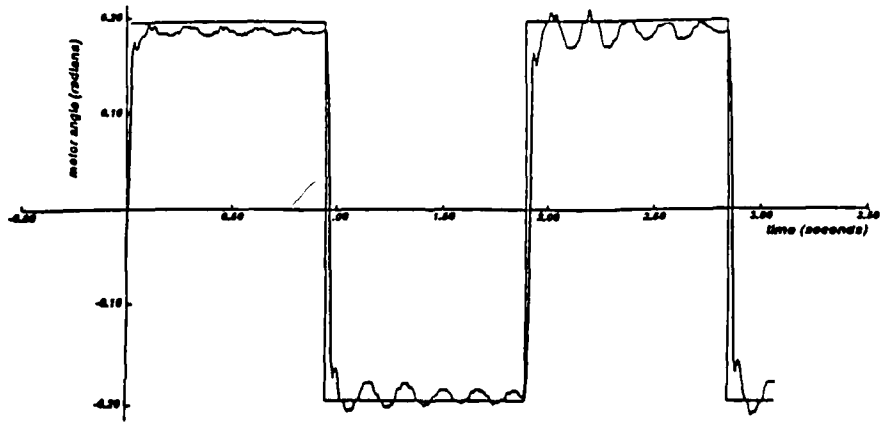

Figure 18: Closed-loop motor position response using Coulomb friction compensation of ± 0.132 *amps.* with a limit of 2 *mrad.*, but not motor-beam decoupling (two-mass beam)

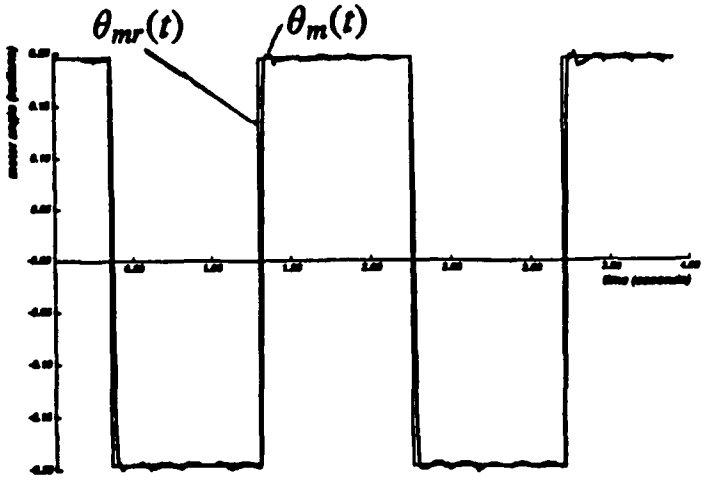

Figure 19: Closed-loop motor position response using Coulomb friction compensation of ± 0.132 *amps*. with a limit of 2 *mrad*., and exact motor-beam decoupling obtained by using (30) and the Selspot camera (two-mass beam)

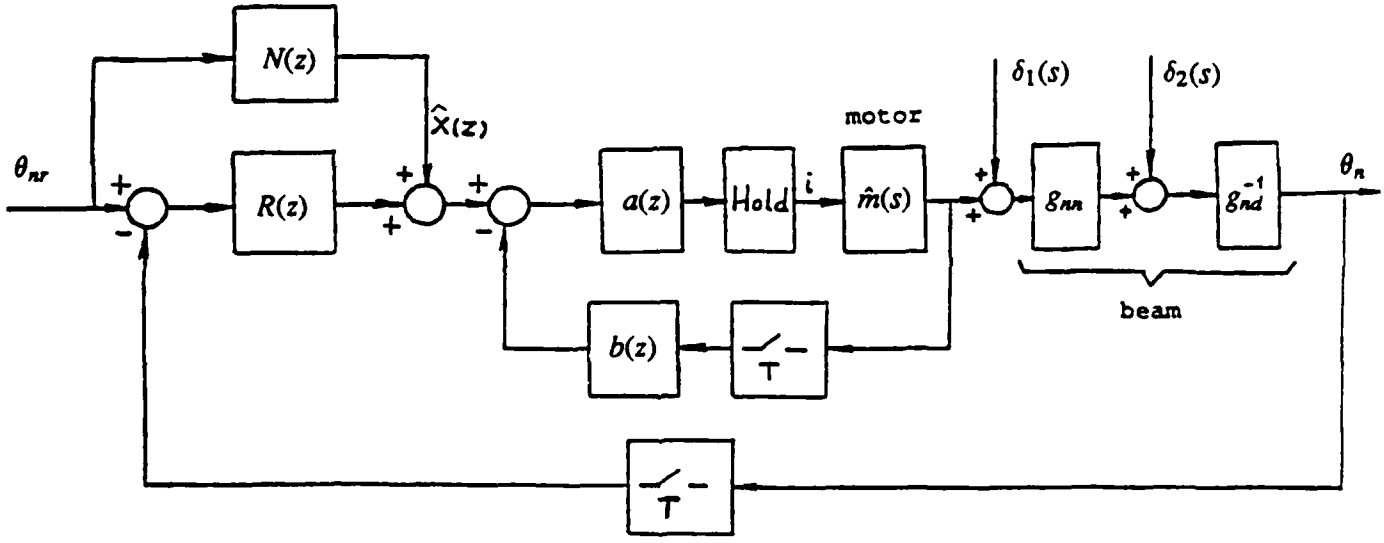

Figure 20: General computer control scheme

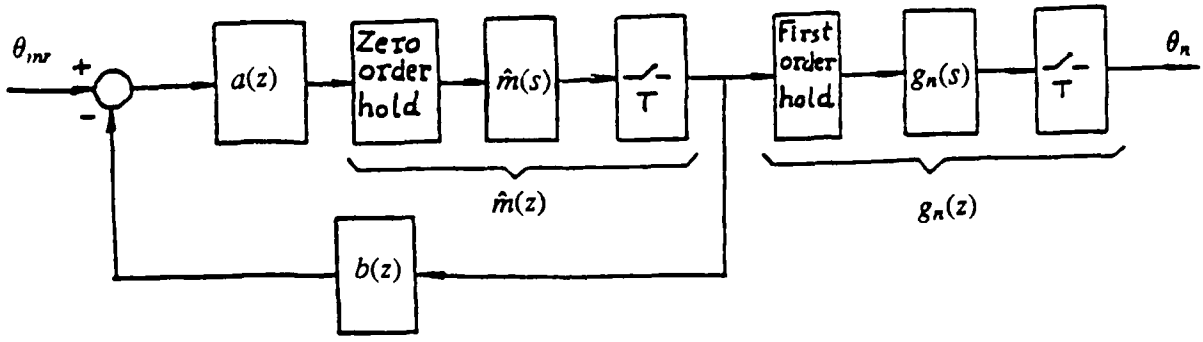

Figure 21: Discretization and reconstruction of the angle of the motor

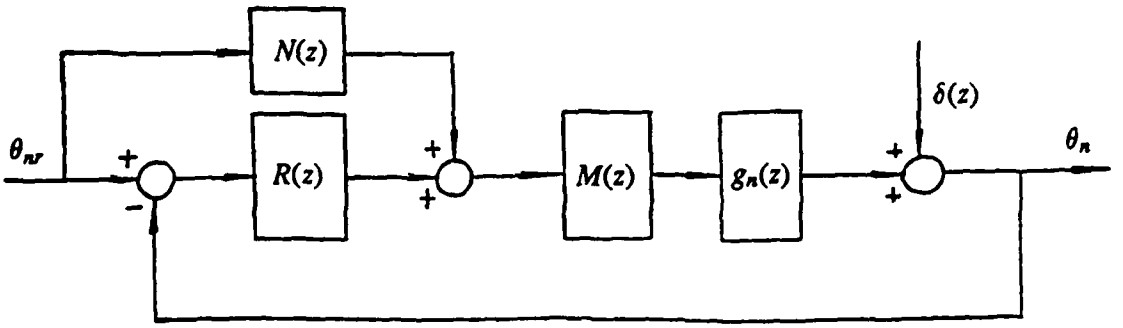

Figure 22: Simplified computer control scheme

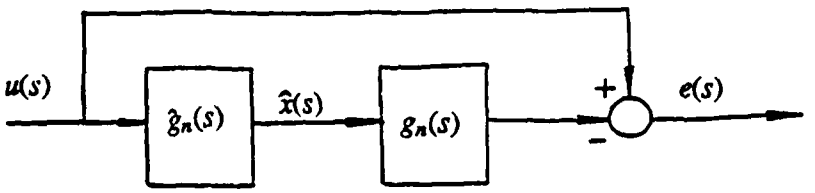

Figure 23: Optimization scheme for the feedforward controller

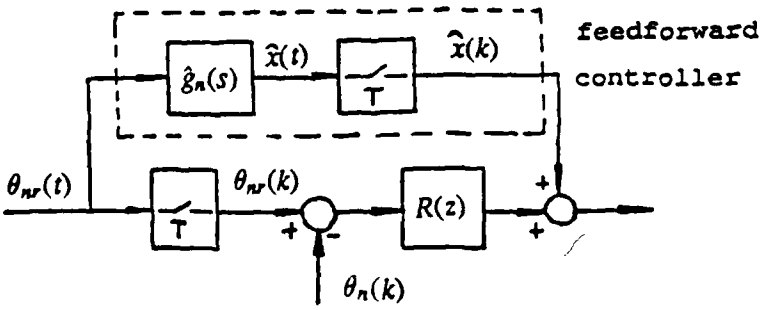

Figure 24: Simplified feedforward scheme

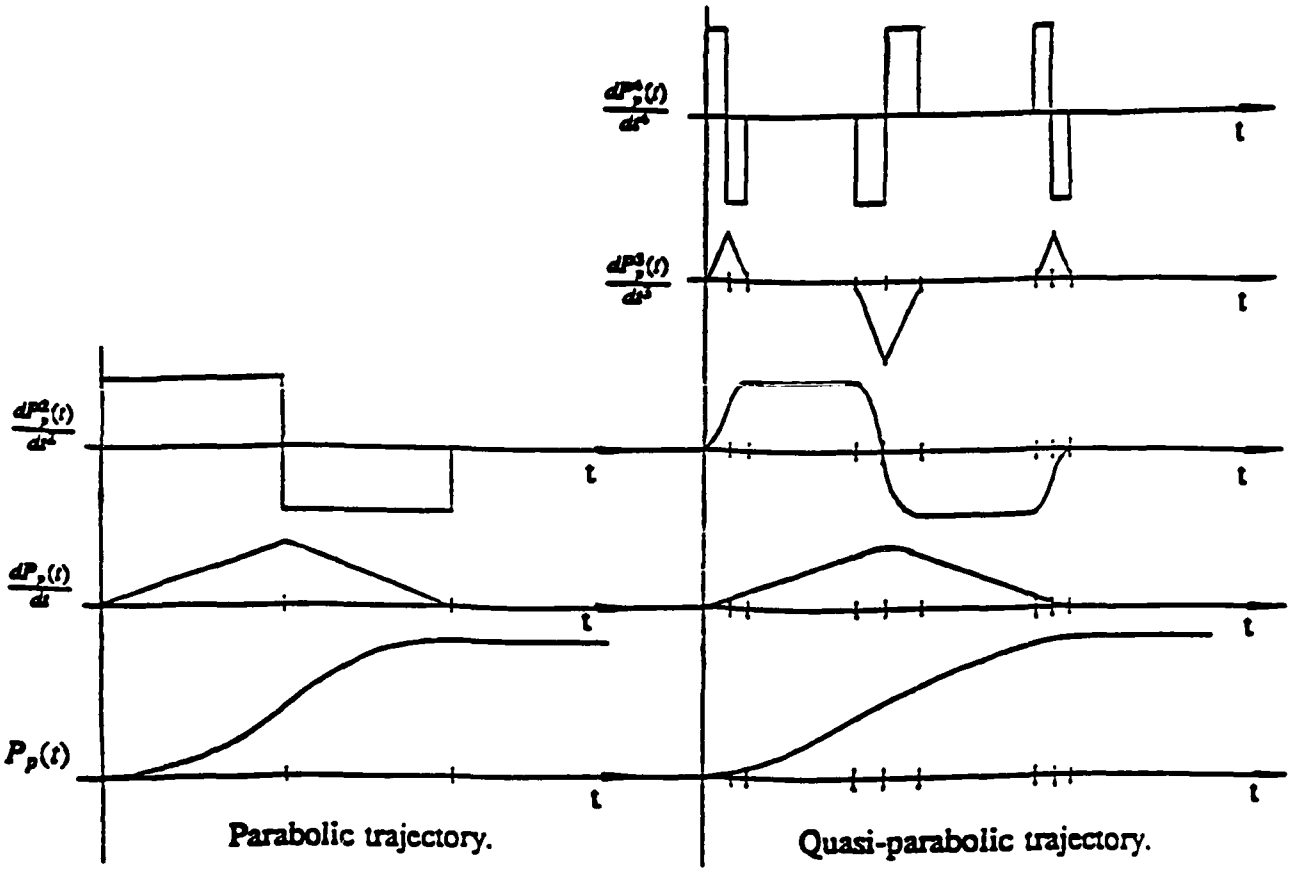

Figure 25: Parabolic and quasi-parabolic trajectories

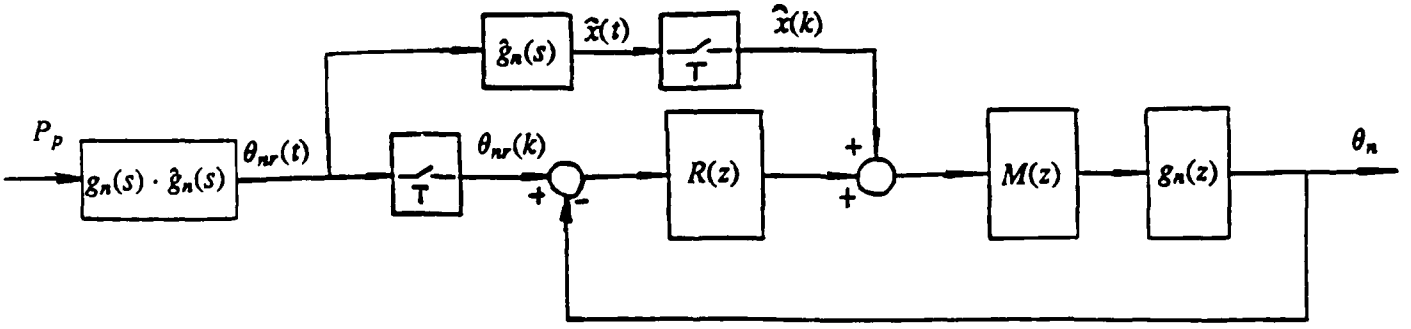

Figure 26: Control scheme using tip position feedback

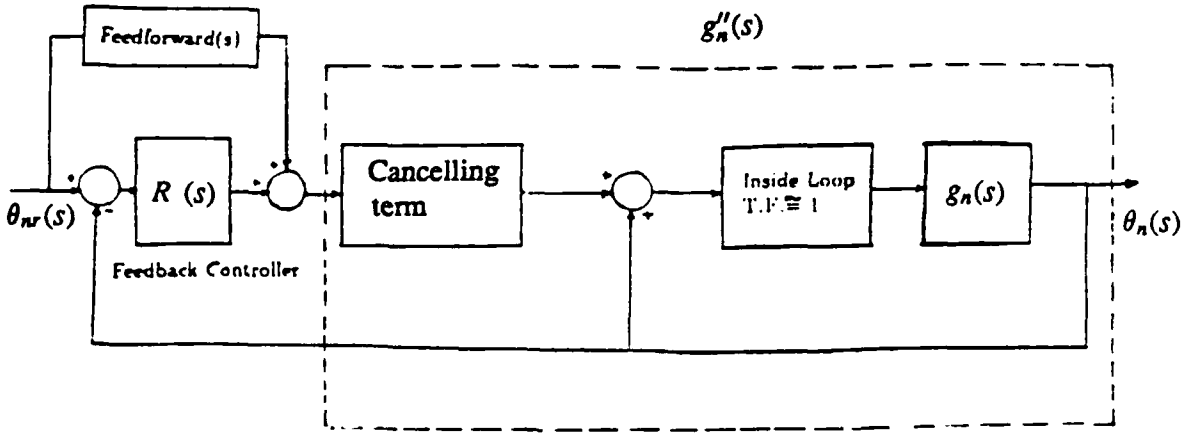

Figure 27: Control scheme cancelling the first vibration mode

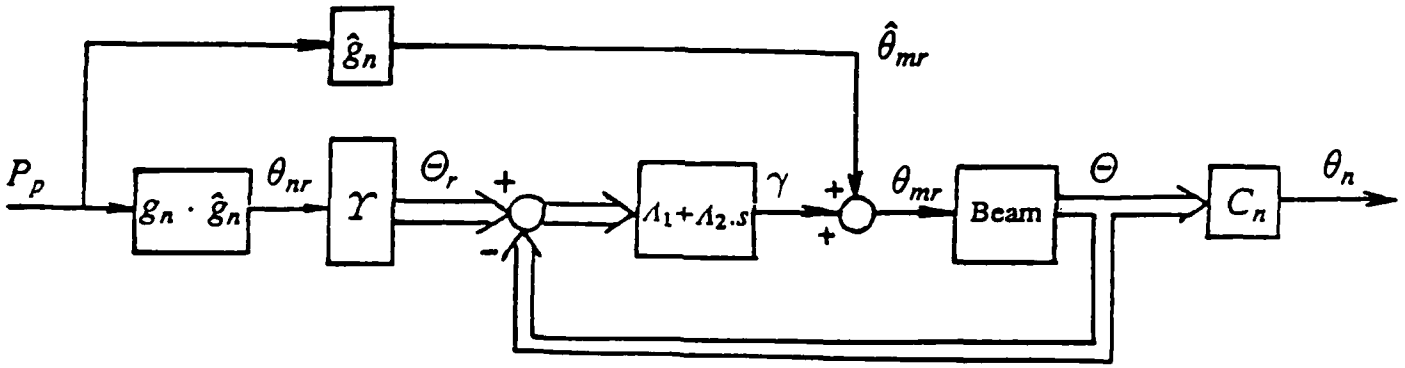

Figure 28: Control scheme sensing intermediate points of the beam

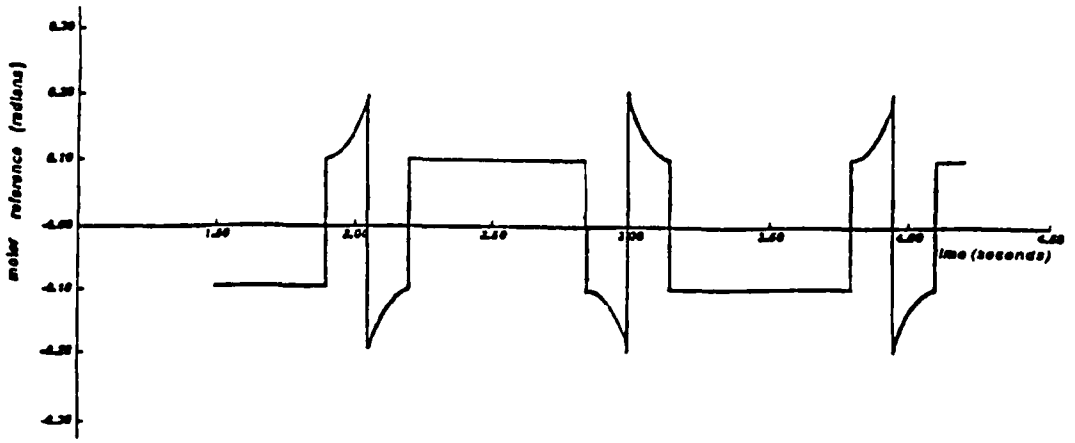

Figure 29: Feedforward signal in the single-mass arm case, having neglected motor loop dynamics

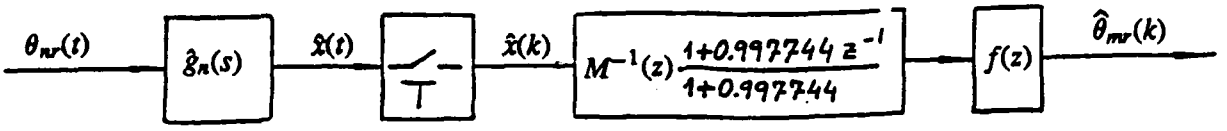

Figure 30: Implementation of the complete feedforward term in the single-mass arm case

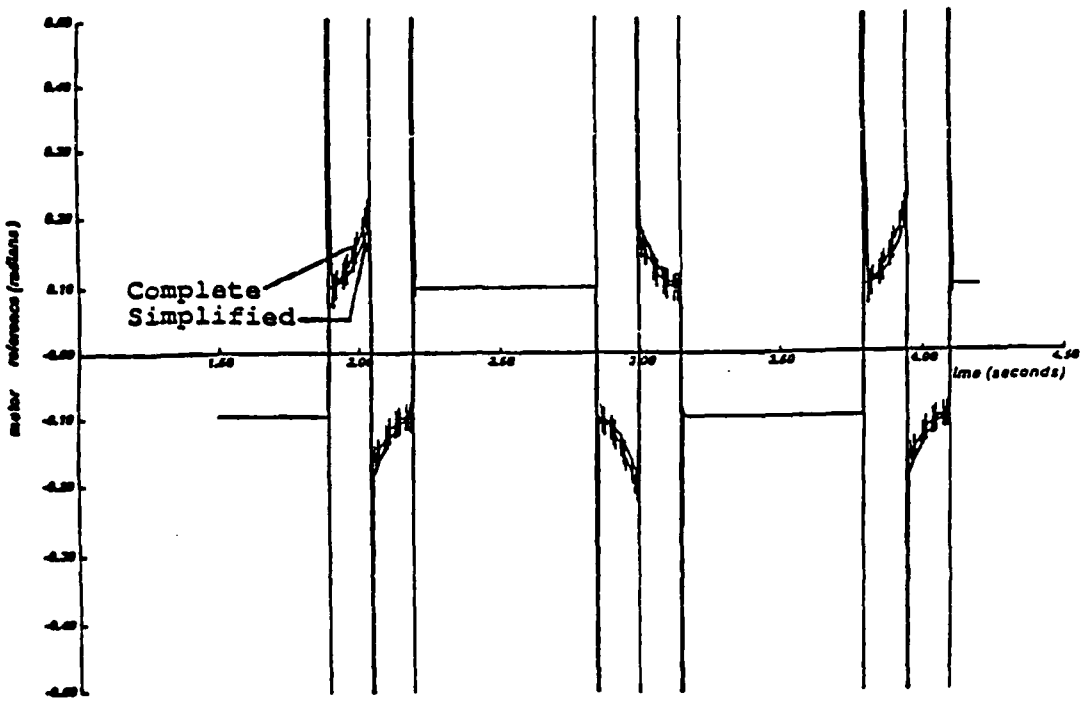

Figure 31: Feedforward signal in the single-mass arm case, taking into account motor loop dynamics

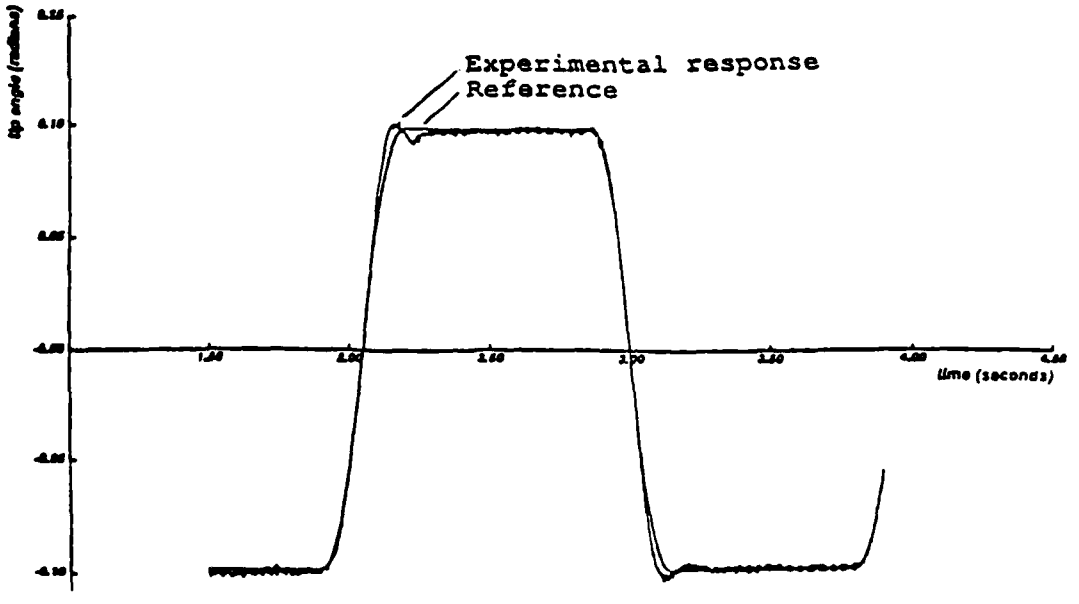

Figure 32: Tip response of the single-mass arm using the first control scheme

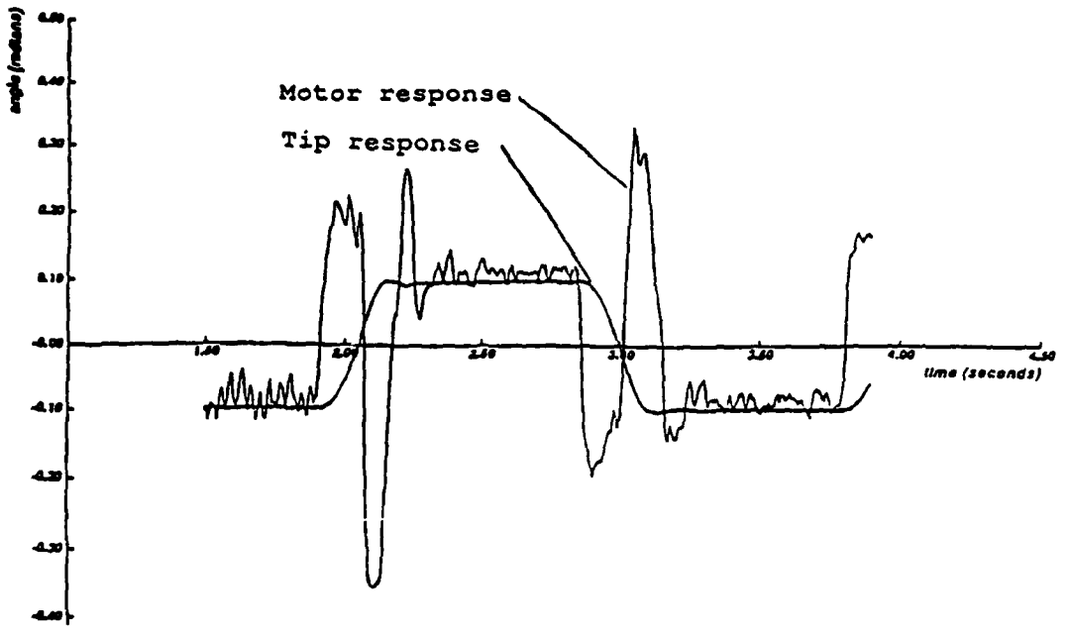

Figure 33: Tip and motor position in the single-mass arm case, using the first control scheme

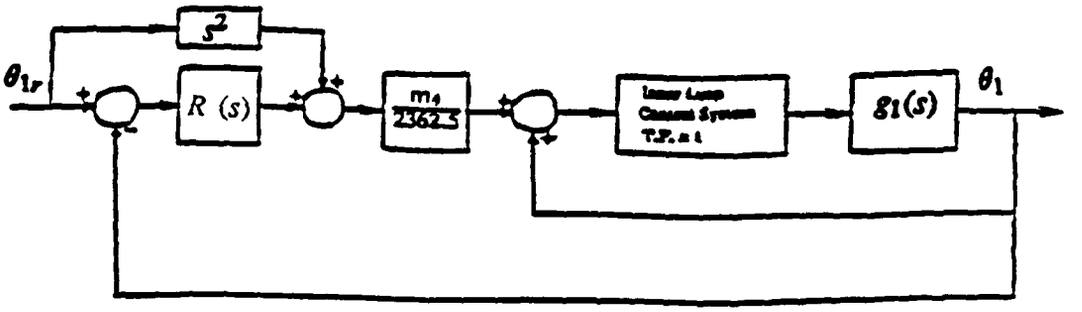

Figure 34: Second control scheme in the case of the single-mass arm

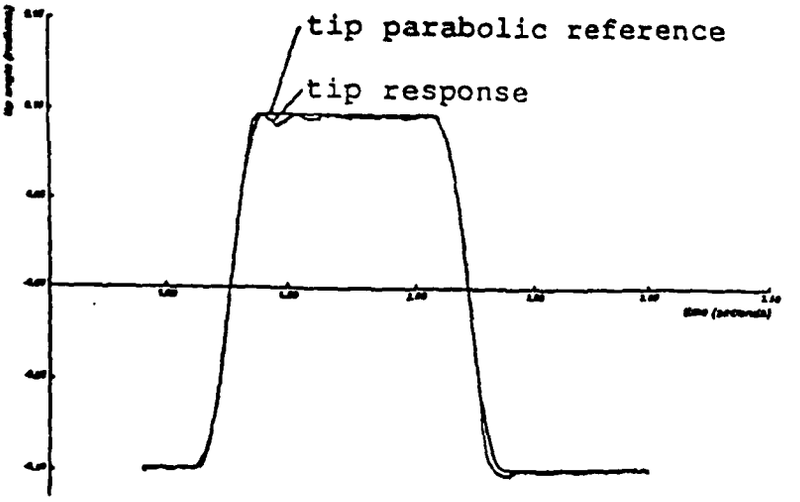

Figure 35: Tip response of the single-mass arm using the second control scheme

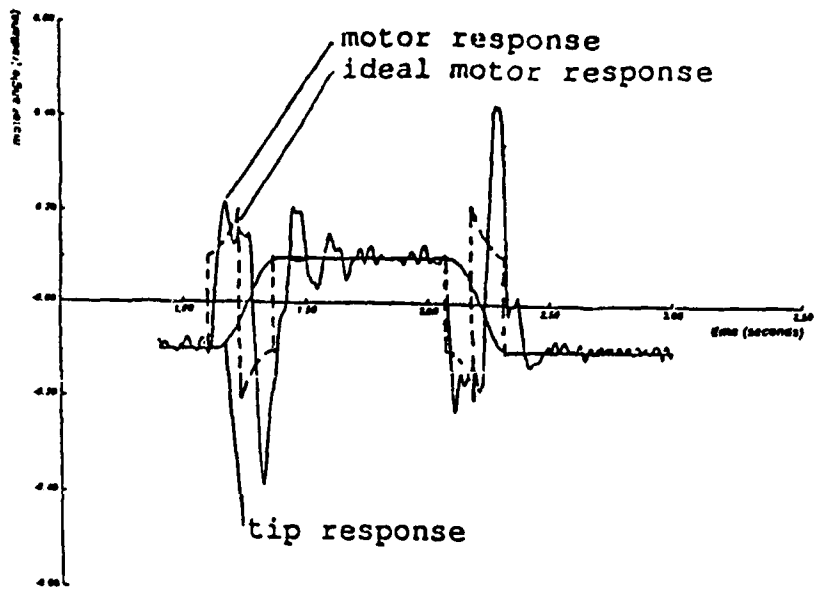

Figure 36: Tip and motor position in the single-mass arm case, using the second control scheme

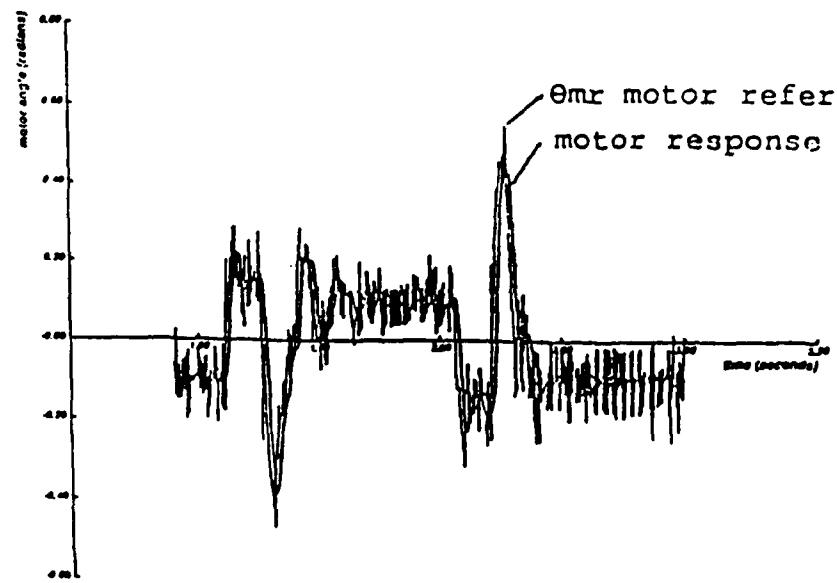

Figure 37: Motor position compared with its reference in the single-mass arm case, using the second control scheme

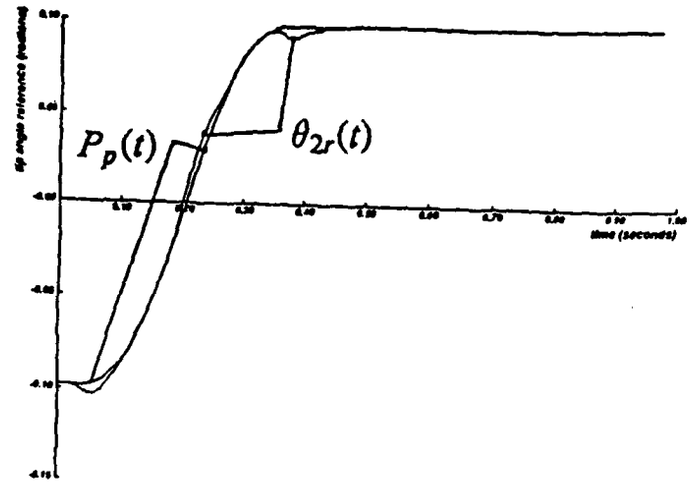

Figure 38: Quasi-parabolic trajectory and optimized tip position reference in the two-mass arm case

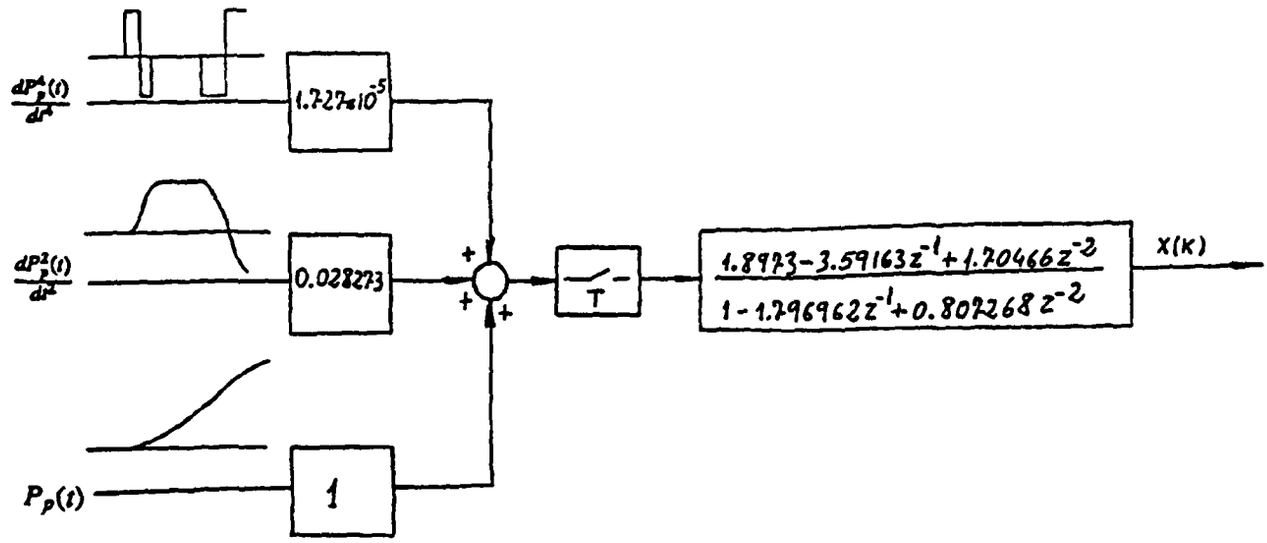

Figure 39: Implementation of the simplified feedforward term in the two-mass arm case

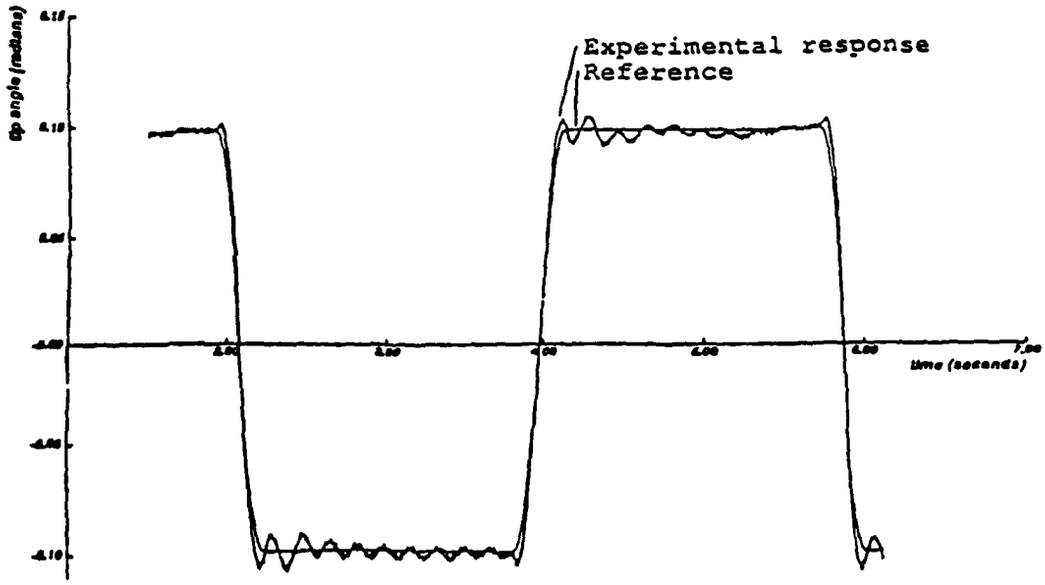

Figure 40: Tip response of the two-mass arm using the first control scheme

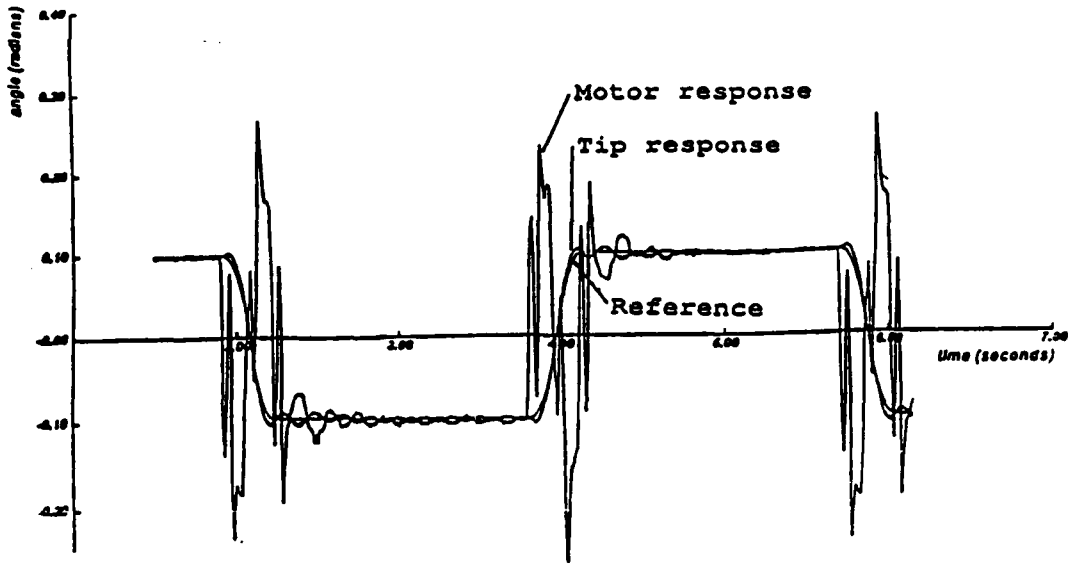

Figure 41: Motor and tip position in the two-mass arm case, using the first control scheme

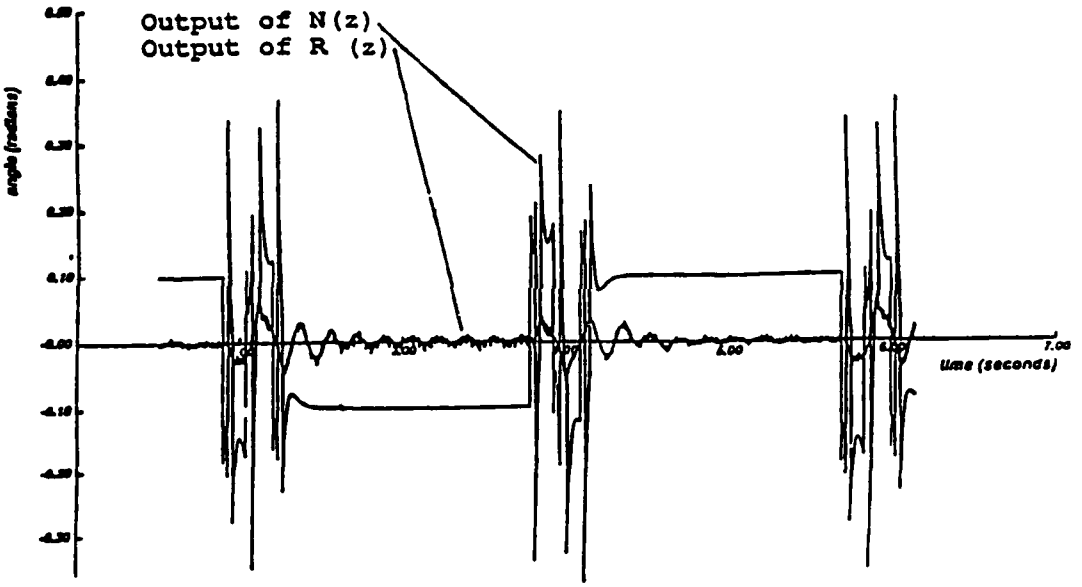

Figure 42: Comparison between the feedforward signal and the signal generated by the feedback controller in the two-mass arm case, using the first control scheme

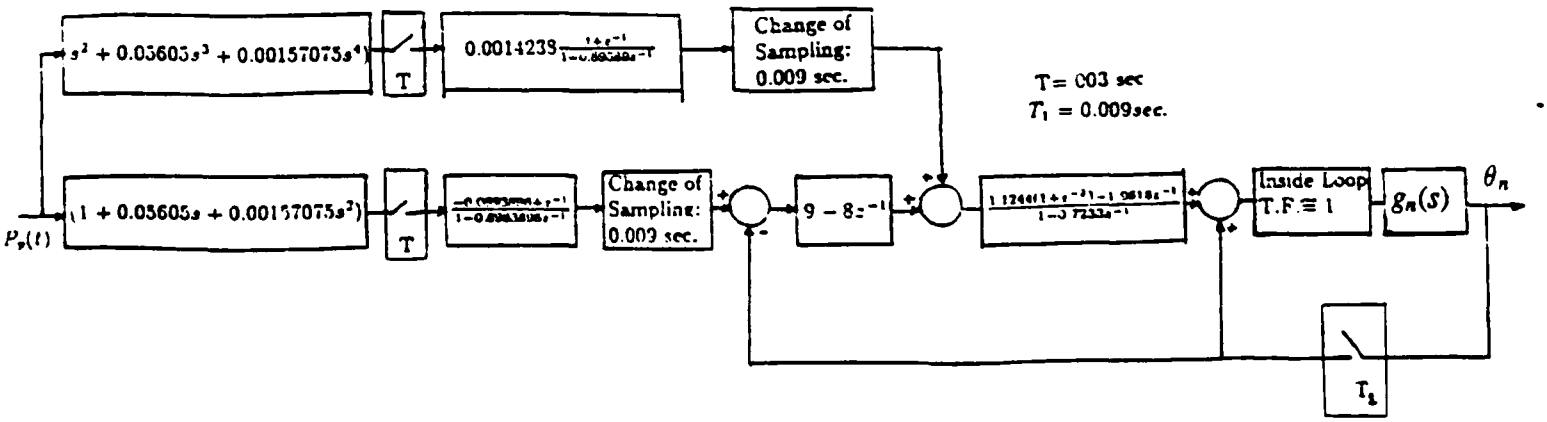

Figure 43: Implementation of the second control scheme in the two-mass arm case

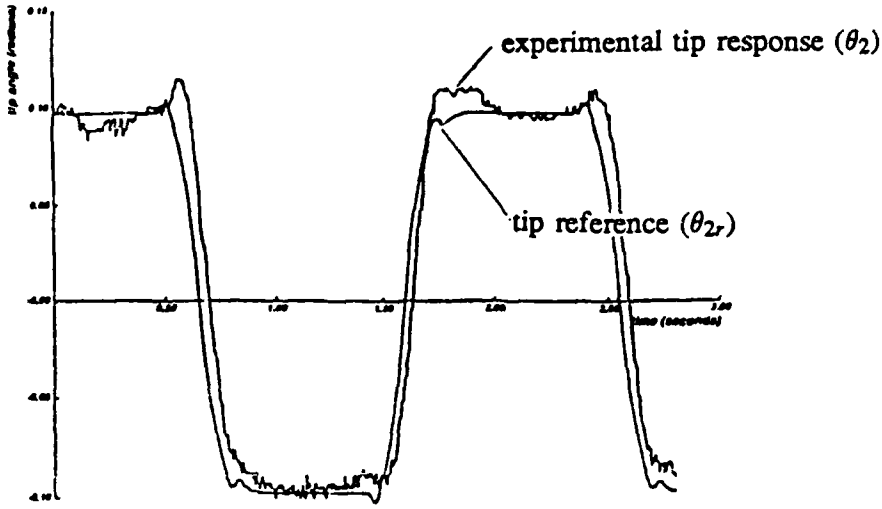

Figure 44: Tip response of the two-mass arm using the second control scheme

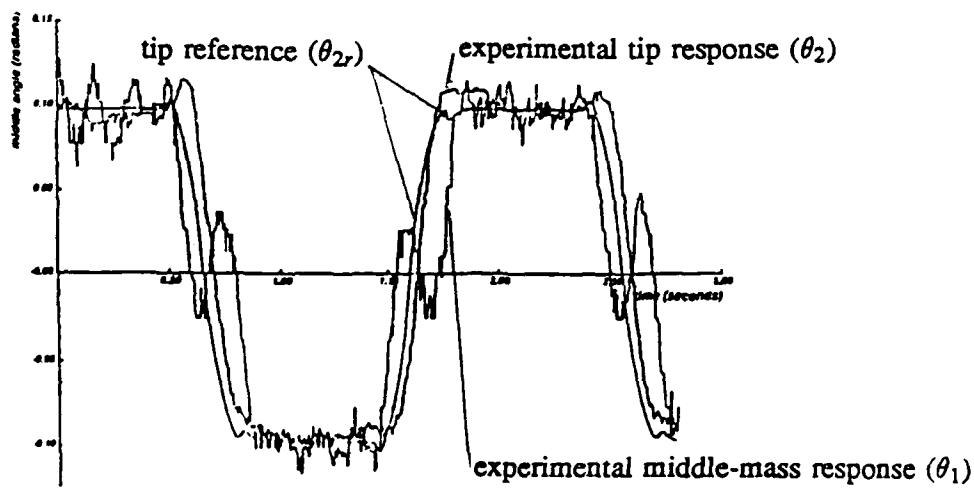

Figure 45: Tip and middle mass position in the two-mass arm case using the second control scheme

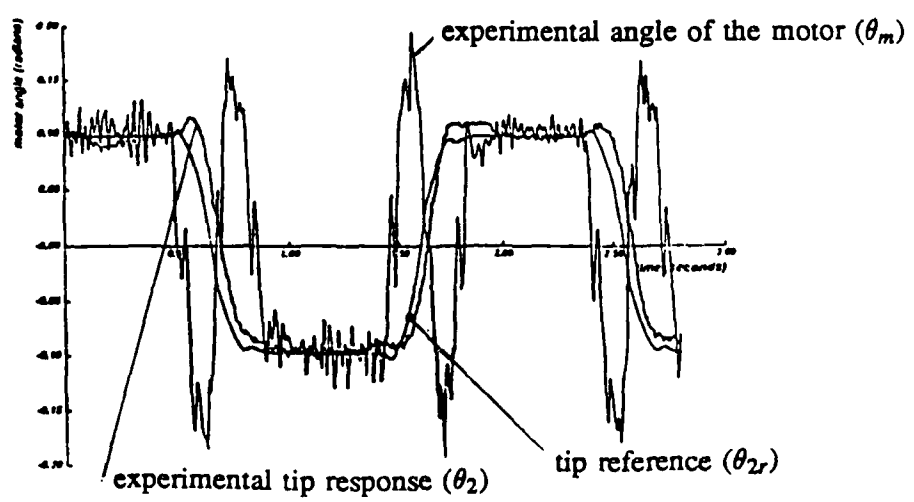

Figure 46: Motor and tip position in the two-mass arm case, using the second control scheme

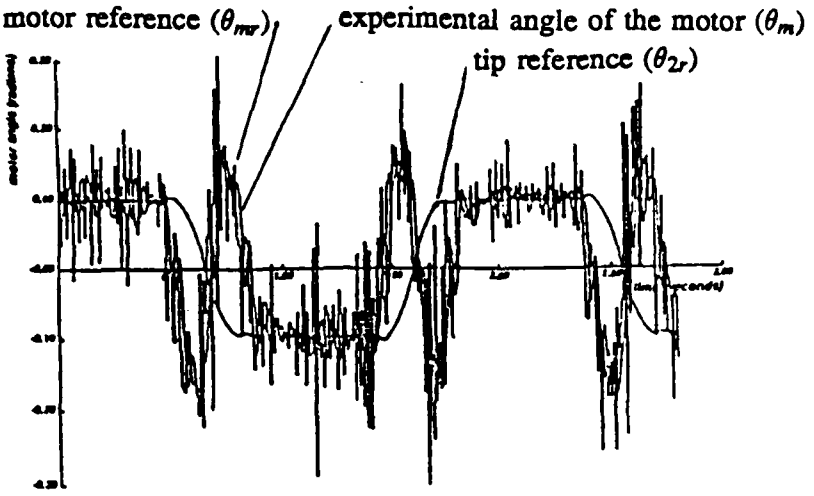

Figure 47: Comparison of the actual and the commanded motor position of the two-mass arm using the second control scheme

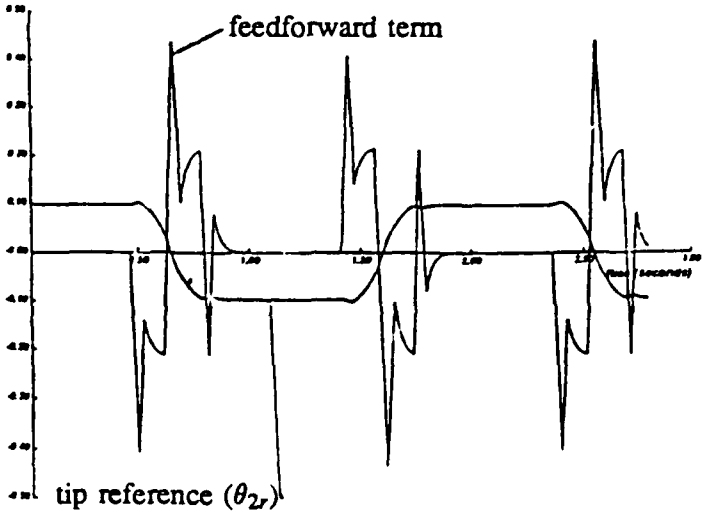

Figure 48: Feedforward signal for the two-mass arm in the second control scheme

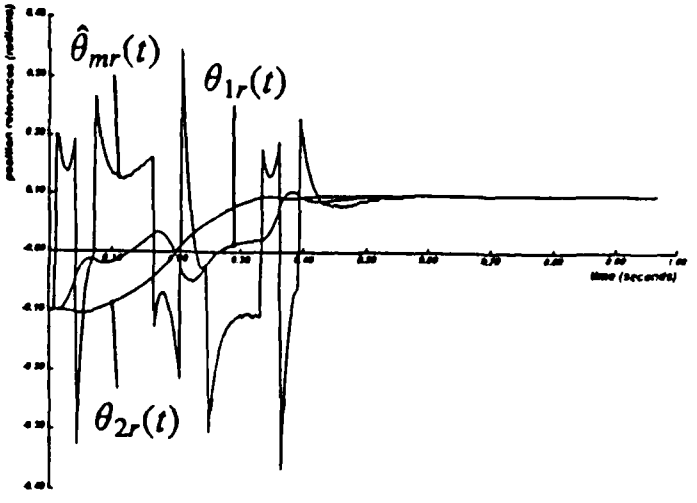

Figure 49: References for the different angles of the two-mass arm using the third control scheme

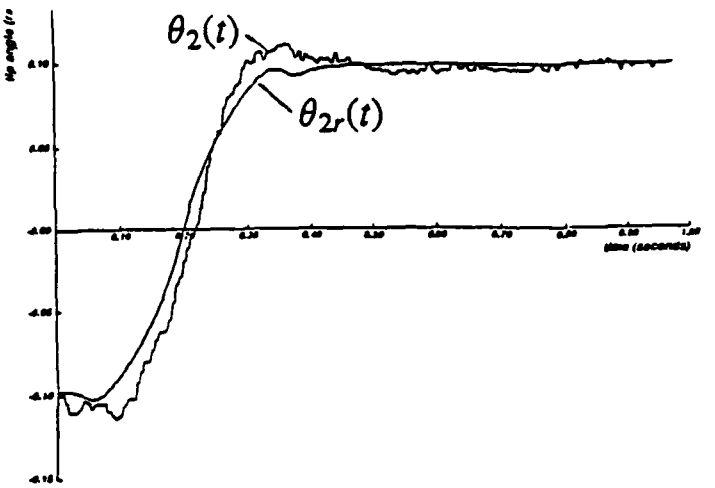

Figure 50: Tip response of the two-mass arm using the third control scheme

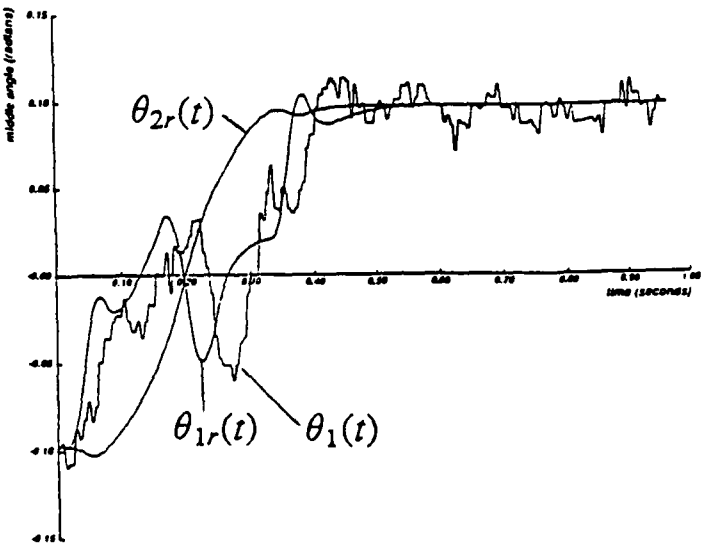

Figure 51: Middle-mass position and its reference in the third control scheme

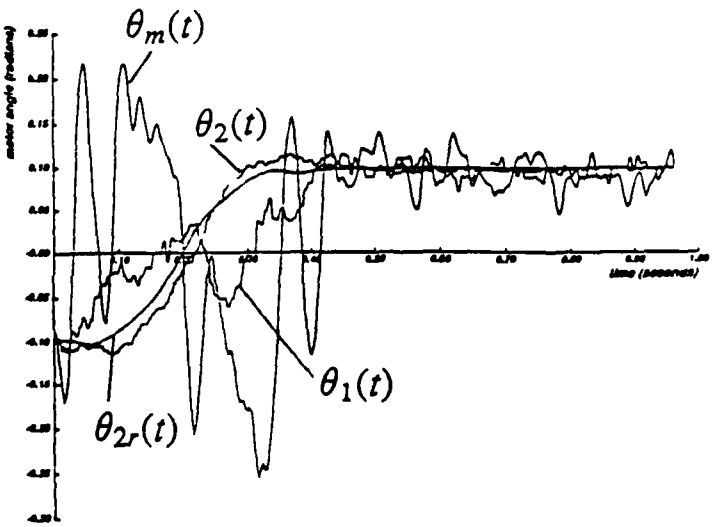

Figure 52: Motor, middle-mass, and tip position in the two-mass arm case, using the third control scheme

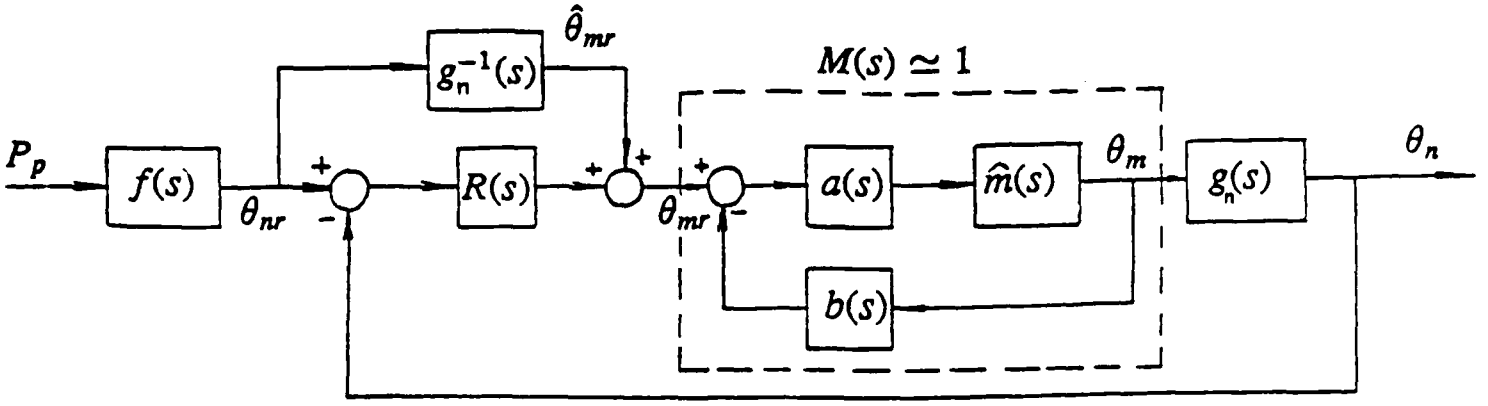

Figure 53: Normalized first control scheme

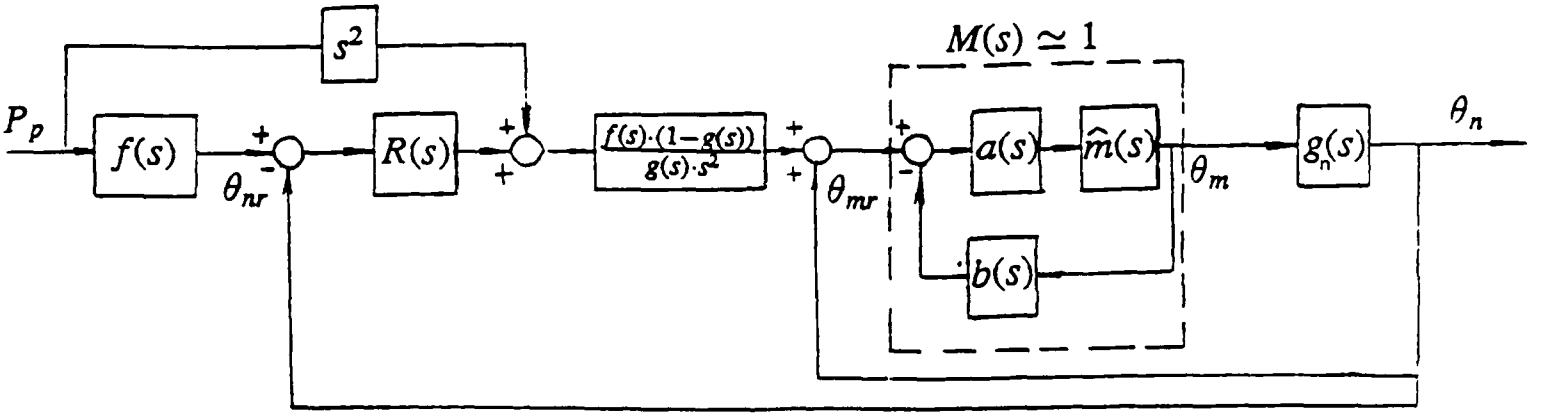

Figure 54: Normalized second control scheme

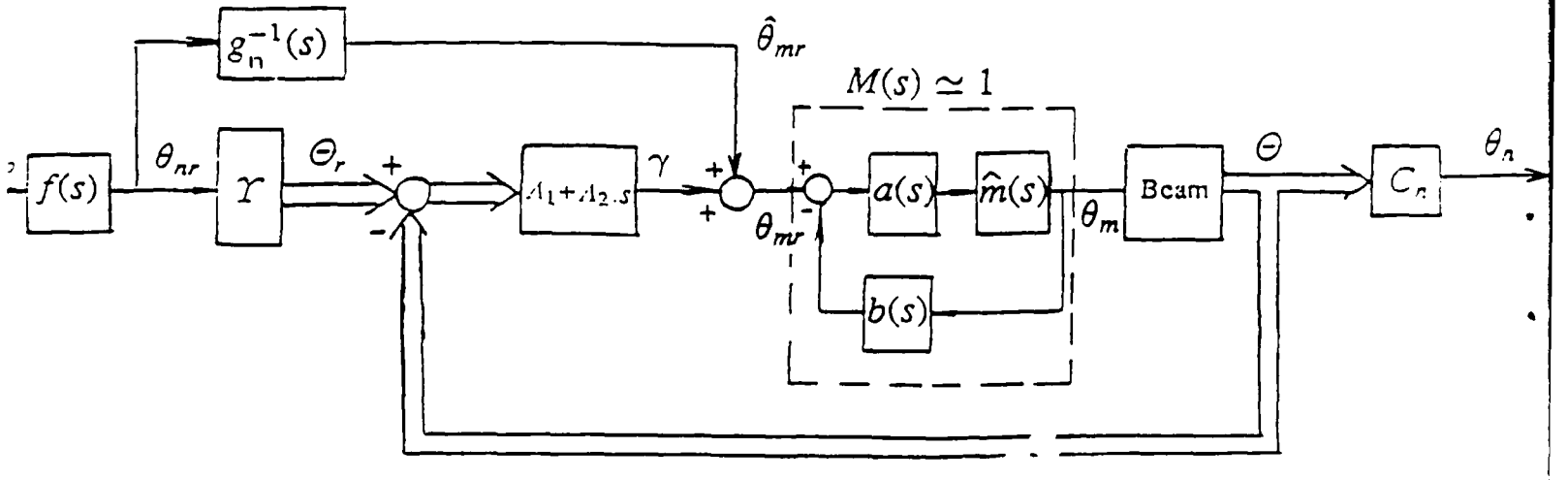

Figure 55: Normalized third control scheme

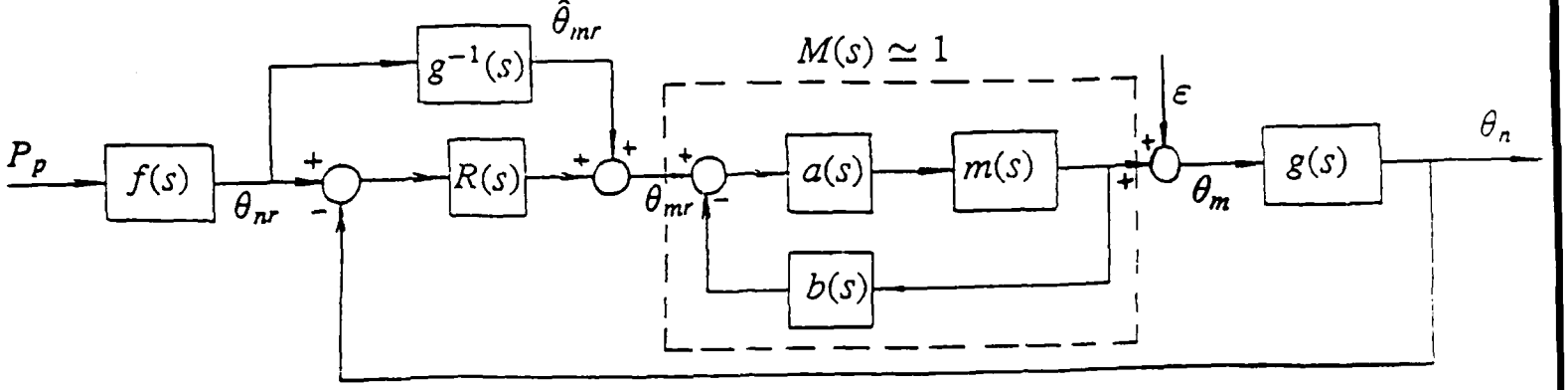

Figure 56: Motor disturbance applied to the first control scheme

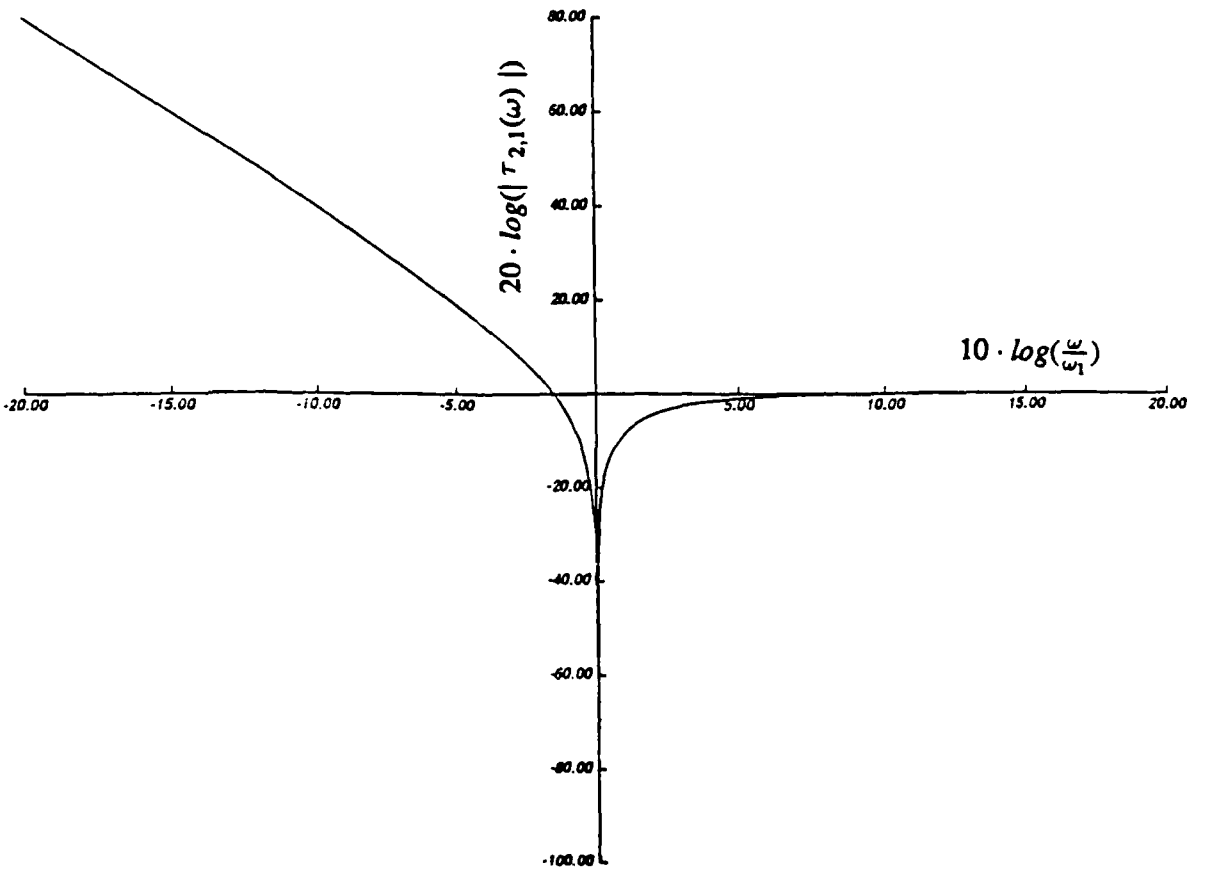

Figure 57: Characteristic that compares sensitivities of schemes 1 and 2 to unmodelled motor loop dynamics in the single-mass arm case

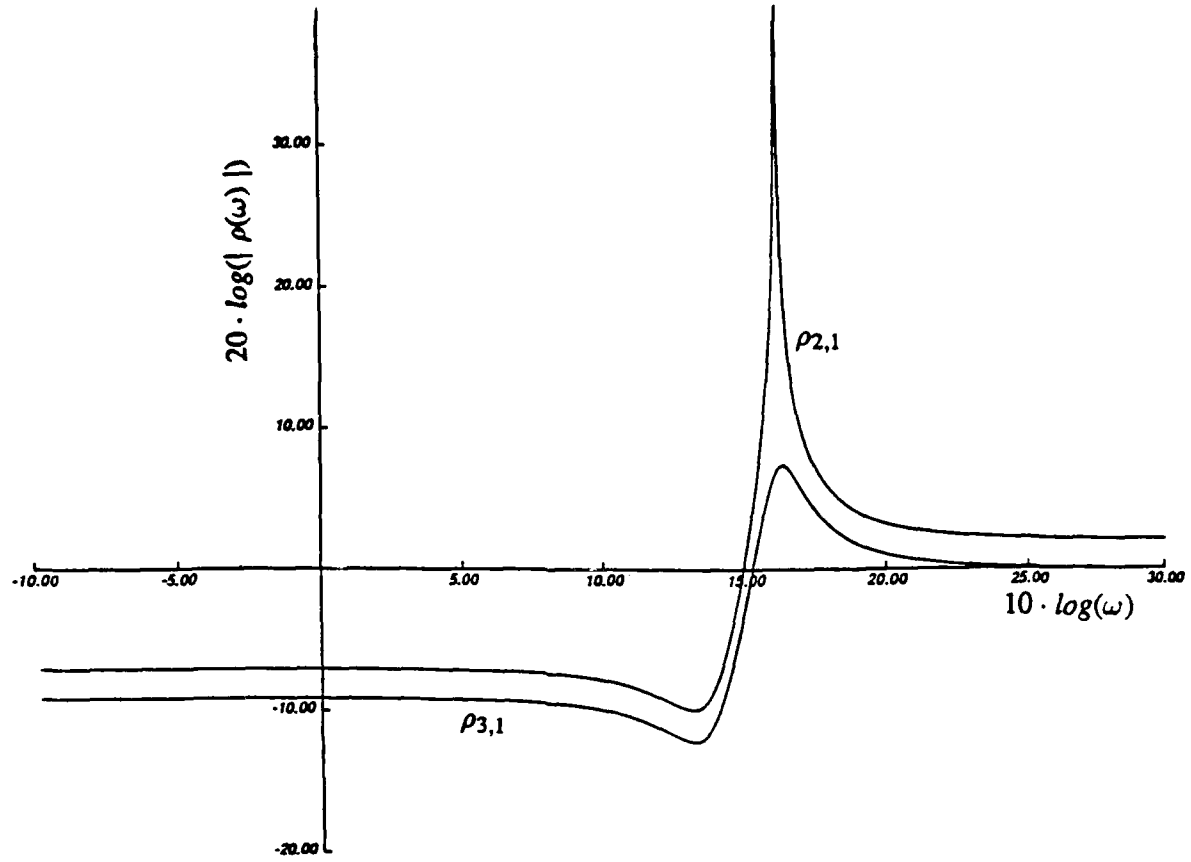

Figure 58: Characteristics that compare rejection properties to motor position perturbations of schemes 1 and 2, and 1 and 3 respectively, in the case of the two-mass arm

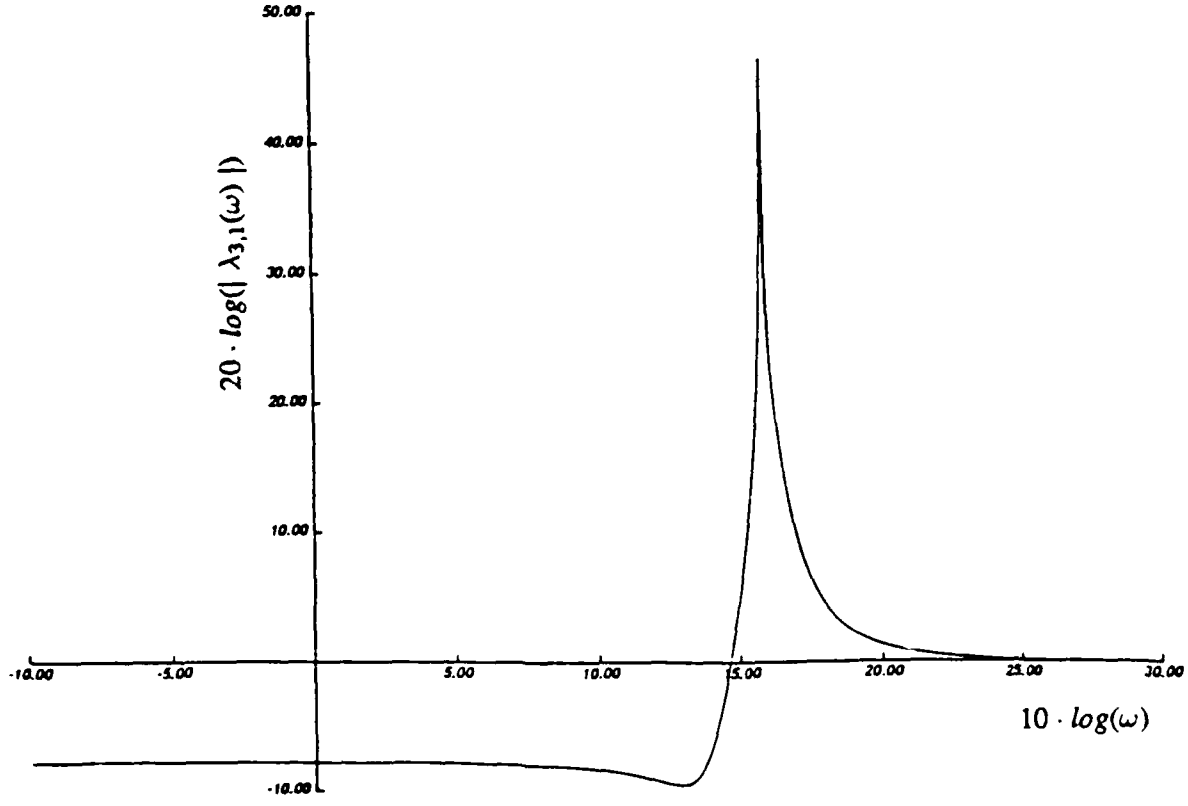

Figure 59: Characteristic that compares sensitivities of schemes 1 and 3 to changes in the tip mass, in the two-mass arm case

References

[1] Cannon, R. H., and Schmitz, E.
Precise Control of Flexible Manipulators.
Robotics Research, 1985.

[2] Matsuno, F., Fukushima, S. et al.
Feedback Control of a Flexible Manipulator with a Parallel Drive Mechanism.
International Journal of Robotics Research. Vol. 6, No. 4, Winter, 1987.

[3] Harahima, F. and Ueshiba, T.
Adaptive Control of Flexible Arm using the End-Point Position Sensing.
Proceedings Japan-Usa Symposium of Flexible Automation. Osaka (Japan), July, 1986.

[4] Siciliano, B., Yuan, B.S. and Book, W.J.
Model Reference Adaptive Control of a One Link Flexible Arm.
25th IEEE Conference on Decision and Control. Athens (Greece), December, 1986.

[5] Rovner, D.M. and Cannon, R.H.
Experiments Towards on-line Identification and Control of a Very Flexible One-Link Manipulator.
International Journal of Robotics Research. Vol. 6, No. 4, Winter, 1987.

[6] Ower, J. C. and Van de Vegte, J.
Classical Control Design for a Flexible Manipulator: Modeling and Control System Design.
IEEE Journal of Robotics and Automation. Vol. RA-3, No. 5, October, 1987.

[7] Kuo, B.C.
Automatic Control Systems. Prentice-Hall, 1982.

[8] Wu, C-h. and Paul. P.
Manipulator Compliance Based on Joint Torque Control.
9th IEEE Conference on Decision and Control. Vol. 1, 1980.

[9] Handlykken, M. and Turner T.
Control System analysis and Synthesis for a Six Degree-of-Freedom Universal Force Reflecting Hand Controller.
9th IEEE Conference on Decision and Control. Vol. 1, 1980.

[10] Walrath, C. D.
Adaptive Gearing Friction Compensation Based on Recent Knowledge of Dynamic Friction.
Automatica. Vol. 20, 1984.

[11] Canudas, C., Astrom K.J., and Braun K.
Adaptive Friction Compensation in DC-Motor Drives.
IEEE Journal of Robotics and Automation. Vol. RA-3, n-6, December, 1987.

[12] Rattan, K.S., Feliu, V., and Brown, H.B.
A Robust Control Scheme for Flexible Arms with Friction in the Joints.
1988 NASA - Air Force Workshop on Space, Operation, Automation and Robotics. Dayton (USA), July, 1988.

[13] Feliu, V.
Diseño Automático con Computador de Sistemas Discretos de Control Multivariables.
Ph.D. Thesis, E.T.S.I. Industriales of Universidad Politécnica of Madrid. September 1982.

[14] Craig, J.J.
Introduction to Robotics. Mechanics & Control. Addison-Wesley Publishing Company, 1986.

[15] Khosla, P.K., and Kanade, T.
Experimental Evaluation of Nonlinear Feedback and Feedforward Control Schemes for Manipulators.
The International Journal of Robotics Research. Vol. 7, n-1. 1988.

[16] Meckl, P.H. and Seering W.P.
Reducing Residual Vibration in Systems with Uncertain Resonances.
IEEE Control Systems Magazine. Vol. 8, no. 2, April 1988.

[17] Kotnick, T., Yurkovich, S. and Ozguner U.
Acceleration Feedback for Control of a Flexible Manipulator Arm
Journal of Robotic Systems. Vol. 5, n-3, June 1988.

[18] Dougherty, H., Tompetrini, K., Levinthal, J. and Nurre, G.
Space Telescope Pointing Control System.
AIAA Journal of Guidance, Control, and Dynamics. Vol. 5, n-4, July-Aug. 1982.

[19] Gebler, B.
Feed-forward Control Strategy for an Industrial Robot with Elastic Links and Joints.
IEEE International Conference on Robotics and Automation. Raleigh (North Carolina-USA), April 1987.

[20] Feliu, V.
A Transformation Algorithm to Estimate System Laplace Transform from Sampled Data.
IEEE Trans. on Systems, Man & Cybernetics. Vol. SMC-16, January 1986.

[21] VanLandingham, H.F.
Introduction to Digital Control Systems. MacMillan Publishing Company, 1985.

[22] Gupta, S.C., and Hasdorff, L.
Fundamentals of Automatic Control. John Wiley & Sons, inc., 1970.

[23] Farrenkopf, R.L.
Optimal Open-Loop Maneuver Profiles for Flexible Spacecraft.
J. Guid. Contr. Vol. 2, no. 6, Nov-Dec., 1979.

[24] Turner, J.D. and Junkins, J.L.

Optimal Large-Angle Single-Axis Rotational Maneuvers of Flexible Spacecrafts.
J. Guid. Contr. Vol. 3, no. 6, Nov-Dec., 1980.

[25] Lee, E.B., and Markus, L.
Foundations of Optimal Control Theory. Krieger Publishing Co.. Florida 1986.

[26] Khosla P.K.
Real-Time Control and Identification of Direct-Drive Manipulators
Ph.D. Thesis, Robotics Institute, Carnegie Mellon University, August 1986.